IMAGE: A MAP OF THE STARS OF THE ORION CONSTELLATION

Print ISSN: 2631-8490 Online ISSN: 2631-8504

JournalPreview

London Journal of Research in Science: Natural & Formal

Volume 25 | Issue 4 | Compilation 1.0

Great Britain
Journals Press

WWW.JOURNALSPRESS.COM

JournalPreview

London Journal of Research in Science: Natural & Formal

Journal Content

In this Issue

Great Britain
Journals Press

Scan to know paper details and
author's profile

Coupling of CO_2 Emissions and Economic Growth Across the U.S. Between 2010 and 2015

Andrew Bagwell, Jeffrey Colby, Caity Duncan, Caroline Fehlman, Nicholas Gastelle, Dennis Gilfillan and Gregg Marland

Appalachian State University

ABSTRACT

To mitigate climate change it will be necessary to reduce greenhouse gas emissions and this transition is likely to involve an impact on economic output. We adopt the U.N. sustainable development indicator 9.4.1, CO_2 emissions per unit of value added, to explore the change over time of the value of economic output as CO_2 emissions change. CO_2/GDP is most often studied at the national level, but data are available for the 2010-2015 time period to estimate CO_2 emissions at the county level in the U.S. Available gridded data allow us to calculate emissions by county for 10 economic sectors, and thus to examine the relationship between CO_2 emissions in counties and the locations, populations, and economic activity of the counties at very fine geographic scale. We explore the 9.4.1 indicator at both the state and county scales in the U.S. for the period 2010 to 2015. These county-level data reveal large heterogeneity with adjacent counties often exhibiting very different trends in CO_2/GDP and states also showing diverse patterns of change. Although CO_2 emissions were decreasing as GDP increased over this interval in the U.S. as a whole, the same was true in only four-fifths of its states and in only around one-third of its counties. There were many counties in which CO_2 increased as GDP declined, or in other combinations of the two variables. Decoupling of CO_2 emissions and economic growth was most apparent in counties with a large fraction of their emissions coming from electricity generation while decoupling was less common in counties with large emissions from the industrial sector.

Keywords: decoupling; CO_2/GDP; U.S. county data; SDG indicator 9.4.1.

Classification: LCC Code: HC110.E5

Language: English

Great Britain
Journals Press

LJP Copyright ID: 925641
Print ISSN: 2631-8490
Online ISSN: 2631-8504

London Journal of Research in Science: Natural & Formal

Volume 25 | Issue 4 | Compilation 1.0

Coupling of CO_2 Emissions and Economic Growth Across the U.S. Between 2010 and 2015

Andrew Bagwell[α], Jeffrey Colby[σ], Caity Duncan[ρ], Caroline Fehlman[Ѡ], Nicholas Gastelle[§], Dennis Gilfillan[χ] and Gregg Marland[ν*]

ABSTRACT

To mitigate climate change it will be necessary to reduce greenhouse gas emissions and this transition is likely to involve an impact on economic output. We adopt the U.N. sustainable development indicator 9.4.1, CO_2 emissions per unit of value added, to explore the change over time of the value of economic output as CO_2 emissions change. CO_2/GDP is most often studied at the national level, but data are available for the 2010-2015 time period to estimate CO_2 emissions at the county level in the U.S. Available gridded data allow us to calculate emissions by county for 10 economic sectors, and thus to examine the relationship between CO_2 emissions in counties and the locations, populations, and economic activity of the counties at very fine geographic scale. We explore the 9.4.1 indicator at both the state and county scales in the U.S. for the period 2010 to 2015. These county-level data reveal large heterogeneity with adjacent counties often exhibiting very different trends in CO_2/GDP and states also showing diverse patterns of change. Although CO_2 emissions were decreasing as GDP increased over this interval in the U.S. as a whole, the same was true in only four-fifths of its states and in only around one-third of its counties. There were many counties in which CO_2 increased as GDP declined, or in other combinations of the two variables. Decoupling of CO_2 emissions and economic growth was most apparent in counties with a large fraction of their emissions coming from electricity generation while decoupling was less common in counties with large emissions from the industrial sector. Counties from large urban concentrations were more likely to be decoupling of CO_2 and GDP. The spatial heterogeneity at the county level suggests the variety and challenges in motivating the decoupling of emissions from economic growth. Understanding the relationship between CO_2 and GDP provides insight for future analyses on where to focus efforts to mitigate CO_2 emissions and on how to reduce emissions in ways that are sensitive to issues of equity and efficiency.

Keywords: decoupling; CO_2/GDP; U.S. county data; SDG indicator 9.4.1.

Authors α σ ρ Ѡ §: Department of Geography and Planning, Appalachian State University, Boone NC, USA;
χ: North Carolina School of Science and Mathematics, Morganton NC, USA;
ν: Research Institute for Environment, Energy and Economics, Appalachian State University, Boone NC, USA;

I. INTRODUCTION

Mitigating global climate change through reduction of greenhouse gas emissions is a challenge of increasing urgency. It is a particular challenge because of the current fundamental interdependence of greenhouse gas emissions with economic production and human development. The primary cause of anthropogenic global climate change is the emission of greenhouse gases (GHGs), most importantly carbon dioxide (CO_2) from fossil-fuel combustion and other industrial processes [1]. A decoupling of CO_2 emissions and the economy, as represented by the Gross Domestic Product (GDP), needs to occur to achieve the global aspirations of combating climate change [e.g., 1, 2, 3]. However, as Haberl et al. [4] note, shifting to renewable energy while sustaining current rates of economic growth may not solve the problem, and "meeting the goals of the Paris Agreement will require new and more effective policies than those deployed so far."

Reducing greenhouse gas emissions and achieving a low carbon economy will likely involve a reorganization of the patterns and scales of human activity. CO_2 emissions per unit of value added (CO_2/GDP) provides a simple measure to explore this transition. Exploring this measure of decoupling emissions across time and space can provide insights to help guide understanding and decision-making.

While combating climate change has been a global priority for decades, progress on international and national public policy has moved slowly. This has driven subnational actors (such as cities, counties, and provinces), as well as non-state actors (such as corporations and non-government organizations) to enact their own policies to reduce their carbon footprints [e.g., 5, 6]. It is apparent that relevant and important decision-making occurs at multiple scales. It is also apparent that current broad differences, including inequities between and within countries, provide different incentives and opportunities for improvement among different demographics. Although CO_2/GDP has been mostly explored at the national level, there is a need to consider subnational variability to understand both national and within-country dynamics of the goals and their pursuit. National indicators may mask strong subnational differences, differences that may be meaningful in several ways - such as understanding the spatial disaggregation of national economies or identifying local challenges, 'successes,' 'failures,' inequities, and/or motivations. There is much insight to be gained by examining the sub-national scale. The linkage of CO_2 emissions and GDP, and their evolution over time at a sub-national scale, should begin to reveal important elements of difference, including equity and social justice.

Products and data are now available to leverage multi-scale earth observations to evaluate indicators such as CO_2/GDP at the national level, but additional tools are needed at the subnational scale to inform regional and local decision makers. This paper explores the subnational distribution of decoupling greenhouse gas emissions in the United States (U.S.) over the period 2010 to 2015. We focus on the U.S. due to the availability of multiple-scale data on CO_2 emissions and GDP. The period 2010 to 2015 is admittedly a short period and yet it provides an opportunity to examine the subnational character of changing directions in CO_2 and GDP. Using the CO_2/GDP indicator we identify eight potential patterns of change over time (which we call cases) and investigate where each case was observed. Insights are provided on the sources of CO_2 emissions and changes in GDP for areas experiencing each case. In section 2 we discuss how we derive our cases, our sources of data, and some key issues of data processing. In section 3 we describe the variability in decoupling at the state and county scales. Section 4 discusses some factors related to this variability and section 5 draws some brief conclusions.

II. MATERIALS AND METHODS

2.1. Decoupling GHG emissions and economic growth - CO_2/GDP

Considering CO_2/GDP as a function of time we can explore changes in the ratio of two related functions, $CO_2(t)$ and GDP(t):

$$\frac{CO_2(t)}{GDP(t)} = CO_2(t) \times GDP(t)^{-1} \tag{1}$$

Defining the proportional growth of each quantity $X(t)$ as $r(X) = \frac{1}{X}\frac{dX}{dt}$ with units of $[\text{time}]^{-1}$, the counterpart for Eq. 1 for proportional growth rates is

$$r(CO_2/GDP) = r\left(CO_2\right) - r(GDP) \tag{2}$$

This allows us to categorize changes of CO_2/GDP into eight specific cases (see Table 1 and Figure 1). These 8 cases are defined by the rate and direction of change for $r\left(CO_2\right)$, $r(GDP)$, and $r\left(CO_2/GDP\right)$; $where\ r(CO_2/GDP)$ is defined by the directions and relative magnitudes of $r\left(CO_2\right)$ and $r(GDP)$. Ideally CO_2/GDP decreases over time - i.e. there is a decrease in the amount of CO_2 emissions per unit of economic output. This may or may not involve continuing economic growth.

The Organization for Economic Co-operation and Development [8] defines decoupling as "breaking the link between 'environmental bads' and 'economic goods'," specifically when "the growth rate of an environmental pressure is less than that of its economic driving force (e.g., GDP) over a given period." Thus, when CO_2/GDP is decreasing, decoupling is occurring (cases 1, 2, and 4 below). Haberl et al. [4] further distinguish between absolute and relative decoupling: "GDP growth coinciding with absolute reductions in emissions or resource use is denoted as 'absolute decoupling' as opposed to 'relative decoupling', where resource use or emissions increase less so than does GDP." By focusing on CO_2/GDP we identify a fourth case of decoupling, case 7, where both CO_2 emissions and GDP are decreasing, but emissions are decreasing faster. Cases 3, 5, 6, and 8 are then classified as "not decoupling" as they are not seeing a decrease in the ratio of CO_2 to GDP over time. Shan et al. [9] have used a similar analysis to examine decoupling of CO_2 emissions and GDP for cities in China. The IPCC [1] similarly distinguishes between absolute and relative decoupling. Our cases 1, 2, 4, and 7 all have negative values of CO_2/GDP, and all qualify as decoupling, but the distinctions in terms of the relative values for the changes in CO_2 and GDP are important and we carry forward the distinctions. Likewise, cases 3, 5, 6, and 8 all qualify as not decoupling but we preserve the important distinctions.

Table 1 and Figure 1 show that there are multiple paths to decreasing CO_2/GDP. Absolute decoupling occurs when CO_2 emissions decrease while GDP increases, cases 1 & 2. Relative decoupling occurs in other cases where the change in CO_2/GDP is negative (i.e. more GDP per unit of CO_2), in case 4, where CO_2 emissions are still increasing but at a decreasing rate with respect to GDP, and in case 7 where the economy is in decline, but CO_2 emissions are declining faster than GDP. Not decoupling likewise occurs in several combinations. In case 3 the economy is growing, but at the cost of increasing CO_2 emissions. Cases 5 and 6 are in economic decline despite increasing CO_2 emissions. Finally, in case 8, both GDP and CO_2 emissions are declining but GDP is declining faster so that the change in CO_2/GDP is positive and decoupling is not occurring. Table 1 provides a vocabulary to characterize and discuss the eight cases.

Table 1: The direction and relative magnitude of changes in CO_2 emissions and GDP define eight cases for the pattern of changes in CO_2/GDP. The last column defines the vocabulary for discussing the eight cases in this paper. See also Figure 1.

Case	r(CO_2)	r(GDP)	r(CO_2/GDP)	Dominant rate	CO_2-GDP relationship
1	-	+	-	r(CO_2)	Absolute Decoupling with steep CO_2 decline
2	-	+	-	r(GDP)	Absolute Decoupling with gentle CO_2 decline
3	+	+	+	r(CO_2)	Not Decoupling with CO_2 growing

4	+	+	-	r(GDP)	Relative Decoupling with CO_2 growing
5	+	-	+	r(CO_2)	Not Decoupling with gentle GDP decline
6	+	-	+	r(GDP)	Not Decoupling with steep GDP decline
7	-	-	-	r(CO_2)	Relative Decoupling with CO_2 declining
8	-	-	+	r(GDP)	Not Decoupling with CO_2 declining

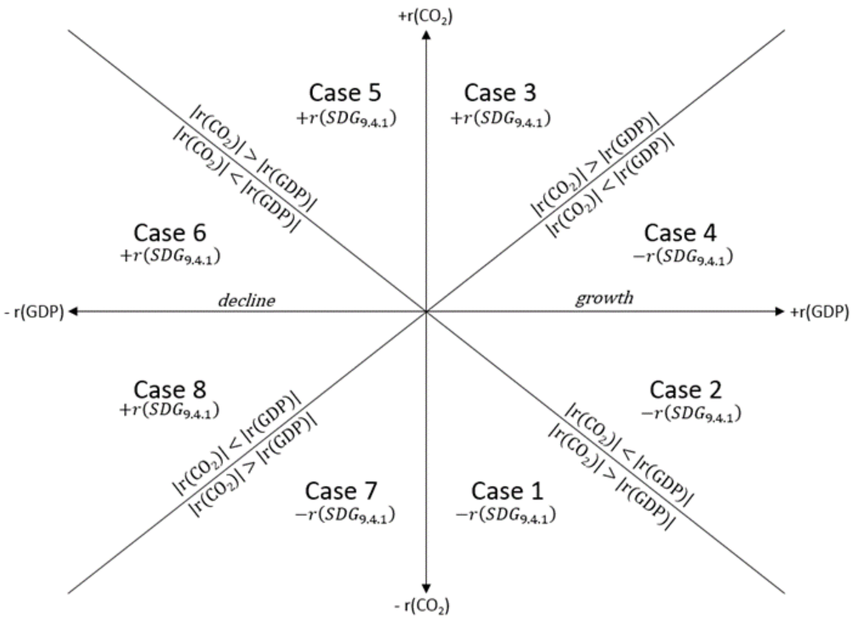

Figure 1: A Cartesian diagram of the eight cases defined in Table 1, where the x-axis is the change in GDP, r(GDP), and the y-axis is the change in CO_2 emissions r(CO_2). The diagonal lines separate whether r(GDP) or r(CO_2) has the greater proportional rate of change (the 'dominant' rate). See also Table 1.

2.2. Data on CO_2 emissions

Data are available on national-level CO_2 emissions from multiple sources. For example, the CDIAC-FF estimates of CO_2 emissions from fossil fuel combustion and cement manufacture provide annual, global measures of anthropogenic CO_2 from all countries for the time period 1751-2020 [10]. Other datasets also provide recent national-level estimates, but with slightly different boundaries of what is or is not included. Datasets may, for example, not include emissions from cement manufacture [11] or may include additional industrial sources of CO_2 [12]. With different system boundaries possible it is important that comparisons across countries or across time use consistent system boundaries for the accounting.

For our analyses at the level of U.S. states we use CO_2 emissions estimates from the U.S. Energy Information Administration for the years 2010-2015 [11]. The EIA obtains emissions estimates based on fuel type (coal, natural gas, petroleum) and does not include emissions from cement manufacture. We have adjusted the state data to account for the difference of the total sum of emissions from all states and the national estimate. The CO_2 emissions estimates are from direct fuel use from all sectors (residential, commercial, industrial, and transportation). The U.S. does not provide uncertainty values for the state-level emissions data, but it is generally expected to be comparable to or slightly larger than the uncertainty of the national estimates which is reported at -2 to +4 %.

To estimate county-level CO_2 emissions, we aggregated data from the Vulcan version 3.0 dataset [13], which provides 1 km x 1 km hourly CO_2 emissions estimates for the United States for the years 2010-2015. Emissions are categorized into ten source sectors and allow us to examine sectoral details to better understand the heterogeneous patterns at the county level: residential, commercial, industrial, electricity production, on-road, non-road, commercial marine vessel, airport, rail, and cement manufacture. For the benefit of graphic display, we have focused on the contiguous U.S. states. The critical Vulcan data that allow construction of CO_2 emissions estimates at the county level are only available for the 2010-2015 interval. The Vulcan estimates of emissions are based on multiple data sources, each with its own uncertainty, so uncertainty at the county level will vary with the mix of emission sources, and uncertainty at the national level is estimated at +/- 8% (13). The state-level Vulcan data are compared to sector and fuel-specific data in the EIA datasets, and the county-level CO_2 emissions data are believed to be sufficiently certain to support meaningful conclusions.

We utilize different CO_2 datasets at different scales to emphasize exploring the construct validity of CO_2/GDP and its eight cases as a useful tool over conserving the numerical consistency across spatial scales. We thus make use of the high accuracy of EIA data at the state level, as well as the analytic freedom afforded by the detailed, sectoral Vulcan data for the county level. Emissions from cement manufacture (which constitute less than 1% of U.S. emissions) are thus not included in the state data. While this affects the numerical values of CO_2/GDP, it has a negligible effect on our area of interest - patterns and trends.

2.3. Data on Economic Output (GDP)

For the U.S., the Department of Commerce, Bureau of Economic Analysis (BEA) [14] maintains data on GDP at the state and county levels. An advantage of confining this analysis to the U.S. is the detailed, multi-scale, spatially-explicit data available on GDP and hence the avoidance of having to derive estimates from national or regional data or assumptions on per capita values.

2.4. Methods and Data Processing

Our county level analysis combined Vulcan 3.0 CO_2 emissions data with county-level GDP data from the BEA. Because Vulcan 3.0 quantifies CO_2 emissions at a resolution of 1 km x 1 km per 1 hour, analysis within a geographic information system was used to convert the data to the county and annual level. The complete Vulcan 3.0 dataset was downloaded from the Oak Ridge National Laboratory Data Archive Center. A county boundary shapefile was acquired from the 2019 U.S. Census Bureau TIGER/Line County data file [15]. Both the Vulcan raster files and U.S. County shapefile were imported into Esri's ArcGIS Pro [16]. The projection of the U.S. County boundaries shapefile was reprojected to the Lambert Conformal Conic 2SP to match the Vulcan 3.0 georeferencing system. Using the Spatial Analyst tool Zonal Statistics as Table [17], the CO_2 emissions estimates were calculated and summarized within the county boundaries provided by the U.S. County boundaries shapefile and reported as a table. Each table contains 3108 records, the total number of counties and county equivalents in the conterminous United States (including 38 independent cities in Virginia). This process was repeated for each of the 6 Vulcan years, as well as for each economic sector.

A table was also created in R for the CO_2/GDP rates of change for both states and counties. This table derived the proportional growth rates for CO_2, GDP, and CO_2/GDP with units of inverse years. This was implemented in the code by taking the log of the ratio between values for 2010 and 2015 for CO_2 emissions and for GDP, which was then divided by five, the time span between the two years. For calculating the CO_2/GDP rates, the difference between the emissions rate and GDP rate was calculated as shown in Equation 2. The output was used to identify which case each state or county belonged in, based on the criteria in Table 1. The absolute and relative rates of change were calculated for the state and county level CO_2/GDP values. The relative change was determined by taking the 2015 value and dividing it by the 2010 value. The absolute change was calculated by taking the difference between the 2010 and 2015 values.

In this analysis the contiguous U.S. was taken to include 3080 counties and county equivalents, including ten of the independent Virginia cities that are not legally included in the counties in which they are geographically embedded (Alexandria, Chesapeake, Hampton, Newport, Norfolk, Portsmouth, Richmond, Roanoke, Suffolk, and Virginia Beach). All 28 of the other independent Virginia cities were processed with the appropriate counties. The District of Columbia was treated as a state comprised of one county.

III. RESULTS

3.1. Decoupling CO_2 emissions and economic growth: changes in CO_2/GDP in the United States at the state level

While CO_2/GDP is often reported as a national aggregate, we focus on the substantial differences found at the state and at the county level in the United States [see also 18]. To track changes over time we focus on the period 2010-2015 as this time interval is supported with the high-resolution VULCAN 3.0 CO_2 emissions dataset [13].

Although the majority of U.S. states (including the District of Columbia, which is absolute decoupling with steep CO_2 decline (case 1), have shown absolute decoupling of greenhouse gas emissions and GDP (cases 1 and 2), with decreasing CO_2 and increasing GDP (Figure 2 and Table 2), there were 8 states with increasing CO_2 emissions over the 2010 to 2015 period. Delaware had the fastest rate of growth in both CO_2 emissions and CO_2/GDP. Four states (Louisiana, Connecticut, Mississippi, and Alaska) had decreasing GDP during this time period. The cases of not decoupling with CO_2 declining (case 8) and not decoupling with steep GDP decline (case 5) were not observed at the state level and only in Connecticut did CO_2 emissions increase while GDP decreased (case 6).

Georgia showed the fastest rate of increasing GDP and the fastest rate of decreasing CO_2/GDP. States decoupling with steep CO_2 decline were the source of an increased fraction of U.S. total CO_2 emissions despite their decreases in absolute total emissions. Almost 80% of U.S. emissions came from states with increasing GDP and declining CO_2 emissions (cases 1 and 2).

Table 2: The 50 U.S. states and the District of Columbia are classified according to the eight cases described in Figure 1 and Table 1, and for each case the total of CO_2 emissions as a fraction of U.S. total emissions for the relevant states is shown for 2010 and 2015. CO_2 data are from the U.S. EIA [11] and GDP data are from the U.S. Bureau of Economic Analysis [14].

CO_2/GDP	Number of states	Portion of 2010 U.S. CO_2 emissions (%)	Portion of 2015 U.S. CO_2 emissions (%)
Absolute Decoupling with steep CO_2 decline (case 1)	22	37.6	40.2
Absolute Decoupling with gentle CO_2 decline (case 2)	18	38.0	37.3
Not Decoupling with CO_2 growing (case 3)	3	0.7	0.6
Relative Decoupling with CO_2 growing (case 4)	4	17	15.2
Not Decoupling with gentle GDP decline (case 5)	0	0	0
Not Decoupling with steep GDP decline (case 6)	1	0.7	0.7
Relative Decoupling with CO_2 declining (case 7)	3	6.0	6.1
Not Decoupling with CO_2 declining (case 8)	0	0	0

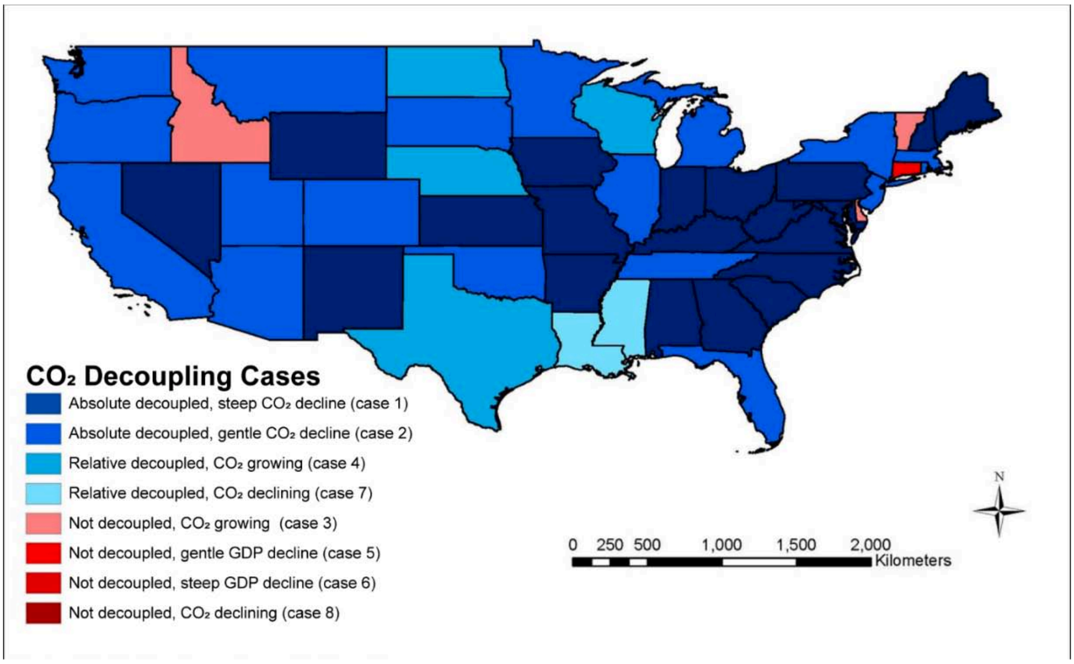

Figure 2: State level mapping of the different cases of CO_2/GDP for the contiguous U.S. states and the District of Columbia. Each state is indicated according to the 8 cases identified for the period 2010 to 2015. Not shown: Alaska is relative decoupling with CO_2 declining (case 7), Hawaii is absolute decoupling with gentle CO_2 decline (case 2), and the District of Columbia is absolute decoupling with steep CO_2 decline (case 1). Cases 1, 2, 4 and 7 (blue) had decreasing CO_2/GDP while cases 3, 5, 6, and 8 (red) had increasing CO_2/GDP. CO_2 data are from the U.S. EIA [11] and GDP data are from the U.S. Bureau of Economic Analysis [14].

3.1. Decoupling CO_2 emissions and economic growth: changes of CO_2/GDP in the United States at the county level

At the county level the spatial distribution of CO_2/GDP cases was complex, with all 8 identified cases represented for the period 2010 to 2015. Approximately one-third of counties in the contiguous United States had growing economies with absolute decoupling of CO_2 emissions and GDP (cases 1 and 2, see Table 3) - whereas almost 80% of the U.S. states exhibited this absolute decoupling (Table 2). Counties with relative decoupling (cases 4 and 7) comprised another one-third of counties and counties not decoupling (cases 3, 5, 6, and 8) comprised the final one-third of counties. Approximately 14% of counties had CO_2 emissions rising despite a declining economy (cases 5 and 6). While 84% of the contiguous states had declining CO_2 emissions, only 53% of the counties did. This shows that national and state-level decreases in CO_2 emissions masked widespread local increases (47% of all counties). Those counties with declining CO_2 emissions (cases 1, 2, 7, and 8) represented 65.8% of emissions from the contiguous U.S. in 2010, and 59.3% in 2015. The counties with decreasing emissions had a gross decrease in emissions of 162.4 Mt CO_2 between 2010 and 2015. The cases with increasing emissions represented a gross increase of 69.3 Mt C, leading to a net decrease of 93.1 Mt C in the contiguous United States.

Table 3: The contiguous U.S. includes 3080 counties and county equivalents, with representatives of all 8 cases for the changes in CO_2/GDP from 2010 to 2015 described in Table 1 and Figure 1. The portions of CO_2 emissions for the contiguous U.S. are shown for 2010 and 2015. The District of Columbia is treated as a state comprised of a single county. CO_2 data are from Gurney et al., [13], and GDP data are from the U.S. Bureau of Economic Analysis [14].

Case	Number of counties	Percent of 2010 CO_2 emissions	Percent of 2015 CO_2 emissions
Absolute Decoupling with steep CO_2 decline (case 1)	316	23.1	19.9
Absolute Decoupling with gentle CO_2 decline (case 2)	708	21.1	21.5
Not Decoupling with CO_2 growing (case 3)	326	8.7	11.8
Relative Decoupling with CO_2 growing (case 4)	674	20.4	22.8
Not Decoupling with gentle GDP decline (case 5)	177	2.5	3.3
Not Decoupling with steep GDP decline (case 6)	254	2.6	2.8
Relative Decoupling with CO_2 declining (case 7)	301	16.5	12.8
Not Decoupling with CO_2 declining (case 8)	324	5.1	5.1

The geographic distribution of the cases at the county level is presented in Figure 3. At this scale all 8 cases appeared broadly across the country. Recognizing that we use different sources for estimates of CO_2 emissions data at the state and county levels, it appears that even for states that were characterized as undergoing absolute decoupling with growing economies, such as Iowa, North Carolina, and West Virginia, each of the 8 cases appeared for counties within them. Texas (relative decoupling with CO_2 growing - case 4) and Mississippi (relative decoupling with CO_2 declining - case 7) also included counties with all 8 cases. Even though there was only one state with growing CO_2 emissions despite decreasing GDP (cases 5 and 6) (Connecticut), there were over 430 counties nationally with these changes. In some states, a small number of counties with large economies dominated the state-level trend, such as in Chittenden County in Vermont and New Castle County in Delaware, both of which were not decoupling, growing economies (case 3).

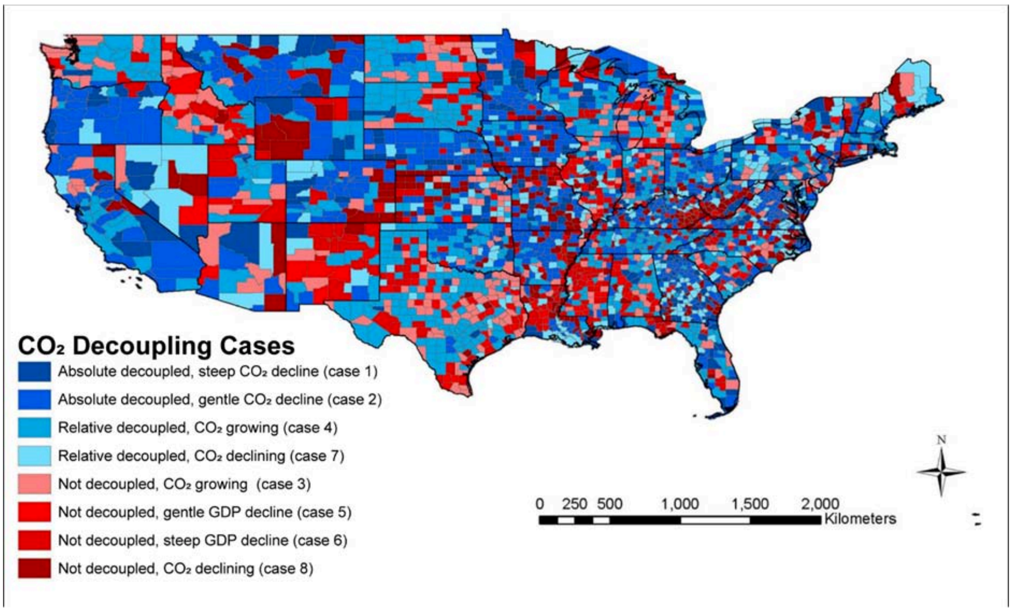

Figure 3: County level mapping of the different cases of CO_2 decoupling for the contiguous U.S. states and the District of Columbia. Each county is indicated according to the 8 cases identified for the trend in CO_2/GDP for the period 2010 to 2015. Cases 1, 2, 4 and 7 (blue) had decreasing values for CO_2/GDP while cases 3, 5, 6, and 8 (red) had increasing values for CO_2/GDP. CO_2 data are from Gurney et al [13] and GDP data are from the U.S. Bureau of Economic Analysis [14].

Table 4 summarizes the cases in terms of average values and relative annual changes in CO_2 emissions. For the time period 2010 to 2015 counties characterized as not decoupling with CO_2 growing and not decoupling with gentle GDP decline (cases 3 and 5) showed, on average, the largest relative increases in emissions, at 4.49 and 3.28 %/year respectively. Counties with relative decoupling with CO_2 declining (case 7) had the largest relative decreases in emissions, at 4.94 %/year, followed by counties with absolute decoupling and steep CO_2 decline (case 1), at 3.92 %/year. Counties from cases 1 and 7 were also the counties with the largest absolute values for average CO_2 emissions. With both of these classes of counties decoupling, this suggests that decoupling in the U.S. as a whole was being driven in significant measure by reducing the emissions from high-emitting counties.

Table 4: Average values for CO_2 emissions and average annual rate of change in CO_2 emissions for all counties in each of the 8 cases. The time interval represented is 2010-2015. Primary data are from Gurney et al. [13].

Case	Average total CO_2 Emissions (kt C per county in 2015)	Annual relative change in CO_2 emissions (% C emissions per county per year)
Absolute Decoupling with steep CO_2 decline (case 1)	963	-3.92
Absolute Decoupling with gentle CO_2 decline (case 2)	465	-0.751
Not Decoupling with CO_2 growing (case 3)	556	4.49
Relative Decoupling with CO_2 growing (case 4)	518	1.08
Not Decoupling with gentle GDP decline (case 5)	285	3.28
Not Decoupling with steep GDP decline (case 6)	170	0.910
Relative Decoupling with CO_2 declining (case 7)	652	-4.94
Not Decoupling with CO_2 declining (case 8)	241	-0.793

IV. DISCUSSION

Having observed the subnational variation in changes of CO_2/GDP, we explore some of the characteristics of the eight different cases identified. We suggest that understanding the causes of subnational variability in decoupling of CO_2 emissions and economic growth is important to understanding our ability to achieve sustainability at a global level. We make a first attempt at exploring this in the U.S. by looking at decoupling at the county level and some of characteristics of the different cases of decoupling, including the sources of emissions by economic sector, the rural-urban continuum, and the concentration of population.

4.1. CO_2 Emissions at the county level by economic sector

Figure 4 shows the average magnitude of CO_2 emissions from each economic sector for 2010 and 2015, for each of the eight cases of decoupling. Table 5 shows the average emissions change in each sector for each case as a percent and as total megatons of C (MtC). Together Figure 4 and Table 5 show, for example, that for the set of counties with absolute decoupling with steep CO_2 decline (case 1), on average, electrical production was the dominant source of emissions (with over 50 % of the total in both 2010 and 2015) and that emissions from electrical production declined by 28% from 2010 to 2015. Similarly, in the set of counties with absolute decoupling with gentle CO_2 decline (case 2), on average, on-road emissions were the largest contribution, contributing 35% of emissions in each year while declining by 1.1% from 2010 to 2015. On-road emissions increased in counties with relative decoupling with CO_2 growing and in counties not decoupling with CO_2 growing (cases 3 and 4). Whether electricity production or on-road emissions was the dominant contribution to emissions has generally defined whether r(GDP) or r(CO_2) was the dominant factor in the 2010-2015 change in CO_2/GDP.

Overall, the sector contributing the most to decreases in CO_2 emissions was electricity generation, with a total reduction of 91.9 Mt C from 2010 to 2015. Commercial marine vessels (cmv) were a distant second with a total 10.1 Mt C decrease, however cmv had by far the largest percent change, at -40% from 2010-2015, with rail the second largest percent change at +24%. CO_2 emissions from electricity production, while experiencing the greatest decreasing change, remained the largest source of emissions. The second largest source of emissions, on-road, saw relatively little change from 2010 to 2015. In cases where $r\left(CO_2\right)$ was the principal driver of change (cases 1, 3, 5, and 7), whether decoupling or not, electricity production was the largest source of emissions. Where on-road emissions were the dominant source, r(CO_2) was not the dominant factor in changing CO_2/GDP. In cases where on-road emissions were the dominant source of emissions, GDP was the principal factor in the evolution of CO_2/GDP (cases 2, 4, and 6). The exception was where there was not decoupling despite declining CO_2 (case 8), where electricity production was the major source of emissions but GDP was the dominant factor in driving the change in CO_2/GDP (case 8). Almost by definition, most of the CO_2 emission reductions occurred in counties with absolute decoupling with steep CO_2 decline or with relative decoupling with CO_2 declining (cases 1 and 7).

Airport, commercial, and rail-related CO_2 emissions went up, on average, in all cases (with a few exceptions), and residential emissions went down in all cases, which suggests that changes in these sectors are occurring nationwide irrespective of local trajectories in decoupling. The largest increases in emissions were from the commercial sector - notably in three of the four cases with increasing GDP (cases 2, 3 and 4) - although the only case with negative values for the commercial sector was for counties with absolute decoupling with steep CO_2 decline (case 1). Industrial sector emissions increased in counties not decoupling with CO_2 growing and relative decoupling with CO_2 growing (cases 3 and 4) counties while decreasing notably in counties with absolute decoupling with steep CO_2 decline and relative decoupling with CO_2 declining (cases 1 and 7). Industrial sector emissions increased by smaller amounts in case 5 and 6 counties while decreasing in case 2 and 8 counties. The industrial sector is perceived as hard to decarbonize and the energy mix has remained relatively unchanged (see [19] and [1]).

In sum, the set of counties with increasing total emissions of CO_2 from 2010 to 2015, on average, (cases 3, 4, 5, and 6) had increases from both the electric power and industrial sectors while the set of counties with decreasing total emissions (cases 1, 2, 7, and 8) had, on average, decreases from both the electric power and industrial sectors. Note that some of the decrease in CO_2 emissions per unit of electricity generated was offset by increases in total electrical production, especially in case 3 counties (not decoupling with CO_2 growing). However, change in electrical production was still the driving factor in transitioning toward a lower carbon economy [20]. Electricity generation highlights the linkages among counties. Although the CO_2 emissions from the generation will be accounted in one county the product power can be employed in nearby counties. The same is true for emissions from industrial facilities in that the products can be widely employed outside of where the emissions occur. What is being observed now is the availability of technologies to produce electricity with lower CO_2 emissions.

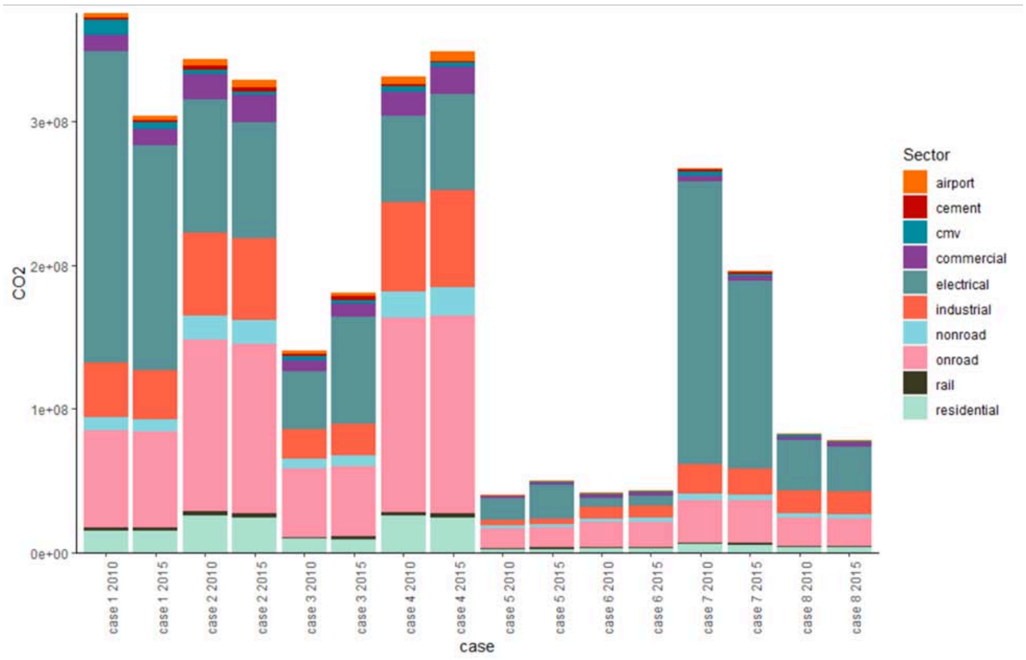

Figure 4: Average CO2 emissions by economic sector, in 2010 and 2015, for the set of counties in each of the identified cases for trend in CO_2 decoupling. Commercial marine vessels are indicated as cmv. Quantities are presented in tons of carbon contained in emitted CO_2, where 3.667 tons of CO_2 contain one ton of carbon. CO_2 data are calculated from Gurney et al. [13].

Table 5: Average change in the percentage and in the magnitude of CO_2 emissions (in megatons carbon) by case and sector for U.S. counties from 2010 to 2015. Summing across the table rows of the total of emissions does not always agree due to rounding. Columns indicate whether decoupling was taking place. CMV is commercial marine vehicles.

Sector	Decoupling (Case 1)	Decoupling (Case 2)	Not (Case 3)	Decoupling (Case 4)	Not (Case 5)	Not (Case 6)	Decoupling (Case 7)	Not (Case 8)	Total
Airport	<1% (0.006)	6% (0.3)	19% (0.4)	14% (0.8)	37% (0.2)	35% (0.2)	4% (0.05)	10% (0.06)	11% (2.0)
Cement	-16% (-0.3)	5% (0.1)	32% (0.7)	-16% (-0.2)	72% (0.3)	-24% (-0.1)	-18% (-0.2)	-43% (-0.007)	3% (0.3)
CMV	-57% (-6.0)	-30% (-1.1)	6% (0.1)	-25% (-0.1)	25% (0.07)	-37% (-0.3)	-52% (-1.8)	-34% (-0.5)	-40% (-10.4)

Commercial	-<1% (-0.06)	9% (1.5)	16% (1.3)	11% (1.9)	9% (0.1)	12% (0.2)	7% (0.2)	9% (0.2)	9% (5.4)
Electrical	-28% (-60)	-13% (-12.1)	86% (34.1)	12% (7.1)	54% (8.2)	14% (0.9)	-34% (-66.7)	-10% (-3.5)	-14% (-91.9)
Industrial	-10% (-3.7)	-<1% (-0.4)	10% (2.0)	9% (5.9)	9% (0.3)	4% (0.3)	-12% (-2.5)	-3% (-0.4)	<1% (1.4)
Non-road	-<1% (-0.8)	-1% (0.2)	4% (0.3)	4% (0.7)	6% (0.1)	3% (0.08)	-<1% (-0.004)	-1% (-0.004)	1% (0.9)
On-road	-2% (-1.1)	-1% (-1.6)	2% (0.9)	2% (2.6)	3% (0.4)	<1% (0.1)	-2% (-0.5)	-2% (-0.4)	<1% (0.3)
Rail	15% (0.3)	-1% (-0.004)	54% (0.8)	23% (0.6)	82% (0.5)	40% (0.3)	29% (0.3)	14% (0.1)	24% (2.8)
Residential	-2% (-0.3)	-5% (-1.3)	–2% (-0.2)	-5% (-1.3)	-5% (-0.1)	-7% (-0.2)	-6% (-0.3)	-4% (-0.2)	-4% (-4.0)
Total	-20% (-71.4)	-4% (-14.8)	29% (40.5)	5% (10.0)	25% (10.1)	4% (1.6)	-27% (-71.4)	-6% (-4.8)	-6% (-93.1)

4.2 The rural-urban character of counties for the eight cases of CO_2 decoupling

A striking observation of the analysis displayed in Figure 3 is the spatial heterogeneity in the pattern of changes in CO_2 decoupling over time. The eight cases for change in CO_2/GDP were all widely observed and the various cases were observed within a single state and among adjacent counties. These variations reflect the spatial disaggregation of the national economy and have the potential to identify differences in economic activity, local inequities, and/or local motivations for addressing the need to decrease CO_2 emissions. The complex heterogeneity reflects intercounty transfers of electricity and of manufactured and agricultural products. It reflects differences in wealth, resources, and opportunity. Over time it will show efforts to combat climate change and how the opportunities, motivations, and cost of mitigating climate change are spatially distributed. We ask whether some of the diversity is related to urban-rural differences and the structure of urban areas.

The rural-urban character of our eight cases (Table 6) is expressed here through the Rural-Urban Continuum Codes (RUCC) of the U.S. Department of Agriculture [21] (see Endnote 1). The RUCC is a classification scheme that distinguishes counties between “metro” (metropolitan) and “non-metro” and classifies metro counties by the population size of the metropolitan area it is a part of and non-metro counties by the degree of urbanization and the adjacency to a metro area. Code 3 to code 4 marks the transition from metro to non-metro counties. The RUCC classification captures both a county’s population and the influence of adjacent metro areas, which can be important when considering local drivers of emissions and GDP. Note that the numbering of non-metro counties alternates between metro-adjacent and non-adjacent as population lowers. Like our decoupling case numbers, RUCC codes are descriptive, not indications of magnitude. RUCC 1 is a county in a metro area of over one million population, RUCC 9 is a county that is completely rural or with population under 2,500.

All eight of the CO_2/GDP cases were found in all nine rural-urban settings. All RUCC codes (except 5) had their highest frequency in CO_2/GDP cases of absolute decoupling with gentle CO_2 decline or relative decoupling with CO_2 growing (cases 2 and 4), the most commonly occurring cases. There is no obvious relationship (Table 6) between rural character and decoupling of CO_2 emissions from economic growth, although 80% of the largest urban areas (RUCC = 1) were decoupling. While there are concentrations one cannot assume, for example, that rural areas consistently exemplified a particular CO_2 per GDP relationship.

Table 6: The relationship between urban-rural character and the CO_2/GDP case for U.S. counties, shown as the number of counties in each category. Rural-urban character is according to the RUCC of the U.S. Department of Agriculture [21] (see text and Endnote 1). Columns indicate whether or not decoupling was taking place.

CO_2/GDP cases	Decoupling (case 1)	Decoupling (case 2)	Not (Case 3)	Decoupling (case 4)	Not (case 5)	Not (case 6)	Decoupling (Case 7	Not (Case 8)	sum
Rural-Urban Continuum Code									
1	61	132	38	113	11	11	33	23	422
2	47	89	47	91	15	30	28	25	372
3	43	72	47	72	17	15	45	36	347
4	27	36	30	49	17	16	28	9	212
5	9	17	18	16	6	5	11	7	89
6	58	103	72	117	43	68	68	59	588
7	40	95	29	87	26	48	47	51	423
8	15	57	19	36	18	21	17	36	219
9	16	107	26	93	24	40	24	78	408
Total	316	708	326	674	177	254	301	324	3080

4.3 County population concentration and the eight cases of CO_2 decoupling

Half of the U.S. population lived in only 146 of the 3080 counties in our study [21] (see Figure 5), meaning that trends and relative changes in CO_2/GDP do not tell the full picture when giving equal weight to every county in the contiguous U.S. The circumstances in these 146 counties do tell the circumstances under which half of the U.S. population was living. Of these 146 counties, only 8 (5%) had decreasing GDP (compared to 34% of all counties) and only 20 (14%) had increasing CO_2/GDP (compared to 35% of all counties). This suggests that large urban areas were indeed disproportionately driving decoupling in the U.S., a potentially important linkage in the relationships among urbanization, population, GDP, and CO_2 emissions.

For contrast, Figure 6 shows the CO_2 decoupling case for the 146 least populous counties. Of these counties 46 (32%) had decreasing GDP and 51 (35%) had CO_2/GDP increasing, both percentages typical of the country as a whole.

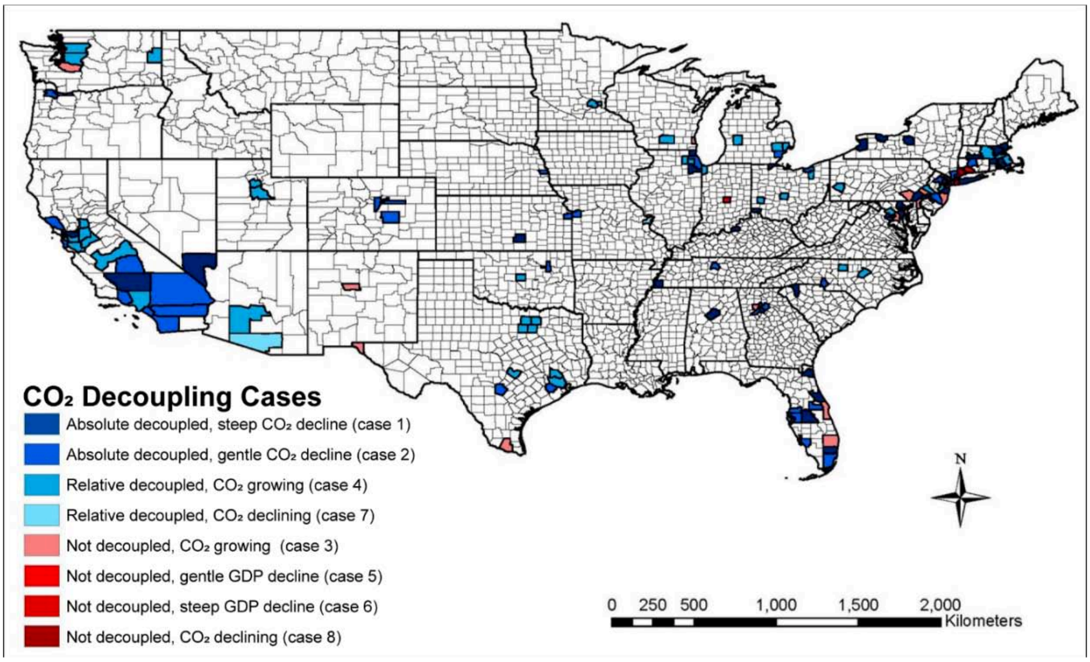

Figure 5: The CO_2/GDP case for the most populous 146 counties in the U.S. These counties collectively encompassed 50% of the U.S. population. These 146 counties represented only 4.7% of the counties included in this analysis and were all, except one, RUCC category 1. Not shown, Honolulu County in Hawaii, which is absolute decoupling with gentle CO_2 decline (case 2). CO_2 data are from Gurney et al. [13], GDP data are from the U.S. Bureau of Economic Analysis [14], and population data are from the U.S. Census Bureau [22].

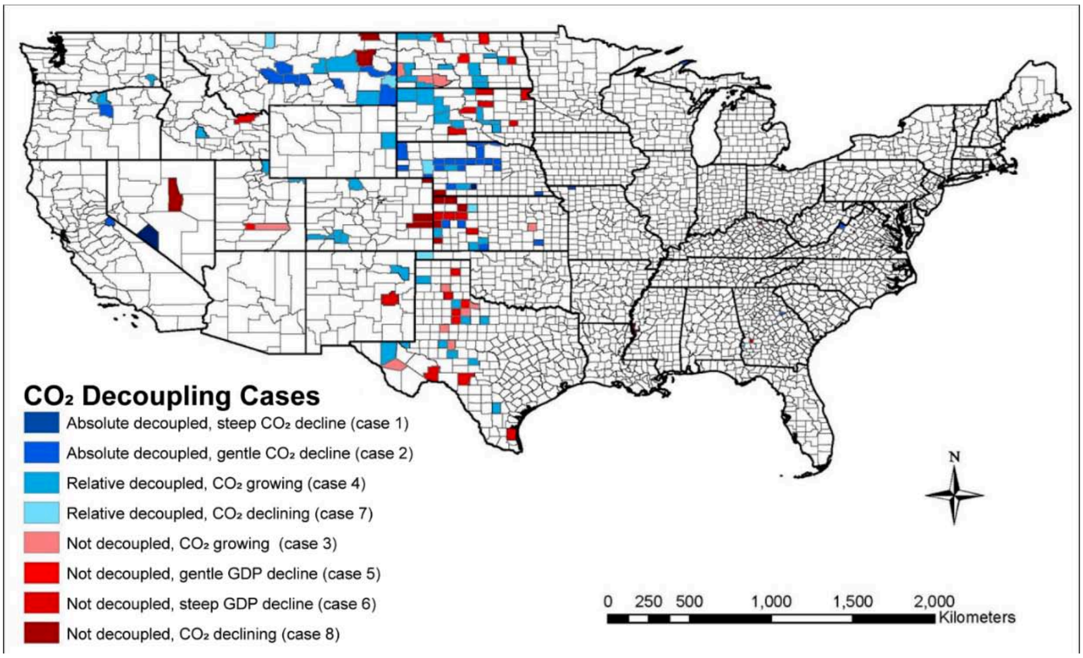

Figure 6: The CO_2/GDP case for the least populous 146 counties in the U.S. In contrast to Figure 5, these 146 counties encompass 0.08 % of the U.S. population. CO_2 data are from Gurney et al. [13], GDP data are from the U.S. Bureau of Economic Analysis [14], and population data are from the U.S. Census Bureau [22].

V. CONCLUSIONS

This study provides a context to characterize the changing relationship and broad heterogeneity in the nature of decoupling between CO_2 emissions and GDP in the United States over the years 2010 to 2015. Sustainable Development Goal Indicator 9.4.1, CO_2/GDP, was adopted by the UN [23, 24] in order to examine and monitor the decoupling of CO_2 emissions and economic development at the national level but use at the national level (which shows decoupling in the U.S.) risks missing the insights that are revealed when we examine the indicator at subnational scales. Even at the state level in the U.S. CO_2/GDP suggests homogeneity as 46 states and the District of Columbia showed decoupling of CO_2 emissions and GDP for the period 2010 to 2015. Only eight states showed increasing CO_2 emissions. To the contrary, whereas CO_2 emissions over the 2010 to 2015 interval were reduced broadly, largely from electric power generation, the decoupling of CO_2 emissions and economic development varied widely when examined at the county level. Whereas 90% of states showed decoupling of CO_2 emissions, only 65% of U.S. counties had decoupling of CO_2 emissions and GDP.

We have defined eight cases to characterize the changing relationship between the magnitude and direction of changes of CO_2 emissions and GDP and we show that all eight cases prevail in counties across the country and across the rural-urban landscape. Of 3080 counties and county equivalents in the conterminous U.S., 1024 counties showed an increase in GDP with a decrease in CO_2 emissions for the period 2010 to 2015 (absolute decoupling, our cases 1 and 2). In another 625 counties CO_2 emissions decreased but GDP decreased as well (cases 7 and 8).

Approximately one-third of U.S. counties were not decoupling emissions from economic growth over the period 2010 to 2015. The data show that decoupling CO_2 emissions from economic growth was very sector specific and dominated by the electrical generating sector. Many counties with large CO_2 contributions from electrical generation were experiencing declining CO_2 emissions with continuing economic growth (cases 1, 2, and 4). Counties with rapidly growing emissions from the electrical, industrial, and other sectors were not decoupling whether GDP was growing (case 3) or declining (case 5). Of counties with declining GDP, 431 had emissions increasing (cases 5 and 6) while 625 had emissions declining (cases 7 and 8).

On average, counties in three of our four cases of decoupling were characterized by decreasing emissions from the electricity sector. For cases with decreasing CO_2 emissions there were decreasing emissions in both the electrical and industrial sectors. If CO_2 emissions were growing there was growth in both the industrial and electrical sectors and three of the four cases of not decoupling were characterized by increasing emissions sources in both the electrical and industrial sectors. High emitting counties tended to be decoupling CO_2 emissions from economic growth and reducing emissions. But the heterogeneity was widespread. States that showed absolute decoupling of emissions from economic growth still contained counties with increasing emissions and economic decline.

The challenge going forward is to balance economic growth and CO_2 emissions. Decoupling now largely reflects changes in the electrical sector and the electrical sector provides services that extend beyond county boundaries. The needed reductions in emissions will require emissions reductions from the broader economy and carry the risk that reductions in one place are offset by increases elsewhere. The rise in electric transportation could create such a circumstance as emissions from road transport decrease in one county while emissions from electrical generation in another county are stable or increasing. Neither climate goals nor social equity are served by relocating emissions sources across counties, states, or countries.

Although we did not show a systematic relationship between CO_2 decoupling and rural/urban character, for the 124 counties that were home to half of the U.S. population CO_2/GDP was decreasing in 86%. The most striking feature of our characterization of decoupling is the heterogeneity observed at county-level spatial resolution. If a significant decrease in reliance on CO_2 emissions is to occur for the U.S. it will have to involve more geographic areas and have a greater involvement across economic sectors.

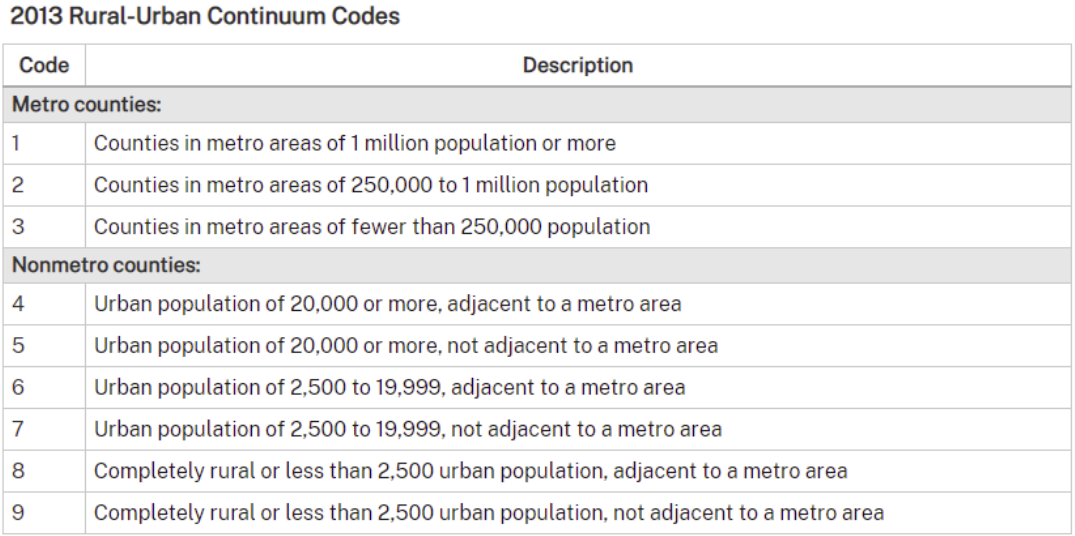

2013 Rural-Urban Continuum Codes

Code	Description
Metro counties:	
1	Counties in metro areas of 1 million population or more
2	Counties in metro areas of 250,000 to 1 million population
3	Counties in metro areas of fewer than 250,000 population
Nonmetro counties:	
4	Urban population of 20,000 or more, adjacent to a metro area
5	Urban population of 20,000 or more, not adjacent to a metro area
6	Urban population of 2,500 to 19,999, adjacent to a metro area
7	Urban population of 2,500 to 19,999, not adjacent to a metro area
8	Completely rural or less than 2,500 urban population, adjacent to a metro area
9	Completely rural or less than 2,500 urban population, not adjacent to a metro area

Endnote: Rural-Urban Continuum Codes from the U.S. Department of Agriculture [21]

Author Contributions: Conceptualization, A.B., J.C., C.D., C.F., N.G., D.G., and G.M.; methodology, A.B., J.C., C.D., C.F., N.G., D.G., and G.M.; software, A.B., C.D., C.F., and N.G.; validation, A.B., C.D., C.F., and N.G.; formal analysis, A.B., J.C., C.D., C.F., N.G., D.G., and G.M.; data curation, A.B., C.D., C.F., and N.G.; writing-original draft preparation, J.C., D.G., and G.M., writing-review and editing, A.B., J.C., C.D., C.F., N.G., D.G., and G.M.; visualization, A.B., C.D., C.F., and N.G.; project administration, J.C., D.G., and G.M. All the authors have read and agreed to the published version of the manuscript.

Funding: This research received no external funding.

Acknowledgments: We thank the Research Institute for Environment, Energy, and Economics (RIEEE) at Appalachian State University for providing funding for this research.

Conflicts of Interest: The authors declare no conflicts of interest.

REFERENCES

1. IPCC. Climate Change 2022: Mitigation of Climate Change, Working Group III Contribution to the IPCC Sixth Assessment Report, Chapter 2 Emissions Trends and Drivers, Cambridge University Press, **2022**, 216-294. https://www.ipcc.ch/report/sixth-assessment-report-working-group-3/.
2. Tapio, P. Towards a theory of decoupling: degrees of decoupling in the EU and the case of road traffic in Finland between 1970 and 2001. *Transport Policy* **2005**, 12, 137-151.
3. Wiedenhofer, D.; Virag, D.; Kalt, G.; Plank, B.; Streeck, J.; Pichler, M.; Mayer, A.; Krausmann, F.; Brockway, P.; Schaffartzik, A.; Fishman, T.; Hausknost, D.; Leon-Gruchalski, B.; Sousa, T.; Creutzig, F, Haberl, H. A systematic review of the evidence on decoupling of GDP, resource use and GHG emissions, part I: bibliometric and conceptual mapping. *Environ. Res. Lett* **2020**, 15, 1-15.
4. Haberl, H.; Wiedenhofer, D.; Virag, D.; Kalt, G.; Plank, B.; Brockway, P.; Fishman, T.; Hausknost, D.; Krausmann, F.; Leon-Gruchalski, B.; Meyer, A.; Pichler, M.; Schaffartzik, A.; Sousa, T.; Streeck,

J.; Creutzig, F. A systematic review of evidence on decoupling of GDP, resource use and GHG emissions, part II: synthesizing the insights. *Environ. Res. Lett* **2020**, 15, 1-42.

5. Hsu, A.; Moffat, A.S.; Weinfurter, A.J.; Schwartz, J.D.2015. Towards a new climate diplomacy. *Nature Climate Change* **2015**, 5, 501–503.
6. Patarasuk, R.; Gurney, K.R.; O'Keeffe, D.; Song, Y.; Huang, J.; Rao, P.; Martin, B.; Lin, J.C.; Mendoza, D.; Ehleringer, J.R. Urban high-resolution fossil fuel CO_2 emissions quantification and exploration of emission drivers for potential policy applications, *Urban Ecosystem* **2016**, 19, 1013-1039.
7. IPCC. Climate Change 2021: The Physical Science Basis. Contribution of Working Group I to the Sixth Assessment Report of the Intergovernmental Panel on Climate Change, Cambridge University Press, **2021**, 1-2409. https://www.ipcc.ch/report/ar6/wg1/
8. OECD. Organization for Economic Co-operation and Development, Indicators to Measure Decoupling of Environmental Pressure from Economic Growth, The OECD Environment Programme, **2002**. https://www.oecd.org/env/indicators-modelling-outlooks/1933638.pdf
9. Shan, Y.; Fang, S.; Cai, B.; Zhou, Y.; Li, D.; Feng, K.; Hubacek, K. Chinese cities exhibit varying degrees of decoupling of economic growth and CO_2 emissions between 2005 and 2015, *One Earth* **2021**, 4, 1-11.
10. Hefner, M. and G. Marland, 2023. Global, Regional, and National Fossil-Fuel CO2 Emissions: 1751-2020 CDIAC-FF, Research Institute for Environment, Energy, and Economics, Appalachian State University. https://rieee.appstate.edu/projects-programs/cdiac
11. U.S. Energy Information Administration, State Energy-related Carbon Dioxide Emissions Tables. Available online: https://www.eia.gov/environment/emissions/state/ (accessed on 24 January, 2024).
12. EDGAR - Emissions Database for Global Atmospheric Research. Joint Research Center, European Commission. Available online: https://edgar.jrc.ec.europa.eu/ (accessed on 24 January, 2024).
13. Gurney, K.R., Liang, J.; Patarasuk, R.; Song, Y.; Huang, J.; Roest, G. The Vulcan Version 3.0 high-resolution fossil fuel CO_2 emissions for the United States. *Journal of Geophysical Research: Atmospheres* **2020**, 125, 1-27.
14. U.S. BEA, Data by Topic, Gross Domestic Product, U.S. Department of Commerce, Bureau of Economic Analysis. Available online: https://bea.gov/data/gdp (accessed on 24 January, 2024).
15. U.S. Census Bureau, TIGER/Line Shapefiles. Available online: https://www.census.gov/geographies/mapping-files/time-series/geo/tiger-line-file.html (accessed on 24 January, 2024).
16. Esri, Resources for ArcMap. Available online: https://www.esri.com/ en-us/arcgis/products/arcgis-desktop/resources (accessed on 24 January, 2024).
17. Esri, Zonal Statistics as Table (Spatial Analyst). Available online: https://pro.arcgis.com /en/pro-app/latest/tool-reference/spatial-analyst/zonal-statistics-as-table.htm (accessed on 24 January, 2024).
18. Saha, D.; Jaeger, J. Ranking 41 US States Decoupling Emissions and GDP Growth, *World Resources Institute* 2020, 1-10. https://www.wri.org/ insights/ranking-41-us-states-decoupling-emissions-and-gdp-growth.
19. Sovacool, B.K., Geels, F.W.; Iskandarova, M. Industrial clusters for deep decarbonization. *Science* 2022, 378, 601-604.
20. U.S. EPA, 2021. U.S. Environmental Protection Agency. Inventory of U.S. Greenhouse Gas Emissions and Sinks: 1990-2019. Available online: https://www.epa.gov/ghgemissions/inventory-us-greenhouse-gas-emissions-and-sinks-1990-2019 (accessed on 24 January, 2024).
21. U.S.D.A., Rural-Urban Continuum Codes. U.S. Department of Agriculture, Economic Research Service. Available online: https://www.ers.usda.gov/data-products/rural-urban-continuum-codes.aspx (accessed on 24 January, 2024).

22. U.S. Census Bureau, County Population Totals, 2010-2020. Available online: https://www.census.gov/programs-surveys/popest/technical-documentation/research/evaluation-estimates/2020-evaluation-estimates/2010s-counties-total.html (accessed on 24 January, 2024).
23. U.N., Transforming our World: the 2030 Agenda for Sustainable Development, The United Nations, **2015**, 1-41. https://sdgs.un.org/2030agenda.
24. U.N., Report of the Inter-Agency and Expert Group on SDG Indicators E/CN.3/2016/2/Rev.1), United Nations, **2016**, 1-25. https://unstats.un.org/sdgs/iaeg-sdgs/

This page is intentionally left blank

The Radii and Densities of Elementary Particles and Periodic Table Nucleons

Ardeshir Irani

ABSTRACT

We calculate the size as the radius of a sphere, along with the density of all the elementary particles of the first column of the Standard Model of Particle Physics viz. the Up and Down quarks, the electron, the electron neutrino, the proton, the neutron, and the nuclei of all the elements and isotopes of the Periodic Table, using their known masses and the previously calculated radii (r) of the electron and the electron neutrino since $r_e/r_{\nu_e} = m_e/m_{\nu_e}$, can be extended further to calculate r_p, r_n, r_{Up}, r_{Down} and their densities, and $r_{Nucleon\ Number}$ with a Table of nucleon radii that increase and nucleon density that decrease as the number of nucleons increase. The radii of the largest size nuclei can be observed experimentally by electron microscopes as confirmation of the theoretical calculations.

Keywords: radius, density, electron, electron neutrino, proton, neutron, up quark, down quark, table of nuclear radiuses and densities.

Classification: LCC Code: QC793.5

Language: English

Great Britain
Journals Press

LJP Copyright ID: 925642
Print ISSN: 2631-8490
Online ISSN: 2631-8504

London Journal of Research in Science: Natural & Formal

Volume 25 | Issue 4 | Compilation 1.0

The Radii and Densities of Elementary Particles and Periodic Table Nucleons

Ardeshir Irani

ABSTRACT

We calculate the size as the radius of a sphere, along with the density of all the elementary particles of the first column of the Standard Model of Particle Physics viz. the Up and Down quarks, the electron, the electron neutrino, the proton, the neutron, and the nuclei of all the elements and isotopes of the Periodic Table, using their known masses and the previously calculated radii (r) of the electron and the electron neutrino since $r_e/r_{\nu_e} = m_e/m_{\nu_e}$*, can be extended further to calculate* r_p, r_n, r_{Up}, r_{Down} *and their densities, and* $r_{Nucleon\ Number}$ *with a Table of nucleon radii that increase and nucleon density that decrease as the number of nucleons increase. The radii of the largest size nuclei can be observed experimentally by electron microscopes as confirmation of the theoretical calculations.*

Keyterms: radius, density, electron, electron neutrino, proton, neutron, up quark, down quark, table of nuclear radiuses and densities.

Author: Downey Research Institute, Downey, California, USA.

I. INTRODUCTION

We consider only the elementary particles of the first column of the Standard Model of Particle Physics because the elementary particles of the second and third columns are all unstable except for the three neutrinos of all three columns that are known to change flavor. The unstable elementary particles of the second and third columns decay into the elementary particles of the first column, and that is the reason the atoms that make up the four states of matter and the elements of the Periodic Table consist of protons, neutrons, and electrons as the building blocks of the Universe. We calculate for only stable nuclei and their isotopes, not considering unstable nuclei with exceptions made either because of their abundance, longevity or importance to calculate their radii and densities.

II. RADIUS CALCULATIONS

Starting with the radius of the electron = $4.68\text{x}10^{-16}$m (Reference 1) and the radius of the electron neutrino = $2\text{x }10^{-21}$m (Reference 2) and the mass of the electron = 0.511 MeV/c^2 and the mass of the electron neutrino = 2.2 eV/c^2 from the Standard Model of Particle Physics we see that the ratio of their radii is equal to the ratio of their masses. $r_e/r_{\nu_e} = m_e/m_{\nu_e} = 4.68\text{x}10^{-16}/2\text{x}10^{-21} = 0.511\text{x}10^{6}/2.2 = 2.3\text{x } 10^{5}$. We use this equality ratio of the radius and mass to calculate the radius of the proton, the neutron, the Up and Down Quarks, and the elements of the Periodic Table.

For the Proton: $r_p/r_e = m_p/m_e$, $r_p = (938.27/0.511)\text{ x }4.68\text{x}10^{-16} = 8.593\text{x}10^{-13}\text{m } 8.59\text{x}10^{-13}\text{m}$.

For the Neutron: $r_n/r_e = m_n/m_e$, $r_n = (939.57/0.511)\text{ x }4.68\text{x}10^{-16} = 8.605\text{x}10^{-13}\text{m } 8.61\text{x}10^{-13}\text{m}$.

For the Up Quark: $r_{Up}/r_e = m_{Up}/m_e$, r_{Up} = (2.3/0.511) x $4.68\text{x}10^{-16}$ = $2.1\text{x}10^{-15}$m.

For the Down Quark: $r_{Down}/r_e = m_{Down}/m_e$, r_{Down} = (4.8/0.511) x $4.68\text{x}10^{-16}$ = $4.4\text{x}10^{-15}$m.

We change the unit of calculation from MeV/c^2 to atomic mass units (u) for convenience while calculating the sizes of the stable nuclei and their stable isotopes.

$r_{H1}/r_e = m_{H1}/m_e$, r_{H1}= (1.0078u/$5.49\text{x}10^{-4}$u) x$4.68\text{x}10^{-16}$m = $.859\text{x}10^{-12}$m. = $8.59\text{x}10^{-13}$m. The formula we use is $r_X = 8.52x10^{-13}\ m_X$ and we use the Tables of Nuclear Data (Reference 3) to determine m_X where **x** refers to the nucleon number and m_X refers to the mass of that nucleus in amu (u) to calculate the radius r_X of its nucleus in meters.

1. Hydrogen H ($r_{1,2}$) m_{H1} → $8.59\text{x}10^{-13}$m, m_{H2} → $1.72\text{x}10^{-12}$m.

Implying r_{H1} = $8.59\text{x}10^{-13}$m, r_{H2} = $1.72\text{x}10^{-12}$m, and so on for all the remaining elements that have been calculated below:

2. Helium He ($r_{3,4}$) m_{He3} → $2.57\text{x}10^{-12}$m, m_{He4} →$3.41\text{x}10^{-12}$m.
3. Lithium Li ($r_{6,7}$) m_{Li6} → $5.13\text{x}10^{-12}$m, m_{Li7} →$5.98\text{x}10^{-12}$m.
4. Beryllium Be ($r_{8,9}$) m_{Be8} → $6.82\text{x}10^{-12}$m, m_{Be9} → $7.68\text{x}10^{-12}$m.
5. Boron B ($r_{10.11}$) m_{B10} → $8.53\text{x}10^{-12}$m, m_{B11} → $9.38\text{x}10^{-12}$m.
6. Carbon C ($r_{12,13}$) m_{C12} → $1.02\text{x}10^{-11}$m, m_{C13} → $1.11\text{x}10^{-11}$m.
7. Nitrogen N ($r_{14,15}$) m_{N14} → $1.19\text{x}10^{-11}$m, m_{N15} → $1.28\text{x}10^{-11}$m.
8. Oxygen O ($r_{16.17.18}$) $m_{O16 \rightarrow}$ $1.36\text{x}10^{-11}$m, m_{O17} → $1.45\text{x}10^{-11}$m, m_{O18} → $1.53\text{x}10^{-11}$m.
9. Fluorine F (r_{19}) m_{F19} → $1.62\text{x}10^{-11}$m.
10. Neon Ne ($r_{20,21,22}$) m_{Ne20} → $1.70\text{x}10^{-11}$m, m_{Ne21} → $1.79\text{x}10^{-11}$m, m_{Ne22} → $1.87\text{x}10^{-11}$m.
11. Sodium Na (r_{23}) m_{Na23} → $1.96\text{x}10^{-11}$m.
12. Magnesium Mg ($r_{X23,25,26}$) m_{Mg24} → $2.04\text{x}10^{-11}$m, m_{Mg25} → $2.13\text{x}10^{-11}$m, m_{Mg26} → $2.21\text{x}10^{-11}$m.
13. Aluminium Al (r_{27}) m_{Al27} → $2.30\text{x}10^{-11}$m.
14. Silicon Si ($r_{28,29,30}$) m_{Si28} → $2.38\text{x}10^{-11}$m, m_{Si29} → $2.47\text{x}10^{-11}$m, m_{Si30} →$2.55\text{x}10^{-11}$m.
15. Phosphorous P (r_{31}) m_{P31} → $2.64\text{x}10^{-11}$m.
16. Sulphur S ($r_{32,33,34,36}$) m_{S32} → $2.72\text{x}10^{-11}$m, m_{S33} → $2.81\text{x}10^{-11}$m, m_{S34} → $2.89\text{x}10^{-11}$m, m_{S36} → $3.06\text{x}10^{-11}$m.
17. Chlorine Cl ($r_{35,37}$) m_{Cl35} → $2.98\text{x}10^{-11}$m, m_{Cl37} → $3.15\text{x}10^{-11}$m.

18. Argon Ar ($r_{36,38,40}$) $m_{Ar36} \rightarrow 3.06\text{x}10^{-11}$m, $m_{Ar38} \rightarrow 3.23\text{x}10^{-11}$m, $m_{Ar40} \rightarrow 3.40\text{x}10^{-11}$m.

19. Potassium K ($r_{39,40,41}$) $m_{K39} \rightarrow 3.32\text{x}10^{-11}$m, $m_{K40} \rightarrow 3.41\text{x}10^{-11}$m, $m_{K41} \rightarrow 3.49\text{x}10^{-11}$m.

20. Calcium Ca ($r_{40,42,43,44,46,48}$) $m_{Ca40} \rightarrow 3.40\text{x}10^{-11}$m, $m_{Ca42} \rightarrow 3.58\text{x}10^{-11}$m, $m_{Ca43} \rightarrow 3.66\text{x}10^{-11}$m, $m_{Ca44} \rightarrow 3.75\text{x}10^{-11}$m, $m_{Ca46} \rightarrow 3.92\ \text{x}10^{-11}$m, $m_{Ca48} \rightarrow 4.09\ \text{x}10^{-11}$m.

21. Scandium Sc (r_{45}) $m_{Sc45} \rightarrow 3.83\text{x}10^{-11}$m.

22. Titanium Ti ($r_{46,47,48,49,50}$) $m_{Ti46} \rightarrow 3.92\text{x}10^{-11}$m, $m_{Ti47} \rightarrow 4.00\text{x}10^{-11}$m, $m_{Ti48} \rightarrow 4.09\text{x}10^{-11}$m, $m_{Ti49} \rightarrow 4.17\text{x}10^{-11}$m, $m_{Ti50} \rightarrow 4.26\ \text{x}10^{-11}$m.

23. Vanadium V ($r_{50,51}$) $m_{V50} \rightarrow 4.26\text{x}10^{-11}$m, $m_{V51} \rightarrow 4.34\text{x}10^{-11}$m.

24. Chromium Cr ($r_{50,52,53,54}$) $m_{Cr50} \rightarrow 4.26\text{x}10^{-11}$m, $m_{Cr52} \rightarrow 4.43\text{x}10^{-11}$m, $m_{Cr53} \rightarrow 4.51\text{x}10^{-11}$m, $m_{Cr54} \rightarrow 4.60\text{x}10^{-11}$m.

25. Manganese Mn (r_{55}) $m_{Mn55} \rightarrow 4.68\text{x}10^{-11}$m.

26. Iron Fe ($r_{54,56,57,58}$) $m_{Fe54} \rightarrow 4.60\text{x}10^{-11}$m, $m_{Fe56} \rightarrow 4.77\text{x}10^{-11}$m, $m_{Fe57} \rightarrow 4.85\text{x}10^{-11}$m, $m_{Fe58} \rightarrow 4.94\text{x}10^{-11}$m.

27. Cobalt Co (r_{59}) $m_{Co59} \rightarrow 5.02\text{x}10^{-11}$m.

28. Nickel Ni ($r_{58,60,61,62,64}$) $m_{Ni58} \rightarrow 4.94\text{x}10^{-11}$m, $m_{Ni60} \rightarrow 5.11\text{x}10^{-11}$m, $m_{Ni61} \rightarrow 5.19\text{x}10^{-11}$m, $m_{Ni62} \rightarrow 5.28\text{x}10^{-11}$m, $m_{Ni64} \rightarrow 5.45\ \text{x}10^{-11}$m.

29. Copper Cu ($r_{63,65}$) $m_{Cu63} \rightarrow 5.36\text{x}10^{-11}$m, $m_{Cu65} \rightarrow 5.53\text{x}10^{-11}$m.

30. Zinc Zn ($r_{64,66,67,68,70}$) $m_{Zn64} \rightarrow 5.45\text{x}10^{-11}$m, $m_{Zn66} \rightarrow 5.62\text{x}10^{-11}$m, $m_{Zn67} \rightarrow 5.70\text{x}10^{-11}$m, $m_{Zn68} \rightarrow 5.79\text{x}10^{-11}$m, $m_{Zn70} \rightarrow 5.96\ \text{x}10^{-11}$m.

31. Gallium Ga ($r_{69,71}$) $m_{Ga69} \rightarrow 5.87\text{x}10^{-11}$m, $m_{Ga71} \rightarrow 6.04\text{x}10^{-11}$m.

32. Germanium Ge ($r_{70,72,73,74,76}$) $m_{Ge70} \rightarrow 5.96\text{x}10^{-11}$m, $m_{Ge72} \rightarrow 6.13\text{x}10^{-11}$m, $m_{Ge73} \rightarrow 6.21\text{x}10^{-11}$m, $m_{Ge74} \rightarrow 6.30\text{x}10^{-11}$m, $m_{Ge76} \rightarrow 6.47\ \text{x}10^{-11}$m.

33. Arsenic As (r_{75}) $m_{As75} \rightarrow 6.38\text{x}10^{-11}$m.

34. Selenium Se ($r_{74,76,77,78,80,82}$) $m_{Se74} \rightarrow 6.30\text{x}10^{-11}$m, $m_{Se76} \rightarrow 6.47\text{x}10^{-11}$m, $m_{Se77} \rightarrow 6.55\text{x}10^{-11}$m, $m_{Se78} \rightarrow 6.64\text{x}10^{-11}$m, $m_{Se80} \rightarrow 6.81\ \text{x}10^{-11}$m, $m_{Se82} \rightarrow 6.98\ \text{x}10^{-11}$m.

35. Bromine Br $(r_{79,81})$ $m_{Br79} \rightarrow 6.72\text{x}10^{-11}$m, $m_{Br81} \rightarrow 6.89\text{x}10^{-11}$m.

36. Krypton Kr $(r_{78,80,82,83,84,86})$ $m_{Kr78} \rightarrow 6.64\text{x}10^{-11}$m, $m_{Kr80} \rightarrow 6.81\text{x}10^{-11}$m, $m_{Kr82} \rightarrow 6.98\text{x}10^{-11}$m, $m_{Kr83} \rightarrow 7.06\text{x}10^{-11}$m, $m_{Kr84} \rightarrow 7.15\ \text{x}10^{-11}$m, $m_{Kr86} \rightarrow 7.32\ \text{x}10^{-11}$m.

37. Rubidium Rb $(r_{85,87})$ $m_{Rb85} \rightarrow 7.23\text{x}10^{-11}$m, $m_{Rb87} \rightarrow 7.40\text{x}10^{-11}$m.

38. Strontium Sr $(r_{84,86,87,88})$ $m_{Sr84} \rightarrow 7.15\text{x}10^{-11}$m, $m_{Sr86} \rightarrow 7.32\text{x}10^{-11}$m, $m_{Sr87} \rightarrow 7.40\text{x}10^{-11}$m, $m_{Sr88} \rightarrow 7.49\text{x}10^{-11}$m.

39. Yttrium Y (r_{89}) $m_{Y89} \rightarrow 7.57\text{x}10^{-11}$m.

40. Zirconium Zr $(r_{90,91,92,94,96})$ $m_{Zr90} \rightarrow 7.66\text{x}10^{-11}$m, $m_{Zr91} \rightarrow 7.75\text{x}10^{-11}$m, $m_{Zr92} \rightarrow 7.83\text{x}10^{-11}$m, $m_{Zr94} \rightarrow 8.00\text{x}10^{-11}$m, $m_{Zr96} \rightarrow 8.17\ \text{x}10^{-11}$m.

41. Niobium Nb (r_{93}) $m_{Nb93} \rightarrow 7.92\text{x}10^{-11}$m.

42. Molybdenum Mo $(r_{92,94,95,96,97,98,100})$ $m_{Mo92} \rightarrow 7.83\text{x}10^{-11}$m, $m_{Mo94} \rightarrow 8.00\text{x}10^{-11}$m, $m_{Mo95} \rightarrow 8.09\text{x}10^{-11}$m, $m_{MO96} \rightarrow 8.17\text{x}10^{-11}$m, $m_{Mo97} \rightarrow 8.26\ \text{x}10^{-11}$m, $m_{MO98} \rightarrow 8.34\text{x}10^{-11}$m, $m_{Mo100} \rightarrow 8.51\text{x}10^{-11}$m.

43. Technetium Tc $(r_{97,98,99})$ $m_{Tc97} \rightarrow 8.26\text{x}10^{-11}$m, $m_{Tc98} \rightarrow 8.34\text{x}10^{-11}$m, $m_{Tc99} \rightarrow 8.43\text{x}10^{-11}$m.

44. Ruthenium Ru$(r_{96,98,99,100,101,102,104})$ $m_{Ru96} \rightarrow 8.17\text{x}10^{-11}$m, $m_{Ru98} \rightarrow 8.34\text{x}10^{-11}$m, $m_{Ru99} \rightarrow 8.43\text{x}10^{-11}$m, $m_{Ru100} \rightarrow 8.51\text{x}10^{-11}$m, $m_{Ru101} \rightarrow 8.60\ \text{x}10^{-11}$m, $m_{Ru102} \rightarrow 8.68\text{x}10^{-11}$m, $m_{Ru104} \rightarrow 8.86\text{x}10^{-11}$m.

45. Rhodium Rh (r_{103}) $m_{Rh103} \rightarrow 8.77\text{x}10^{-11}$m.

46 Palladium Pd $(r_{102,104,105,106,107,108,110})$

$m_{Pd102} \rightarrow 8.68\text{x}10^{-11}$m, $m_{Pd104} \rightarrow 8.86\text{x}10^{-11}$m, $m_{Pd105} \rightarrow 8.94\text{x}10^{-11}$m, $m_{Pd106} \rightarrow 9.02\text{x}10^{-11}$m, $m_{Pd107} \rightarrow 9.11\ \text{x}10^{-11}$m, $m_{Pd108} \rightarrow 9.19\text{x}10^{-11}$m, $m_{Pd110} \rightarrow 9.36\text{x}10^{-11}$m.

47. Silver Ag $(r_{107,109})$ $m_{Ag107} \rightarrow 9.11\text{x}10^{-11}$m, $m_{Ag109} \rightarrow 9.28\text{x}10^{-11}$m.

48. Cadmium Cd $(r_{106,108,110,111,112,113,114,116})$ $m_{Cd106} \rightarrow 9.02\text{x}10^{-11}$m, $m_{Cd108} \rightarrow 9.19\text{x}10^{-11}$m, $m_{Cd110} \rightarrow 9.36\text{x}10^{-11}$m, $m_{Cd111} \rightarrow 9.45\text{x}10^{-11}$m, $m_{CD112} \rightarrow 9.53\ \text{x}10^{-11}$m, $m_{Cd\ 113} \rightarrow 9.62\text{x}10^{-11}$m, $m_{Cd114} \rightarrow 9.70\text{x}10^{-11}$m, $m_{Cd116} \rightarrow 9.88\text{x}10^{-11}$m.

49. Indium In $(r_{113,115})$ $m_{In113} \rightarrow 9.62\text{x}10^{-11}$m, $m_{In\ 115} \rightarrow 9.79\text{x}10^{-11}$m.

50. Tin Sn ($r_{112,114,115,116,117,118,119,120,122,124}$) $m_{Sn112} \rightarrow 9.53\text{x}10^{-11}$m, $m_{Sn114} \rightarrow 9.70\text{x}10^{-11}$m, $m_{Sn115} \rightarrow 9.79\text{x}10^{-11}$m, $m_{Sn116} \rightarrow 9.88\text{x}10^{-11}$m, $m_{Sn117} \rightarrow 9.96\ \text{x}10^{-11}$m, $m_{Sn118} \rightarrow 10.05\text{x}10^{-11}$m, $m_{Sn119} \rightarrow 10.13\text{x}10^{-11}$m, $m_{Sn120} \rightarrow 10.22\text{x}10^{-11}$m, $m_{Sn122} \rightarrow 10.39\text{x}10^{-11}$m, $m_{Sn124} \rightarrow 10.56\text{x}10^{-11}$m.

51. Antimony Sb ($r_{121,123,125}$) $m_{Sb121} \rightarrow 10.30\text{x}10^{-11}$m, $m_{Sb123} \rightarrow 10.47\text{x}10^{-11}$m, $m_{Sb125} \rightarrow 10.64\text{x}10^{-11}$m.

52. Tellurium Te ($r_{120,122,123,124,125,126,128,130}$)

$m_{Te120} \rightarrow 10.22\text{x}10^{-11}$m, $m_{Te122} \rightarrow 10.39\text{x}10^{-11}$m, $m_{Te123} \rightarrow 10.47\text{x}10^{-11}$m, $m_{Te124} \rightarrow 10.56\text{x}10^{-11}$m, $m_{Te125} \rightarrow 10.64\ \text{x}10^{-11}$m, $m_{Te126} \rightarrow 10.73\text{x}10^{-11}$m, $m_{Te128} \rightarrow 10.90\text{x}10^{-11}$m, $m_{Te130} \rightarrow 11.07\text{x}10^{-11}$m.

53. Iodine I (r_{127}) $m_{I127} \rightarrow 10.81\text{x}10^{-11}$m.

54. Xenon Xe ($r_{124,126,128,129,130,131,132,134,136}$) $m_{Xe124} \rightarrow 10.56\text{x}10^{-11}$m, $m_{Xe126} \rightarrow 10.73\text{x}10^{-11}$m, $m_{Xe128} \rightarrow 10.91\text{x}10^{-11}$m, $m_{Xe129} \rightarrow 10.98\text{x}10^{-11}$m, $m_{Xe130} \rightarrow 11.07\text{x}10^{-11}$m, $m_{Xe131} \rightarrow 11.15\text{x}10^{-11}$m, $m_{Xe132} \rightarrow 11.24\text{x}10^{-11}$m, $m_{Xe134} \rightarrow 11.41\text{x}10^{-11}$m, $m_{Xe136} \rightarrow 11.58\text{x}10^{-11}$m.

55. Cesium Cs (r_{133}) $m_{Cs133} \rightarrow 11.32\text{x}10^{-11}$m.

56. Barium Ba ($r_{130,132,134,135,136,137,138}$) $m_{Ba130} \rightarrow 11.07\text{x}10^{-11}$m, $m_{Ba132} \rightarrow 11.24\text{x}10^{-11}$m, $m_{Ba134} \rightarrow 11.41\text{x}10^{-11}$m, $m_{Ba135} \rightarrow 11.49\text{x}10^{-11}$m, $m_{Ba136} \rightarrow 11.58\text{x}10^{-11}$m, $m_{Ba137} \rightarrow 11.66\text{x}10^{-11}$m, $m_{Ba138} \rightarrow 11.75\text{x}10^{-11}$m.

57. Lanthanum La ($r_{138,139}$) $m_{La138} \rightarrow 11.75\text{x}10^{-11}$m, $m_{La139} \rightarrow 11.83\text{x}10^{-11}$m.

58. Cesium Ce ($r_{136,138,140,142}$) $m_{Ce136} \rightarrow 11.58\text{x}10^{-11}$m, $m_{Ce138} \rightarrow 11.75\text{x}10^{-11}$m, $m_{Ce140} \rightarrow 11.92\text{x}10^{-11}$m, $m_{Ce142} \rightarrow 12.09\text{x}10^{-11}$m.

59. Praseodymium Pr (r_{141}) $m_{Pr141} \rightarrow 12.01\text{x}10^{-11}$m.

60. Neodymium Nd ($r_{142,143,144,145,146,148,150}$) $m_{Nd142} \rightarrow 12.09\text{x}10^{-11}$m, $m_{Nd143} \rightarrow 12.18\text{x}10^{-11}$m, $m_{Nd144} \rightarrow 12.26\text{x}10^{-11}$m, $m_{Nd145} \rightarrow 12.35\text{x}10^{-11}$m, $m_{Nd146} \rightarrow 12.43\text{x}10^{-11}$m, $m_{Nd148} \rightarrow 12.60\text{x}10^{-11}$m, $m_{Nd150} \rightarrow 12.77\text{x}10^{-11}$m.

61. Promethium Pm ($r_{145,146,147}$) $m_{Pm145} \rightarrow 12.35\text{x}10^{-11}$m, $m_{Pm146} \rightarrow 12.43\text{x}10^{-11}$m, $m_{Pm147} \rightarrow 12.52\text{x}10^{-11}$m.

62. Samarium Sm ($r_{144,147,148,149,150,152,154}$) $m_{Sm144} \rightarrow 12.26\text{x}10^{-11}$m, $m_{Sm147} \rightarrow 12.52\text{x}10^{-11}$m, $m_{Sm148} \rightarrow 12.60\text{x}10^{-11}$m, $m_{Sm149} \rightarrow 12.69\text{x}10^{-11}$m, $m_{Sm150} \rightarrow 12.77\text{x}10^{-11}$m, $m_{Sm152} \rightarrow 12.94\text{x}10^{-11}$m, $m_{Sm154} \rightarrow 13.11\text{x}10^{-11}$m.

63. Europium Eu ($r_{151,153}$) $m_{Eu151} \rightarrow 12.86\text{x}10^{-11}$m, $m_{Eu153} \rightarrow 13.03\text{x}10^{-11}$m.

64. Gadolinium Gd ($r_{152,154,155,156,157,158,160}$) $m_{Gd152} \rightarrow 12.94\text{x}10^{-11}$m, $m_{Gd154} \rightarrow 13.11\text{x}10^{-11}$m, $m_{Gd155} \rightarrow 13.20\text{x}10^{-11}$m, $m_{Gd156} \rightarrow 13.28\text{x}10^{-11}$m, $m_{Gd157} \rightarrow 13.37\text{x}10^{-11}$m, $m_{Gd158} \rightarrow 13.46\text{x}10^{-11}$m, $m_{Gd160} \rightarrow 13.63\text{x}10^{-11}$m.

65. Terbium Tb (r_{159}) $m_{Tb159} \rightarrow 13.54\text{x}10^{-11}$m.

66. Dysprosium Dy ($r_{156,158,160,161,162,163,164}$) $m_{Dy156} \rightarrow 13.28\text{x}10^{-11}$m, $m_{Dy158} \rightarrow 13.46\text{x}10^{-11}$m, $m_{Dy160} \rightarrow 13.63\text{x}10^{-11}$m, $m_{Dy161} \rightarrow 13.71\text{x}10^{-11}$m, $m_{Dy162} \rightarrow 13.80\text{x}10^{-11}$m, $m_{Dy163} \rightarrow 13.88\text{x}10^{-11}$m, $m_{Dy164} \rightarrow 13.97\text{x}10^{-11}$m.

67. Holmium Ho (r_{165}) $m_{Ho165} \rightarrow 14.05\text{x}10^{-11}$m.

68. Erbium Er ($r_{162,164.166,167,168,170}$) $m_{Er162} \rightarrow 13.80\text{x}10^{-11}$m, $m_{Er164} \rightarrow 13.97\text{x}10^{-11}$m, $m_{Er166} \rightarrow 14.14\text{x}10^{-11}$m, $m_{Er167} \rightarrow 14.22\text{x}10^{-11}$m, $m_{Er168} \rightarrow 14.31\text{x}10^{-11}$m, $m_{Er170} \rightarrow 14.48\text{x}10^{-11}$m.

69. Thulium Tm (r_{169}) $m_{Tm169} \rightarrow 14.39\text{x}10^{-11}$m.

70. Ytterbium Yb ($r_{168,170,171,172,173,174,176}$) $m_{Yb168} \rightarrow 14.31\text{x}10^{-11}$m, $m_{Yb170} \rightarrow 14.48\text{x}10^{-11}$m, $m_{Yb171} \rightarrow 14.56\text{x}10^{-11}$m, $m_{Yb172} \rightarrow 14.65\text{x}10^{-11}$m, $m_{Yb173} \rightarrow 14.73\text{x}10^{-11}$m, $m_{Yb174} \rightarrow 14.82\text{x}10^{-11}$m, $m_{Yb176} \rightarrow 14.99\text{x}10^{-11}$m.

71. Lutetium Lu ($r_{175,176}$) $m_{Lu175} \rightarrow 14.90\text{x}10^{-11}$m, $m_{Lu176} \rightarrow 14.99\text{x}10^{-11}$m.

72. Hafnium Hf ($r_{174,176,177,178,179,180}$) $m_{Hf174} \rightarrow 14.82\text{x}10^{-11}$m, $m_{Hf176} \rightarrow 14.99\text{x}10^{-11}$m, $m_{Hf177} \rightarrow 15.08\text{x}10^{-11}$m, $m_{Hf178} \rightarrow 15.16\text{x}10^{-11}$m, $m_{Hf179} \rightarrow 15.25\text{x}10^{-11}$m, $m_{Hf180} \rightarrow 15.33\text{x}10^{-11}$m.

73. Tantalum Ta ($r_{180,181}$) $m_{Ta180} \rightarrow 15.33\text{x}10^{-11}$m, $m_{Ta181} \rightarrow 15.42\text{x}10^{-11}$m.

74. Tungsten W ($r_{180,182,183.184,186}$) $m_{W180} \rightarrow 15.33\text{x}10^{-11}$m, $m_{W182} \rightarrow 15.50\text{x}10^{-11}$m, $m_{W183} \rightarrow 15.59\text{x}10^{-11}$m, $m_{W184} \rightarrow 15.67\text{x}10^{-11}$m, $m_{W186} \rightarrow 15.84\text{x}10^{-11}$m.

75. Rhenium Re ($r_{185,187}$) $m_{Re185} \rightarrow 15.76\text{x}10^{-11}$m, $m_{Re187} \rightarrow 15.93\text{x}10^{-11}$m.

76. Osmium Os ($r_{184,186,187,188,189.190,192}$) $m_{Os184} \rightarrow 15.67\text{x}10^{-11}$m, $m_{Os186} \rightarrow 15.84\text{x}10^{-11}$m, $m_{Os187} \rightarrow 15.93\text{x}10^{-11}$m, $m_{Os188} \rightarrow 16.01\text{x}10^{-11}$m, $m_{Os189} \rightarrow 16.10\text{x}10^{-11}$m, $m_{Os190} \rightarrow 16.18\text{x}10^{-11}$m, $m_{Os192} \rightarrow 16.36\text{x}10^{-11}$m.

77. Iridium Ir ($r_{191,193}$) $m_{Ir191} \rightarrow 16.27\text{x}10^{-11}$m, $m_{Ir193} \rightarrow 16.44\text{x}10^{-11}$m.

78. Plutonium Pt ($r_{190,192,194,195,196,198}$) $m_{Pt190} \rightarrow 16.18x10^{-11}$m, $m_{Pt192} \rightarrow 16.36x10^{-11}$m, $m_{Pt194} \rightarrow 16.53x10^{-11}$m, $m_{Pt195} \rightarrow 16.61x10^{-11}$m, $m_{Pt196} \rightarrow 16.70x10^{-11}$m, $m_{Pt198} \rightarrow 16.87x10^{-11}$m.

79. Gold Au (r_{197}) $m_{Au197} \rightarrow 16.78x10^{-11}$m.

80. Mercury Hg ($r_{196,198,199,200,201,201,202,204}$) $m_{Hg196} \rightarrow 16.70x10^{-11}$m, $m_{Hg198} \rightarrow 16.87x10^{-11}$m, $m_{Hg199} \rightarrow 16.95x10^{-11}$m, $m_{Hg200} \rightarrow 17.04x10^{-11}$m, $m_{Hg201} \rightarrow 17.12x10^{-11}$m, $m_{Hg202} \rightarrow 17.21x10^{-11}$m, $m_{Hg204} \rightarrow 17.38x10^{-11}$m.

81. Thallium Tl ($r_{203,205}$) $m_{Tl203} \rightarrow 17.29x10^{-11}$m, $m_{Tl205} \rightarrow 17.46x10^{-11}$m.

82. Lead Pb ($r_{204,206,207,208}$) $m_{Pb204} \rightarrow 17.38x10^{-11}$m, $m_{Pb206} \rightarrow 17.55x10^{-11}$m, $m_{Pb207} \rightarrow 17.63x10^{-11}$m, $m_{Pb208} \rightarrow 17.72x10^{-11}$m, which is the last of the Stable Nuclides.

83. Bismuth Bi (r_{209}) $m_{Bi209} \rightarrow 17.81x10^{-11}$m.

84. Polonium Po ($r_{208,209}$) $m_{Po208} \rightarrow 17.72x10^{-11}$m, $m_{Po209} \rightarrow 17.81x10^{-11}$m.

85. Astatine At ($r_{207,208,209,210,211}$) $m_{At207} \rightarrow 17.63x10^{-11}$m, $m_{At208} \rightarrow 17.72x10^{-11}$m, $m_{At209} \rightarrow 17.81x10^{-11}$m, $m_{At210} \rightarrow 17.89x10^{-11}$m, $m_{At211} \rightarrow 17.98x10^{-11}$m.

86. Radon Rn (r_{222}) $m_{Rn222} \rightarrow 18.92x10^{-11}$m.

87. Francium Fr ($r_{223,224,225}$) $m_{Fr223} \rightarrow 19.01x10^{-11}$m, $m_{Fr224} \rightarrow 19.09x10^{-11}$m, $m_{Fr225} \rightarrow 19.17x10^{-11}$m.

88. Radium Ra ($r_{226,228}$) $m_{Ra226} \rightarrow 19.26x10^{-11}$m, $m_{Ra228} \rightarrow 19.43x10^{-11}$m.

89. Actinium Ac (r_{227}) $m_{Ac227} \rightarrow 19.34x10^{-11}$m.

90. Thorium Th ($r_{229,230,232}$) $m_{Th229} \rightarrow 19.51x10^{-11}$m, $m_{Th230} \rightarrow 19.60x10^{-11}$m, $m_{Th232} \rightarrow 19.77x10^{-11}$m.

91. Protactinium Pa (r_{231}) $m_{Pa231} \rightarrow 19.68x10^{-11}$m.

92. Uranium U or Ur ($r_{232,233,234,235,236,238}$) $m_{U232} \rightarrow 19.77x10^{-11}$m, $m_{U233} \rightarrow 19.86x10^{-11}$m, $m_{U234} \rightarrow 19.94x10^{-11}$m, $m_{U235} \rightarrow 20.03x10^{-11}$m, $m_{U236} \rightarrow 20.11x10^{-11}$m, $m_{U238} \rightarrow 20.28x10^{-11}$m.

93. Neptunium Np ($r_{236,237}$) $m_{Np236} \rightarrow 20.11x10^{-11}$m, $m_{Np237} \rightarrow 20.20x10^{-11}$m.

94. Plutonium Pu ($r_{236,238,239,240,241.242,244}$) $m_{Np236} \rightarrow 20.11x10^{-11}$m, $m_{Np238} \rightarrow 20.28x10^{-11}$m, $m_{Np239} \rightarrow 20.37x10^{-11}$m, $m_{Np240} \rightarrow 20.45x10^{-11}$m, $m_{Np241} \rightarrow 20.54x10^{-11}$m, $m_{Np242} \rightarrow 20.62x10^{-11}$m, $m_{Np244} \rightarrow 20.79x10^{-11}$m.

95. Americium Am ($r_{241,242,243}$) m_{Am241} → 20.54x10^{-11}m, m_{Am242} → 20.62x10^{-11}m, m_{Am243} → 20.71x 10^{-11}m.

96.Curium Cm ($r_{245,246,247,248}$) m_{Cm245} → 20.88x10^{-11}m, m_{Cm246} → 20.96x10^{-11}m, m_{Cm247} → 21.05x 10^{-11}m, m_{Cm248} → 21.14x10^{-11}m.

97. Berkelium Bk (r_{247}) m_{Bk247} → 21.05x10^{-11}m.

98. Californium Cf ($r_{249,250,251,252}$) m_{Cf249} → 21.22x10^{-11}m, m_{Cf250} → 21.31x10^{-11}m, m_{Cf251} → 21.39x 10^{-11}m, m_{Cf252} → 21.48x10^{-11}m.

99. Einsteinium Es ($r_{252,253,254,255,256,257}$) m_{Es252} → 21.48x10^{-11}m, m_{Es253} → 21.56x10^{-11}m, m_{Es254} → 21.64x10^{-11}m, m_{Es255} → 21.73x10^{-11}m, m_{Es256} → 21.82x10^{-11}m, m_{Es257} → 21.90x10^{-11}m.

100. Fermion Fm ($r_{253,257}$) m_{Fm253} → 21.56x10^{-11}m, m_{Fm257} → 21.90x10^{-11}m.

101. Mendelevium Md ($r_{257,258,259,260}$) m_{Md257} → 21.90x10^{-11}m, m_{Md258} → 21.99x10^{-11}m, m_{Md259} → 22.08x10^{-11}m, m_{Md260} → 22.16x10^{-11}m.

All nuclei beyond nuclear number 260 are very unstable (have very short half-lives) and therefore are not being considered. The same instability applies to nuclei numbers between 212 and 221 that will also be left out of the Table. The reason for the instability pertains to their large number and the way the protons and neutrons are situated within the nucleus. Since the nucleon binding forces act over short distances as the nucleus gets larger in size the binding forces which acts over only a few neighboring nucleons cannot compete with the longer range electrical repulsive forces between protons, hence the nucleus becomes unstable.

III. DENSITY CALCULATIONS

Density (ρ) = Mass/Volume = Mass / ($4\pi r^3/3$) using the values of r from the Radius Calculations and the known values of Mass.

Electron ρ = 2.12x10^{15} Kg/m^3.

Electron Neutrino ρ = 1.18x10^{26} Kg/m^3.

Up Quark ρ = 1.06x10^{14} Kg/m^3.

Down Quark ρ = 2.41x10^{13} Kg/m^3.

Proton and Neutron Density ρ = 6.30x10^{8} Kg/m^3.

The Radius and Density Table of the Nucleons of the Periodic Table are used to correct the mistakes made in Physics Textbooks that all sized nuclei have the same Density (Reference 4) of 2.3x10^{17} *kg*/m^3

based on the incorrect assumption that the radius of all nuclei is proportional to $A^{\frac{1}{3}}$ *where A is their Mass Number, and therefore their Density is independent of their Mass Number.*

. Within the Table S = Stable Nucleus and U = Unstable Nucleus. Simplifying the formula ρ = M/V to: ρ = (No. of Nucleons x 3.99x 10^{-28})/ r^3 Kg/m^3 we get:

Number of Nucleons.	Radius in m.	Density in Kg/m^3.
1 H-S	8.59x10^{-13}	6.30x10^{8}
2 H-S	1.72x10^{-12}	1.57x10^{8}
3 He-S	2.57x10^{-12}	7.05x10^{7}
4 He-S	3.41x10^{-12}	4.03x10^{7}
5 -----------------	Does Not Exist.	------------------
6 Li-S	5.13x10^{-12}	1.77x10^{7}
7 Li-S	5.98x10^{-12}	1.31x10^{7}
8 Be-U	6.82x10^{-12}	1.01x10^{7}
9 Be-S	7.68x10^{-12}	7.93x10^{6}
10 B-S	8.53x10^{-12}	6.43x10^{6}
11 B-S	9.38x10^{-12}	5.32x10^{6}
12 C-S	1.02x10^{-11}	4.51x10^{6}
13 C-S	1.11x10^{-11}	3.79x10^{6}
14 N-S	1.19x10^{-11}	3.31x10^{6}
15 N-S	1.28x10^{-11}	2.85x10^{6}
16 O-S	1.36x10^{-11}	2.54x10^{6}
17 O-S	1.45x10^{-11}	2.22x10^{6}
18 O-S	1.53x10^{-11}	2.01x10^{6}
19 F-S	1.62x10^{-11}	1.78x10^{6}
20 Ne-S	1.70x10^{-11}	1.62x10^{6}
21 Ne-S	1.79x10^{-11}	1.46x10^{6}
22 Ne-S	1.87x10^{-11}	1.34x10^{6}
23 Na-S	1.96x10^{-11}	1.22x10^{6}
24 Mg-S	2.04x10^{-11}	1.13x10^{6}
25 Mg-S	2.13x10^{-11}	1.03x10^{6}
26 Mg-S	2.21x10^{-11}	9.61x10^{5}
27 Al-S	2.30x10^{-11}	8.85x10^{5}
28 Si-S	2.38x10^{-11}	8.29x10^{5}
29 Si-S	2.47x10^{-11}	7.68x10^{5}
30 Si-S	2.55x10^{-11}	7.22x10^{5}
31 P-S	2.64x10^{-11}	6.72x10^{5}
32 Sulphur-S	2.72x10^{-11}	6.34x10^{5}
33 Sulphur-S	2.81x10^{-11}	5.93x10^{5}
34 Sulphur-S	2.89x10^{-11}	5.62x10^{5}

35 Cl-S	$2.98x10^{-11}$	$5.28x10^{5}$
36Sulphur,Ar-S	$3.06x10^{-11}$	$5.01x10^{5}$
37 Cl-S	$3.15x10^{-11}$	$4.72x10^{5}$
38 Ar-S	$3.23x10^{-11}$	$4.50x10^{5}$
39 K-S	$3.32x10^{-11}$	$4.25x10^{5}$
40 Ar, Ca-S	$3.40x10^{-11}$	$4.06x10^{5}$
41 K-S	$3.49x10^{-11}$	$3.85x10^{5}$
42 Ca-S	$3.58x10^{-11}$	$3.65x10^{5}$
43 Ca-S	$3.66x10^{-11}$	$3.50x10^{5}$
44 Ca-S	$3.75x10^{-11}$	$3.33x10^{5}$
45 Sc-S	$3.83x10^{-11}$	$3.20x10^{5}$
46 Ca, Ti-S	$3.92x10^{-11}$	$3.05x10^{5}$
47 Ti-S	$4.00x10^{-11}$	$2.93x10^{5}$
48 Ti-S	$4.09x10^{-11}$	$2.80x10^{5}$
49 Ti-S	$4,17x10^{-11}$	$2.70x10^{5}$
50 Ti-S	$4.26x10^{-11}$	$2.58x10^{5}$
51 V-S	$4.34x10^{-11}$	$2.49x10^{5}$
52 Cr-S	$4.43x10^{-11}$	$2.39x10^{5}$
53 Cr-S	$4.51x10^{-11}$	$2.31x10^{5}$
54 Cr, Fe-S	$4.60x10^{-11}$	$2.21x10^{5}$
55 Mn-S	$4.68x10^{-11}$	$2.14x10^{5}$
56 Fe-S	$4.77x10^{-11}$	$2.06x10^{5}$
57 Fe-S	$4.85x10^{-11}$	$1.99x10^{5}$
58 Fe, Ni-S	$4.94x10^{-11}$	$1.92x10^{5}$
59 Co-S	$5.02x10^{-11}$	$1.86x10^{5}$
60 Ni-S	$5.11x10^{-11}$	$1.79x10^{5}$
61 Ni-S	$5.19x10^{-11}$	$1.74x10^{5}$
62 Ni-S	$5.28x10^{-11}$	$1.68x10^{5}$
63 Cu-S	$5.36x10^{-11}$	$1.63x10^{5}$
64 Ni, Zn-S	$5.45x10^{-11}$	$1.58x10^{5}$
65 Cu-S	$5.53x10^{-11}$	$1.53x10^{5}$
66 Zn-S	$5.62x10^{-11}$	$1.48x10^{5}$
67 Zn-S	$5.70x10^{-11}$	$1.44x10^{5}$
68 Zn-S	$5.79x10^{-11}$	$1.40x10^{5}$
69 Ga-S	$5.87x10^{-11}$	$1.36x10^{5}$
70 Zn, Ge-S	$5.96x10^{-11}$	$1.32x10^{5}$
71 Ga-S	$6.04x10^{-11}$	$1.29x10^{5}$
72 Ge-S	$6.13x10^{-11}$	$1.25x10^{5}$

73 Ge-S	$6.21x10^{-11}$	$1.22x10^{5}$
74 Ge, Se-S	$6.30x10^{-11}$	$1.18x10^{5}$
75 As-S	$6.38x10^{-11}$	$1.15x10^{5}$
76 Ge, Se-S	$6.47x10^{-11}$	$1.12x10^{5}$
77 Se-S	$6.55x10^{-11}$	$1.09x10^{5}$
78 Se-S	$6.64x10^{-11}$	$1.06x10^{5}$
79 Br-S	$6.72x10^{-11}$	$1.04x10^{5}$
80 Se, Kr-S	$6.81x10^{-11}$	$1.01x10^{5}$
81 Br-S	$6.89x10^{-11}$	$9.88x10^{4}$
82 Kr-S	$6.98x10^{-11}$	$9.62x10^{4}$
83 Kr-S	$7.06x10^{-11}$	$9.41x10^{4}$
84 Kr, Sr-S	$7.15x10^{-11}$	$9.17x10^{4}$
85 Rb-S	$7.23x10^{-11}$	$8.97x10^{4}$
86 Kr, Sr-S	$7.32x10^{-11}$	$8.75x10^{4}$
87 Sr-S	$7.40x10^{-11}$	$8.57x10^{4}$
88 Sr-S	$7.49x10^{-11}$	$8.36x10^{4}$
89 Y-S	$7.57x10^{-11}$	$8.19x10^{4}$
90 Zr-S	$7.66x10^{-11}$	$7.99x10^{4}$
91 Zr-S	$7.75x10^{-11}$	$7.80x10^{4}$
92 Zr, Mo-S	$7.83x10^{-11}$	$7.65x10^{4}$
93 Nb-S	$7.92x10^{-11}$	$7.47x10^{4}$
94 Zr, Mo-S	$8.00x10^{-11}$	$7.33x10^{4}$
95 Mo-S	$8.09x10^{-11}$	$7.16x10^{4}$
96 Mo, Ru-S	$8.17x10^{-11}$	$7.02x10^{4}$
97 Mo-S	$8.26x10^{-11}$	$6.87x10^{4}$
98 Mo, Ru-S	$8.34x10^{-11}$	$6.74x10^{4}$
99 Tc-U, Ru-S	$8.43x10^{-11}$	$6.59x10^{4}$
100 Ru-S	$8.51x10^{-11}$	$6.47x10^{4}$
101 Ru-S	$8.60x10^{-11}$	$6.34x10^{4}$
102 Ru, Pd-S	$8.68x10^{-11}$	$6.22x10^{4}$
103 Rh-S	$8.77x10^{-11}$	$6.09x10^{4}$
104 Ru, Pd-S	$8.86x10^{-11}$	$5.97x10^{4}$

105 Pd-S	$8.94x10^{-11}$	$5.86x10^{4}$
106 Pd, Cd-S	$9.02x10^{-11}$	$5.76x10^{4}$
107 Ag-S	$9.11x10^{-11}$	$5.65x10^{4}$
108 Pd, Cd-S	$9.19x10^{-11}$	$5.55x10^{4}$
109 Ag-S	$9.28x10^{-11}$	$5.44x10^{4}$
110 Pd, Cd-S	$9.36x10^{-11}$	$5.35x10^{4}$
111 Cd-S	$9.45x10^{-11}$	$5.25x10^{4}$
112 Cd, Sn-S	$9.53x10^{-11}$	$5.16x10^{4}$
113 In-S	$9.62x10^{-11}$	$5.06x10^{4}$
114 Cd, Sn-S	$9.70x10^{-11}$	$4.98x10^{4}$
115 Sn-S	$9.79x10^{-11}$	$4.89x10^{4}$
116 Sn-S	$9.88x10^{-11}$	$4.80x10^{4}$
117 Sn-S	$9.96x10^{-11}$	$4.72x10^{4}$
118 Sn-S	$10.05x10^{-11}$	$4.64x10^{4}$
119 Sn-S	$10.13x10^{-11}$	$4.57x10^{4}$
120 Sn, Te-S	$10.22x10^{-11}$	$4.49x10^{4}$
121 Sb-S	$10.30x10^{-11}$	$4.42x10^{4}$
122 Sn, Te-S	$10.39x10^{-11}$	$4.34x10^{4}$
123 Sb-S	$10.47x10^{-11}$	$4.28x10^{4}$
124 Sn,Te,Xe-S	$10.56x10^{-11}$	$4.20x10^{4}$
125 Te-S	$10.64x10^{-11}$	$4.14x10^{4}$
126 Te, Xe-S	$10.73x10^{-11}$	$4.07x10^{4}$
127 I-S	$10.81x10^{-11}$	$4.01x10^{4}$
128 Xe-S	$10.91x10^{-11}$	$3.93x10^{4}$
129 Xe-S	$10.98x10^{-11}$	$3.89x10^{4}$
130 Xe, Ba-S	$11.07x10^{-11}$	$3.82x10^{4}$
131 Xe-S	$11.15x10^{-11}$	$3.77x10^{4}$
132 Xe, Ba-S	$11.24x10^{-11}$	$3.71x10^{4}$
133 Cs-S	$11.32x10^{-11}$	$3.66x10^{4}$
134 Xe, Ba-S	$11.41x10^{-11}$	$3.60x10^{4}$
135 Ba-S	$11.49x10^{-11}$	$3.55x10^{4}$
136 Ba, Ce-S	$11.58x10^{-11}$	$3.49x10^{4}$

137 Ba-S	$11.66x10^{-11}$	$3.45x10^{4}$
138 Ba, Ce-S	$11.75x10^{-11}$	$3.39x10^{4}$
139 La-S	$11.83x10^{-11}$	$3.35x10^{4}$
140 Ce-S	$11.92x10^{-11}$	$3.30x10^{4}$
141 Pr-S	$12.01x10^{-11}$	$3.25x10^{4}$
142 Nd-S	$12.09x10^{-11}$	$3.21x10^{4}$
143 Nd-S	$12.18x10^{-11}$	$3.16x10^{4}$
144 Sm-S	$12.26x10^{-11}$	$3.12x10^{4}$
145 Nd-S	$12.35x10^{-11}$	$3.07x10^{4}$
146 Nd-S	$12.43x10^{-11}$	$3.03x10^{4}$
147 Pm-U	$12.52x10^{-11}$	$2.99x10^{4}$
148 Nd-S	$12.60x10^{-11}$	$2.95x10^{4}$
149 Sm-U	$12.69x10^{-11}$	$2.91x10^{4}$
150 Sm-S	$12.77x10^{-11}$	$2.87x10^{4}$
151 Eu-S	$12.86x10^{-11}$	$2.83x10^{4}$
152 Sm-S	$12.94x10^{-11}$	$2.80x10^{4}$
153 Eu-S	$13.03x10^{-11}$	$2.76x10^{4}$
154 Sm, Gd-S	$13.11x10^{-11}$	$2.73x10^{4}$
155 Gd-S	$13.20x10^{-11}$	$2.69x10^{4}$
156 Gd, Dy-S	$13.28x10^{-11}$	$2.66x10^{4}$
157 Gd-S	$13.37x10^{-11}$	$2.62x10^{4}$
158 Gd, Dy-S	$13.46x10^{-11}$	$2.59x10^{4}$
159 Tb-S	$13.54x10^{-11}$	$2.56x10^{4}$
160 Gd, Dy-S	$13.63x10^{-11}$	$2.52x10^{4}$
161 Dy-S	$13.71x10^{-11}$	$2.49x10^{4}$
162 Dy, Er-S	$13.80x10^{-11}$	$2.46x10^{4}$
163 Dy-S	$13.88x10^{-11}$	$2.43x10^{4}$
164 Dy, Er-S	$13.97x10^{-11}$	$2.40x10^{4}$
165 Ho-S	$14.05x10^{-11}$	$2.37x10^{4}$
166 Er-S	$14.14x10^{-11}$	$2.34x10^{4}$
167 Er-S	$14.22x10^{-11}$	$2.32x10^{4}$
168 Er, Yb-S	$14.31x10^{-11}$	$2.29x10^{4}$

169 Tm-S	$14.39x10^{-11}$	$2.26x10^{4}$
170 Er, Yb-S	$14.48x10^{-11}$	$2.23x10^{4}$
171 Yb-S	$14.56x10^{-11}$	$2.21x10^{4}$
172 Yb-S	$14.65x10^{-11}$	$2.18x10^{4}$
173 Yb-S	$14.73x10^{-11}$	$2.16x10^{4}$
174 Yb-S	$14.82x10^{-11}$	$2.13x10^{4}$
175 Lu-S	$14.90x10^{-11}$	$2.11x10^{4}$
176 Yb, Hf-S	$14.99x10^{-11}$	$2.08x10^{4}$
177 Hf-S	$15.08x10^{-11}$	$2.06x10^{4}$
178 Hf-S	$15.16x10^{-11}$	$2.04x10^{4}$
179 Hf-S	$15.25x10^{-11}$	$2.01x10^{4}$
180 Hf, W-S	$15.33x10^{-11}$	$1.99x10^{4}$
181 Ta-S	$15.42x10^{-11}$	$1.97x10^{4}$
182 W-S	$15.50x10^{-11}$	$1.95x10^{4}$
183 W-S	$15.59x10^{-11}$	$1.93x10^{4}$
184 W, Os-S	$15.67x10^{-11}$	$1.91x10^{4}$
185 W, Re-S	$15.76x10^{-11}$	$1.89x10^{4}$
186 Os-U	$15.84x10^{-11}$	$1.87x10^{4}$
187 Re-U, Os-S	$15.93x10^{-11}$	$1.85x10^{4}$
188 Os-S	$16.01x10^{-11}$	$1.83x10^{4}$
189 Os-S	$16.10x10^{-11}$	$1.81x10^{4}$
190 Os-S	$16.18x10^{-11}$	$1.79x10^{4}$
191 Ir-S	$16.27x10^{-11}$	$1.77x10^{4}$
192 Os, Pt-S	$16.36x10^{-11}$	$1.75x10^{4}$
193 Ir-S	$16.44x10^{-11}$	$1.73x10^{4}$
194 Pt-S	$16.53x10^{-11}$	$1.71x10^{4}$
195 Pt-S	$16.61x10^{-11}$	$1.70x10^{4}$
196 Pt, Hg-S	$16.70x10^{-11}$	$1.68x10^{4}$
197 Au-S	$16.78x10^{-11}$	$1.66x10^{4}$
198 Pt, Hg-S	$16.87x10^{-11}$	$1.65x10^{4}$
199 Hg-S	$16.95x10^{-11}$	$1.63x10^{4}$
200 Hg-S	$17.04x10^{-11}$	$1.61x10^{4}$

201 Hg-S	$17.12x10^{-11}$	$1.60x10^{4}$
202 Hg-S	$17.21x10^{-11}$	$1.58x10^{4}$
203 Tl-S	$17.29x10^{-11}$	$1.57x10^{4}$
204 Hg-S	$17.38x10^{-11}$	$1.55x10^{4}$
205 Tl-S	$17.46x10^{-11}$	$1.54x10^{4}$
206 Pb-S	$17.55x10^{-11}$	$1.52x10^{4}$
207 Pb-S, At-U	$17.63x10^{-11}$	$1.51x10^{4}$
208 Pb-S; All nuclei > 208 are Unstable.	$17.72x10^{-11}$	$1.49x10^{4}$
209Bi, Po, At-U	$17.81x10^{-11}$	$1.48x10^{4}$
210 At-U	$17.89x10^{-11}$	$1.46x10^{4}$
211 At-U	$17.98x10^{-11}$	$1.45x10^{4}$
222 Rn-U	$18.92x10^{-11}$	$1.31x10^{4}$
223 Fr-U	$19.01x10^{-11}$	$1.30x10^{4}$
224 Fr-U	$19.09x10^{-11}$	$1.28x10^{4}$
225 Fr-U	$19.17x10^{-11}$	$1.27x10^{4}$
226 Ra-U	$19.26x10^{-11}$	$1.26x10^{4}$
227 Ac-U	$19.34x10^{-11}$	$1.25x10^{4}$
228 Ra-U	$19.43x10^{-11}$	$1.24x10^{4}$
229 Th-U	$19.51x10^{-11}$	$1.23x10^{4}$
230 Th-U	$19.60x10^{-11}$	$1.22x10^{4}$
231 Pa-U	$19.68x10^{-11}$	$1.21x10^{4}$
232 Th, Ur-U	$19.77x10^{-11}$	$1.20x10^{4}$
233 Ur-U	$19.86x10^{-11}$	$1.19x10^{4}$
234 Ur-U	$19.94x10^{-11}$	$1.18x10^{4}$
235 Ur-U	$20.03x10^{-11}$	$1.17x10^{4}$
236Ur,Np,Pu-U	$20.11x10^{-11}$	$1.16x10^{4}$
237 Ur, Np-U	$20.20x10^{-11}$	$1.15x10^{4}$
238 Ur, Pu-U	$20.28x10^{-11}$	$1.14x10^{4}$
239 Pu-U	$20.37x10^{-11}$	$1.13x10^{4}$
240 Pu-U	$20.45x10^{-11}$	$1.12x10^{4}$
241 Pu, Am-U	$20.54x10^{-11}$	$1.11x10^{4}$

242 Pu, Am-U	20.62x10^{-11}	1.10x10^{4}
243 Am-U	20.71x10^{-11}	1.09x10^{4}
244 Pu-U	20.79x10^{-11}	1.08x10^{4}
245 Cm-U	20.88x10^{-11}	1.074x10^{4}
246 Cm-U	20.96x10^{-11}	1.066x10^{4}
247 Cm, Bk-U	21.05x10^{-11}	1.06x10^{4}
248 Cm-U	21.14x10^{-11}	1.05x10^{4}
249 Cf-U	21.22x10^{-11}	1.04x10^{4}
250 Cf-U	21.31x10^{-11}	1.03x10^{4}
251 Cf-U	21.39x10^{-11}	1.02x10^{4}
252 Cf, Es-U	21.48x10^{-11}	1.01x10^{4}
253 Es, Fm-U	21.56x10^{-11}	10.07x10^{3}
254 Es-U	21.64x10^{-11}	10.00x10^{3}
255 Es-U	21.73x10^{-11}	9.92x10^{3}
256 Es-U	21.82x10^{-11}	9.83x10^{3}
257 Es, Fm, Md-U	21.90x10^{-11}	9.76x10^{3}
258 Md-U	21.99x10^{-11}	9.68x10^{3}
259 Md-U	22.08x10^{-11}	9.60x10^{3}
260 Md-U	22.16x10^{-11}	9.53x10^{3}

The density of stable nuclei varies from 6.30x10^{8} Kg/m^{3} for 1 nucleus to 1.49x10^{4} Kg/m^{3} for 208 nucleons.

IV. CONCLUSION

All the radii of the elementary particles are fundamental and therefore they should be included, along with the radii and charges of the three neutrinos, in the Table at the end of a University Physics Book in conjunction with the other Physical Constants of nature. The sizes of the nuclei of the elements depend only on the total number of nucleons. If there is an overlap of the number of nucleons between two or more elements their size will be the same. As an example, Barium, Lanthanum, and Cesium can all carry 138 nucleons of the same radius of 11.75x10^{-11}m. Another example would be Hafnium carrying 176 nucleons of radius 14.99x10^{-11}m with Ytterbium and Lutetium; and Hafnium carrying 180 nucleons of radius 15.33x10^{-11}m with Tantalum and Tungsten. The radii and densities of all the nuclei of all the elements of the Periodic Table should be included in Chemistry Textbooks. Densities decrease as the number of nucleons and their radii increase. The strong nuclear attractive force between the nucleons that is short ranged begins to become weaker than the repulsive electric force between the protons that is long ranged until nucleons with higher mass number become unstable.

REFERENCES

1. Irani, A. (2024) Calculations of the Electron Radius. Journal of High Energy Physics, Gravitation and Cosmology, 10, 724-725. doi: 10.4236/jhepgc.2024.102044.
2. Irani, A. (2024) Estimates of the Charges and Size of the Three Types of Neutrinos. *Journal of High Energy Physics, Gravitation and Cosmology*, 10, 1467-1469. doi: 10.4236/jhepgc.2024.104082.
3. Tables of Nuclear Data, Nuclear Data Center, Japan Atomic Energy Agency (JAEA) wwwndc.jaea.go.jp/NuC/
4. Serway & Faughn, College Physics, Fifth Edition, Page 960, Harcourt College Publishers, Orlando, FL 32887-6777.

This page is intentionally left blank

Scan to know paper details and
author's profile

The Study of the Complexity and Capacity of Urban Floristic Diversity in Arid Zones, Exemplified by the City of Bukhara, RUz

Mukhamad I. Gulamov & Saida M. Gafarova

Bukhara State University

ABSTRACT

This study examines the biodiversity of the urban flora in the arid zone of Bukhara city, Republic of Uzbekistan. The research is based on our newly proposed methods—analyzing the complexity and capacity of floral biodiversity. It also incorporates established biodiversity indices: species abundance evenness (probability of species occurrence) and the Shannon index. This is the first time that the values of complexity and power indicators for real ecological systems have been calculated. The findings reveal that the biodiversity of Bukhara's urban flora is characterized by uneven species abundance, with significant dominance of certain tree species (Pinus brutia var. eldarica (Medw.) Silba; Ulmus parvifolia L.; Platycladus orientalis (L.) Franco); shrubs (Rosa chinensis Jacq.; Yucca filamentosa L.), and herbs (Hordeum bulbosum L.; Descurainia Sophia L.; Seteria viridis (L.) P.Beauv; Coreopsis lanceolata L). A high level of complexity and low capacity in the biodiversity structure of the studied urban flora indicate weak resilience, adaptability, and regenerative capacity of the flora. These observations suggest that the general principles (lack of uniformity, unified logic, harmony, purpose, and order) governing biodiversity transformation in nature are disrupted in urban ecosystems due to the imposition of subjective logic, harmony, purpose, and order.

Keywords: urban flora; urban ecosystem; species occurrence frequency; Shannon index; biodiversity complexity; biodiversity capacity.

Classification: LCC Code: QK910

Language: English

Great Britain
Journals Press

LJP Copyright ID: 925643
Print ISSN: 2631-8490
Online ISSN: 2631-8504

London Journal of Research in Science: Natural & Formal

Volume 25 | Issue 4 | Compilation 1.0

The Study of the Complexity and Capacity of Urban Floristic Diversity in Arid Zones, Exemplified by the City of Bukhara, RUz

Mukhamad I. Gulamov[α] & Saida M. Gafarova[σ]

ABSTRACT

This study examines the biodiversity of the urban flora in the arid zone of Bukhara city, Republic of Uzbekistan. The research is based on our newly proposed methods—analyzing the complexity and capacity of floral biodiversity. It also incorporates established biodiversity indices: species abundance evenness (probability of species occurrence) and the Shannon index. This is the first time that the values of complexity and power indicators for real ecological systems have been calculated. The findings reveal that the biodiversity of Bukhara's urban flora is characterized by uneven species abundance, with significant dominance of certain tree species (Pinus brutia var. eldarica (Medw.) Silba; Ulmus parvifolia L.; Platycladus orientalis (L.) Franco); shrubs (Rosa chinensis Jacq.; Yucca filamentosa L.), and herbs (Hordeum bulbosum L.; Descurainia Sophia L.; Seteria viridis (L.) P.Beauv; Coreopsis lanceolata L). A high level of complexity and low capacity in the biodiversity structure of the studied urban flora indicate weak resilience, adaptability, and regenerative capacity of the flora. These observations suggest that the general principles (lack of uniformity, unified logic, harmony, purpose, and order) governing biodiversity transformation in nature are disrupted in urban ecosystems due to the imposition of subjective logic, harmony, purpose, and order.

Keywords: urban flora; urban ecosystem; species occurrence frequency; Shannon index; biodiversity complexity; biodiversity capacity.

Author α σ: Bukhara State University, Bukhara, Uzbekistan.

I. INTRODUCTION

This paper summarizes the results of our previous studies on the biodiversity of urban flora in the arid zone of Central Asia, using the city of Bukhara as a case study. These studies employed the floristic systematic grid method. The primary objectives of this research were:

a. Based on scientific data and personal observations, study the modern physical-geographical and ecological characteristics of the city of Bukhara (Republic of Uzbekistan). The territory of Bukhara covers an area of 143 km^2. The climate is sharply continental and desert-like: winters are very harsh, while summers are hot and dry. The average January temperature is minus 2 degrees Celsius, and in July, it exceeds 40 degrees. The annual precipitation in the Bukhara region ranges from 90–150 mm, mostly in the form of rain. Therefore, Bukhara's territory is classified as an arid zone (Gafarova S.M., Gulamov M.I., 2021).
b. Conduct research and analysis of floral diversity in urban conditions based on field observations and literary data using the city of Bukhara, Republic of Uzbekistan, as a case study. The collected materials were used to systematize the floral diversity of Bukhara, and standard statistical data processing was performed (Gafarova et al., 2024).

Currently, the global discussion on the significance of plant biodiversity for human society is highly pertinent. Life on Earth directly depends on plant biodiversity, which serves as the foundation of existence. Considering the current pace of urbanization worldwide, any research aimed at preserving floral biodiversity is exceedingly necessary. Contemporary ecological situations on the planet confirm this necessity (A Global Standard 2016; Kate 2022; Alves 2024).

Currently, urban areas occupy a small fraction of Earth's surface; some estimates suggest less than 0.1% of the total land area. However, their impact extends over significant distances. It has been calculated that 1 m^2 of urban system consumes 70 times more energy than the corresponding area of a natural ecosystem. To provide food for an urban population of 1 million people, approximately 0.8 million hectares of arable land are required. Cities affect the environment not only as consumers of energy, organic matter, and oxygen but also as powerful sources of pollution (Conservation and Restoration of Biodiversity, 2002).

Vegetation is a fundamental component of urban ecosystems, playing a crucial role in the lives of city residents. The functions of plants in urban areas are diverse and include: Improving the urban microclimate, Food production, Regulating air composition, Absorbing dust and toxic substances, Reducing noise levels, Enhancing the aesthetic appearance of the city and Providing spaces for recreation. In ecosystems, plants play a leading role as sources of food and oxygen, creating conditions for life and shelter for other organisms (Conservation and Restoration of Biodiversity, 2002; Ceplová et al. 2017 a,b; Tretyakova et al. 2018; Jovanović, Glišić, 2021).

One of the pressing issues in this field is the development of methods to study the biodiversity of urban flora in arid zones under urban conditions, aiming to preserve and enhance its floristic structure. The biodiversity of urban flora serves as the foundation that shapes the landscape of urban planning (Christenhusz et al., 2011). Investigating the biodiversity of urban flora requires examining its elementary floristic unit at the regional level (minimum range), species composition, species density (Gafarova et al., 2024), and levels of complexity and capacity. Assessing the complexity and capacity of floristic diversity in urban zones will help determine whether the current levels and rates of urbanization are safe for the ecosystems in question. The concepts of complexity and capacity indicators in biodiversity studies were first introduced by M.I. Gulamov (2017b, 2023).

Biodiversity is a fundamental property of ecosystems, reflecting their complexity and structure. Species diversity determines the complexity of structure and the power of ecosystems (Brodsky, 2002; Lebedeva, Krivolutsky, 2002).

In natural conditions, any ecosystem strives for balance and stability. Moreover, the more complex the ecosystem—i.e., the higher its level of diversity—the more likely it is to maintain stability over time and space (Nikolaikin et al., 2003).

The level of complexity implies the presence of multiple forces in equilibrium. If there is only one force, it is meaningless to talk about its balancing. In this context, complexity is a balanced diversity or a hierarchically complex structure.

The natural increase in species diversity leads to intensified competition among species, reducing the distance between them and increasing mutual pressure. As a result, specialization occurs in biomes, ecosystems, and communities, leading to the differentiation of ecological niches.

Complexity (trade-off) is meaningful only in the presence of diversity. Without diversity, trade-offs are impossible.

Capacity refers to the rate at which work is performed, energy is transferred, or a response is made. In mathematics, the capacity of a set is a characteristic that generalizes the concept of the number of elements in a finite set. This concept is based on natural ideas about comparing sets. If we replace the set of biological species in a specific ecosystem with the concept of biodiversity in that ecosystem, it becomes quite natural to talk about the capacity of biodiversity.

Based on these concepts, the phrase "capacity of diversity (biodiversity)" can be defined as a magnitude characterizing the potential response of diversity (biodiversity) to external forces.

In the context of this work, it is appropriate to consider the capacity of biodiversity as a measure characterizing the potential response of an ecosystem to external factors. To better understand this indicator, an analogy can be drawn with the capacity of a plant.

A plant's capacity is determined by the rate at which it produces oxygen, absorbs carbon dioxide, or purifies the surrounding environment. In this context, the capacity of a tree surpasses that of a shrub or herbaceous cover.

However, when discussing the capacity of biodiversity in the plant world of a specific ecosystem, we are referring not to the capacity of an individual plant species, but rather to the indicator of the overall viability potential of the entire ecosystem. The capacity of plant biodiversity is not simply the sum of the capacities of individual species, but the ability of the ecosystem to sustain functioning, adapt, and recover.

The question of the equivalence of the capacity of biodiversity in trees, shrubs, and grasses is important and requires careful consideration. From the perspectives of physics and biology, the capacity of biodiversity in these plant groups is not equivalent, as their ecological roles and adaptation abilities differ.

Trees, shrubs, and grasses occupy different vegetation layers and perform various ecological functions. Trees form the upper layer, shrubs the middle layer, and herbaceous plants the lower layer. These differences affect their ability to perform photosynthesis, absorb carbon dioxide, and produce oxygen. For example, trees, due to their height and structure, can absorb more carbon dioxide and produce more oxygen compared to shrubs and grasses. Additionally, trees play a key role in climate formation, soil erosion protection, and creating conditions for the habitat of other organisms. Shrubs and grasses also perform important functions, but their impact on the ecosystem differs.

Thus, calculating the capacity of biodiversity for these groups of plants separately is plausible and justified, as their ecological roles and adaptation abilities differ.

The calculation of complexity and capacity indicators for biodiversity is an important tool for assessing and monitoring biodiversity in natural ecosystems. It allows for the determination of the state of the ecosystem, the exploration of its structure, and aids in the development of strategies for conserving species diversity.

This issue is of great significance, as without studying the capacity of biodiversity in the researched geographical landscape (regardless of the scale of the territory), any planning of economic activities can lead to irreversible ecological consequences. All existing ecological disasters on a global scale today are the result of such thoughtless approaches (Brodsky, 2002; Conservation and Restoration of Biodiversity, 2002).

Any activities conducted must take into account the complexity and capacity of the biodiversity of the studied landscape to avoid the emergence of new, more global ecological problems.

The goal of this work is to study the evenness of species abundance, the Shannon index, the complexity, and the capacity of biodiversity in the urban flora of the city of Bukhara, Republic of Uzbekistan, as well as to analyze the results obtained. In the course of the study, we rely on species biodiversity data presented in the work of S.M. Gafarova et al., 2024.

Species abundance evenness is an important tool for assessing the structure of communities in different ecosystems. This method allows for identifying patterns in the distribution of species, determining key species that play an important role in the ecosystem, and tracking changes in the community over time.

1.1 Community structure assessment

Comparing species abundance across different locations or time periods helps identify changes in community composition. This is useful for monitoring the impact of anthropogenic factors, such as climate change or urbanization, on biodiversity.

1.2 Identifying keystone species:

Keystone species have a significant impact on the structure and functioning of an ecosystem. They can regulate the population sizes of other species, influence the physical habitat, and contribute to species diversity. Their removal can lead to substantial changes within the ecosystem.

1.3 Analyzing ecological trends

Species abundance evenness allows for tracking community changes, identifying trends, and predicting potential ecological consequences. This is particularly important for developing biodiversity conservation strategies and the sustainable use of natural resources.

Thus, species abundance evenness is a powerful tool for understanding ecosystem dynamics, identifying keystone species, and assessing the impact of various factors on biodiversity.

II. MATERIALS AND METHODS

From 2021 to 2024, a study was conducted to investigate the biodiversity of the urban flora in the arid zone of Bukhara city, Republic of Uzbekistan. The results of this research were published in 2021 and 2024 (Gafarova, Gulamov, 2021; Gafarova et al., 2024). This was the first such detailed study of the urban flora biodiversity of Bukhara city.

The aim of these works was to utilize the minimal area method, which involves a sample plot that allows for a general characterization of a specific flora. The study relied on data from personal observations, the cadastral map of Bukhara city (Gafarova, Gulamov, 2021), the Bukhara city beautification department, as well as data from H.K. Esanov (Esanov, 2016a,b; Esanov, Sharipova, 2020).

During the study, an area of 45,739 m^2 was surveyed, representing approximately 1.5% of the total vegetative cover of Bukhara city, which, according to cadastral data, amounts to 2,950,100 m^2. For a more detailed understanding, the vegetative cover of Bukhara city comprises 2,950,100 m^2, including (Gafarova, Gulamov, 2021):

Green plantation areas: 954,500 m^2
Annual plantings: 1,034,000 m^2
Perennial plantings: 126,000 m^2
Other types of green spaces: 835,600 m^2

The total number of trees in Bukhara city is 2,536,500, according to the city's cadastral data.

The study encompassed a significant portion of the city's vegetative cover, providing representative data on the urban flora biodiversity of Bukhara. Assessments were conducted across 45 sample plots situated in various parts of Bukhara city—including the northern area (Gijduvan Street), southern area (Navoi Avenue and Piridastgir Street), western area (Khavzi Bodom Street), eastern area (B. Naqshband Street), and central areas (I. Muminov Street, Mustaqillik Street, and M. Iqbol Street)—to ensure maximum representativeness of the urban flora (Gafarova et al., 2024) (Figure 1).

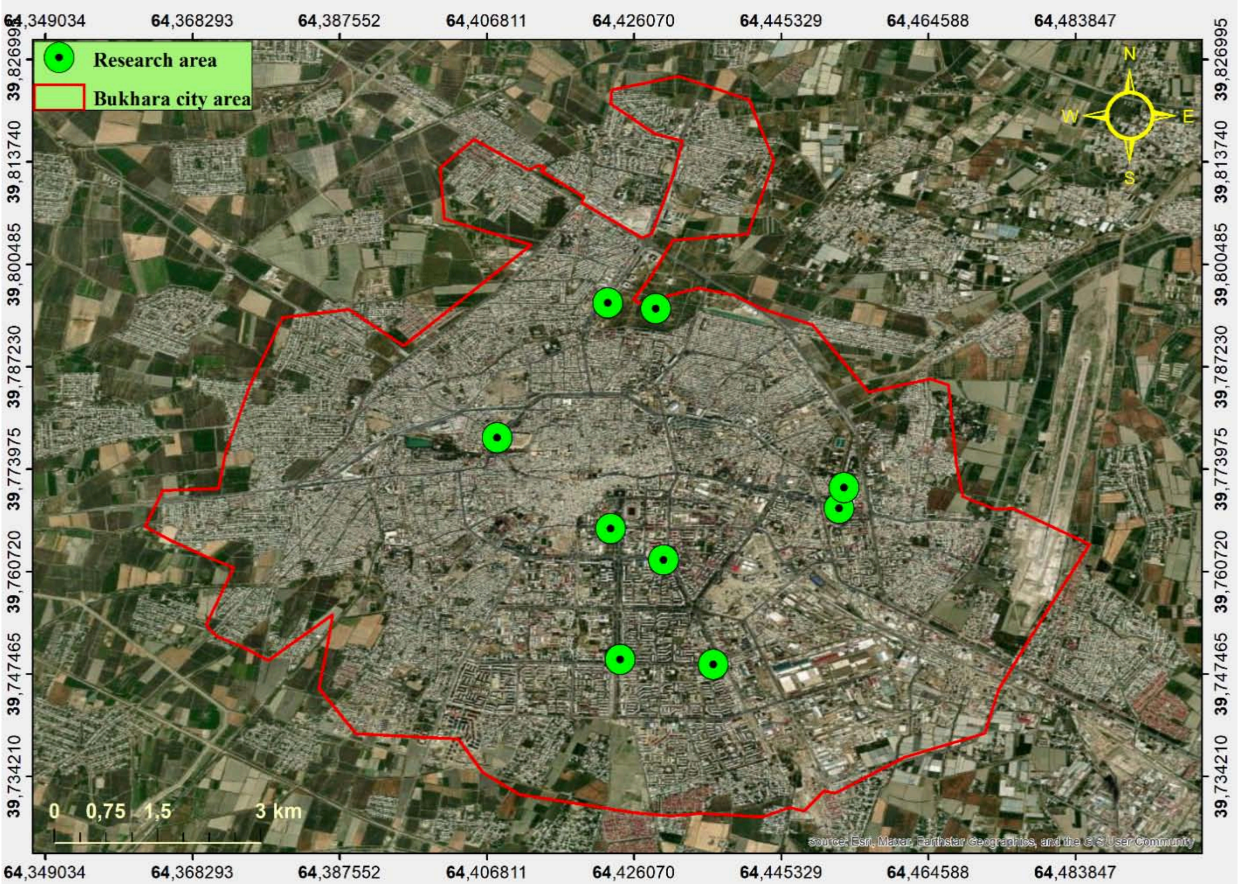

Figure 1: Map of Bukhara city. Observation sites are marked in green.

During the study of the urban flora biodiversity in Bukhara city, sample plots measuring 1,000 m² (35×30 m or 50×20 m) were selected for field research. This plot size was chosen to facilitate the analysis of species biodiversity data across the entire city.

The minimal area method, where the study area represents a sample plot that characterizes a specific flora, is an effective tool for assessing biodiversity. It provides representative data on the composition and structure of vegetation within a limited area, which is particularly useful in urbanized landscapes.

The choice of sample plot size depends on the research objectives, characteristics of the study area, and available resources. In some cases, smaller plots, such as 100 m², may be used for detailed biodiversity analysis. However, to obtain more comprehensive data on vegetation over larger areas, using plots of 1,000 m² may be more appropriate.

It is important to note that selecting the size of sample plots should consider the specific characteristics of the ecosystem under study, resource availability, and research objectives. In urbanized areas like

Bukhara city, utilizing 1,000 m² plots enables effective characterization of the flora and provides data that can be used to assess the state and dynamics of vegetation at the city level.

During the study of the urban flora biodiversity in Bukhara city, detailed floristic descriptions of the surveyed plots were conducted, quantifying the presence of species across different life forms using standard methodologies. Additionally, for each tree, morphometric parameters of the trunk and crown were measured, and their vitality was assessed.

A biodiversity index is a quantitative measure that reflects the variety of species in a specific area or ecosystem. Several methods exist for calculating biodiversity indices, such as the Shannon index, Simpson's index, Pielou's index, and others. These indices can account for various parameters, including species richness, evenness, and relative abundances (Magurran, 1992; Odum, 1986; Geography and Monitoring of Biodiversity, 2002; Gulamov, 2017 b; Gulamov, 2022 a, b).

The Shannon index is a quantitative measure that characterizes the diversity of species in a specific area or ecosystem. A higher value of the index indicates a more diverse and evenly distributed species composition within the ecosystem. This index allows for comparisons of biodiversity across different ecosystems or for tracking changes in biodiversity within the same ecosystem over time.

The formula for calculating the Shannon index includes the frequency of occurrence of each species in the ecosystem. A more even distribution of species leads to a higher Shannon index value, while the dominance of one or a few species results in a lower value.

Calculating the complexity indicator, aligning species abundance (probabilities of species occurrence) and the Shannon index for the biodiversity of the urban flora in the arid zone of Bukhara city, Uzbekistan, will be conducted following the methodology presented in the work of M.I. Gulamov (2017b, 2022a, 2023).

The values of the complexity indicator (C_d) and the capacity (M) of biodiversity for the study of real ecological systems are calculated for the first time. The complexity indicator (C_d) serves a theoretical purpose for assessing the complexity level of an ecological system. In contrast, the capacity (M) of biodiversity has a practical application and evaluates the potential viability of the ecosystem.

Since the C_d and M indicators are being calculated for the first time based on real data, it is challenging to assess them accurately. To evaluate the M indicator, we will use the "first approximation" table provided by M.I. Gulamov (2023).

Table 1: Levels of the "First Approximation" Capacity of Biodiversity Parameter Value

0–0.25	Low Capacity of Biodiversity
0,25–0,5	Approaching the Average Capacity of Biodiversity
0,5–0,75	Above Average Capacity of Biodiversity
0,75–1,0	High Capacity of Biodiversity

Complexity Indicator C_d (Gulamov, 2017):

$C_d = 1 - \frac{1}{N}$, where N – number of species of urban flora in the studied area. Maximum value $C_d \rightarrow 1$.

Species Occurrence Frequency Probability $\left(P_i\right)$ and Shannon Index $(\overline{H})$ (Magurran, 1992; Gulamov, 2022):

$P_i = \frac{n_i}{S}$, where n_i − number of individuals (Ni) of the ith species, S− total number of individuals of all species $(S = \sum n_i)$.

Shannon Index $(\overline{H})$:

$\overline{H} = -\sum P_i lnP_i = \sum P_i ln\frac{1}{P_i}$, where P_i – probability of occurrence of the i − th species $(i = 1, ..., N)$.

Capacity of Biodiversity (M) *(Gulamov, 2023)*

$M = \frac{N}{S}$, where N- number of species of urban flora, S− total number of individuals of all species $(S = \sum n_i)$, n_i − number of individuals of the i − th species.

Based on the data on the biodiversity of the urban flora of Bukhara city presented in our previous work (Gafarova et al., 2024), we will calculate, using the aforementioned methodology, the frequency of species occurrence $\left(P_i\right)$, the complexity indicator (C_d), the Shannon index $(\overline{H})$, and the capacity (M) of biodiversity.

The results of our calculations for the biodiversity of trees, shrubs, and herbs (species occurrence probability $\left(P_i\right)$, complexity indicator (C_d), Shannon index $(\overline{H})$, and capacity (M) of biodiversity) are presented in Tables 2, 3, and 4.

Table 2: Results of calculations for trees

№	Plant Name	n_i	P_i
1	*Albizia julibrissin* Durazz.	46	0,0101
2	*Ailanthus altissima* (Mill.) Swingle	82	0,0180
3	*Acer negundo* L.	14	0,0031
4	*Aesculus hippocastanum* L.	17	0,0037
5	*Catalpa bignonioides* Walter	107	0,0235
6	*Cydonia oblonga* Mill.	38	0,0084
7	*Cupressus arizonica* Greene	41	0,0090
8	*Elaeagnus angustifólia* L.	18	0,0040
9	*Fagus orientalis* Lipsky	3	0,0007
10	*Fraxinus lanceolata* Borkh.	171	0,0376
11	*Gleditsia triacanthos* L.	41	0,0090
12	*Juniperus virginiana* L.	114	0,0251
13	*Juglans regia* L.	1	0,0002
14	*Morus alba* L.	215	0,0473
15	*Morus rubra* L.	265	0,0583
16	*Morus nigra* L.	45	0,0099

17	*Malus domestica* Borkh.	30	0,0066
18	*Maclura pomifera* (Raf) C.K.Schneid	25	0,0055
19	*Paulownia tomentosa* (Thunb.) Steud.	42	0,0092
20	*Pinus brutia var. eldarica* (Medw.) Silba	886	0,1948
21	*Pinus nigra* J.F.Arnold	10	0,0022
22	*Pinus nigra subsp. Pallasiana* (Lamb.) Holmboe	238	0,0523
23	*Picea pungens* Engelm.	3	0,0007
24	*Populus alba L.*	39	0,0086
25	*Populus bachofenii* Wierzb. Ex Rochel	104	0,0229
26	*Platanus orientalis* L.	54	0,0119
27	*Platycladus orientalis* (L.) Franco	557	0,1225
28	*Prunus avium* L.	52	0,0114
29	*Prunus persica* (L.) Batsch	8	0,0018
30	*Prunus cerasus* L.	49	0,0108
31	*Prunus armeníaca* L.	68	0,0150
32	*Prunus domestica L.*	3	0,0007
33	*Prunus communis* L.	5	0,0011
34	*Robinia pseudoacacia* L.	5	0,0011
35	*Quercus robur* L.	54	0,0119
36	*Salix alba* L.	22	0,0048
37	*Salix excelsa* S.G. Gmel	8	0,0018
38	Salix babylonica var.tortuosa x alba var.recticapus (S.X` Sverdlovskaja Isvilistaja 2` V.Schaburov et l. Beljaeva)	4	0,0009
39	*Styphnolobium japonicum (L.) Schott*	*68*	*0,0150*
40	*Tilia cordata Mill.*	*22*	*0,0048*
41	*Thuja occidentalis L.*	*50*	*0,0110*
42	*Ulmus parvifolia L.*	*824*	*0,1812*
43	*Ulmus densa Litv.*	*100*	*0,0220*
Total (S)		*4548*	
Value of the Complexity Coefficient Function (C_d)		*0,9767*	
Value of the Shannon Index $(\overline{H})$		*2,8267*	
Value of the Capacity of Biodiversity (M)		*0,0095*	
Level of Capacity of Biodiversity according to Table 1:		*Low Level of Capacity of Biodiversity*	

Table 3:Results of Calculations for Shrubs

№	Plant Name	n_i	P_i
1	*Tamarix ramosissima* Ledeb.	5	0,0039
2	*Caesalpinia gilliesii* (Wall. Ex Hook.) D.Dietr.	5	0,0039
3	*Catharanthus roseus* (L.) G.Don	12	0,0093
4	*Euonymus japonicas* Thunb.	36	0,0280
5	*Ficus carica* L.	22	0,0171
6	*Hibiscus syriacus* L.	2	0,0016
7	*Jacobaea maritima* (L.) Pelser & Meijden	35	0,0272
8	*Ligustrum vulgare* L.	152	0,1181
9	*Lagerstroemia indica* L.	3	0,0023
10	*Lonicera japonica Thunb.*	2	0,0016
11	*Lycium ruthenicum* Murray	3	0,0023
12	*Mahonia aquifolium* (Pursh) Nutt.	3	0,0023
13	*Parthenocissus quinquefolia* (L.)	20	0,0155
14	*Punica granatum* L.	5	0,0039
15	*Rosa chinensis* Jacq.	409	0,3178
16	*Rosa canina* L.	86	0,0668
17	*Ribes nigrum* L.	23	0,0179
18	*Spartium junceum* L.	7	0,0054
19	*Vitex agnus-castus* L.	3	0,0023
20	*Vítis vinífera* L.	49	0,0381
21	*Yucca filamentosa* L.	405	0,3147
Total (S)		1287	
Value of the Complexity Coefficient Function (C_d)		0,9524	
Value of the Shannon Index ($\overline{H}$)		1,9031	
Value of the Capacity of Biodiversity (M)		0,0163	
Level of Capacity of Biodiversity according to Table 1:		Low Level of Capacity of Biodiversity	

Table 4: Results of Calculations for Herbs

№	Название растений	на м²	n_i	P_i
1	*Alhagi kirghisorum* Schrenk	1-2	67499	0,0023
2	*Achillea millefolium* L.	2-3	112498	0,0037
3	*Aconogonon divaricatum* (L.) Nakai ex Mori	2-3	112498	0,0037
4	*Alcea rosea* L.	1-2	67499	0,0023
5	*Althaea officinalis* L.	2-3	112498	0,0037
6	*Amaranthus tuberculatus* (Moq.) Sauer	4-5	202496	0,0067
7	*Amaranthus viridis* L.	18-20	854981	0,0284

8	*Amaranthus retroflexus* L.	5-6	247495	0,0082
9	*Anagallis arvensis* L.	60 м² – 16 шт	16	0.0000
10	*Anchusa azurea* Mill.	2-3	112498	0,0037
11	*Arctium leiospermum* Juz. et Ye. V. Serg.	1-2	67499	0,0023
12	*Artemisia absinthium* L.	3-4	157497	0,0052
13	*Artemisia annua* L.	12	539988	0,0179
14	*Artemisia vulgaris* L.	4-5	202496	0,0067
15	*Aster amellus L.*	5-6	247495	0,0082
16	*Asperugo procumbens* L.	18-20	854981	0,0284
17	*Atriplex micrantha* C.A. Mey.	17-18	787483	0,0261
18	*Atriplex tatarica* L.	13	584987	0,0194
19	*Bromus tectorim L. ялтирбош*	6-7	292494	0,0097
20	*Bassia hyssopifolia* (Pall.) Kuntze	4-5	202496	0,0067
21	*Bassia scoparia* f. Trichophylla (hort. ex Voss) S. L. Welsh)	2-3	112498	0,0037
22	*Calendula officinalis* L.	3-4	157497	0,0052
23	*Camelina microcarpa* Andrz. ex DC.	1-2	67499	0,0023
24	*Canna generalis* L.H. Bailey & E.Z. Bailey	65 м² – 98 шт	98	0.0000
25	*Capsella bursa-pastoris* subsp. *thracicus* (VELEN.) STOJ. & STEF.	19-20	877481	0,0293
26	*Cardaria repens* (Schrenk) Jarm.	13-14	607487	0,0210
27	*Centaurea solstitialis* L.	1-2	67499	0,0023
28	*Cirsium vulgare* (Savi) Ten.	2-3	112498	0,0037
29	*Chenopodium album* L.	18	809082	0,0268
30	*Convonvulus arvensis* L.	7-8	337493	0,0112
31	*Coreopsis lanceolata* L.	21-22	967479	0,0321
32	*Cuscuta Lehmanniana* L.	4-5	202496	0,0067
33	*Cynodon* dactylon L.	22	989978	0,0329
34	*Cyperus rotundus L.*	10-11	472490	0,0157
35	*Cynanchum acutum* L.	3-4	157497	0,0052
36	*Cynanchum sibiricum* Willd.	2-3	112498	0,0037
37	*Cichorium intybus* L.	1-2	67499	0,0023
38	*Chrysanthemum x koreanum* Hort.	5-6	247495	0,0082
39	*Cucurbita pepo* L.	2-3	112498	0,0037
40	*Datura innoxia* Mill.	60 м² – 5 шт	5	0.0000
41	*Descurainia Sophia* L.	25	1124975	0,0374
42	*Echinochloa crus-galli* (L.) P.Beauv.	5-6	247495	0,0082
43	*Eregeron bonariensis* L.	2-3	112498	0,0037
44	*Erigeron canadensis* L.	1-2	67499	0,0023
45	*Gelosia cristata* L.	2-3	112498	0,0037
46	*Geranium pusillum* L.	1-2	67499	0,0023
47	*Helianthus annuus* L.	32м² – 30 шт	30	0.0000
48	*Heliopsis helianthoides* Summer Night	12-13	562488	0,0187
49	*Hordeum bulbosum* L.	30	1349970	0,0449
50	*Lactuca serriola* L.	5-6	247495	0,0082
51	*Lactuca tatarica* (L.) C.A. Mey.	10	449990	0,0150

52	*Lathyrus aphaca* L.	1	44999	0,0015
53	*Lamium amplexicaule* L.	5	224995	0,0075
54	*Lepidium latifolium* L.	2-3	112498	0,0037
55	*Lepidium ruderale* L.	3-4	157497	0,0052
56	*Leuzea repens* (L.) D.J.N.Hind.	3-4	157497	0,0052
57	*Lolium perenne* L.	21	944979	0,0314
58	*Malva neglecta Wallr.*	5-6	247495	0,0082
59	*Medicago sativa* L.	8-10	404991	0,0134
60	*Melilotus officinalis* (L.) Mill.	12-13	562488	0,0187
61	*Melilotus albus* Medik.	1-2	67499	0,0022
62	*Mentha asiatica* Boriss.	7-8	337493	0,0112
63	*Mirabilis jalapa* L.	5-6	247495	0,0082
64	*Ocimum basilicum* L.	15-16	697485	0,0232
65	*Peganum harmala* L.	1	44999	0,0015
66	*Portulaca oleracea* L.	7-8	337493	0,0112
67	*Portulaca grandiflora* Hook.	1-2	67499	0,0022
68	*Panicum miliaceum* L.	7-8	337493	0,0112
69	*Phaseolus vulgaris* L.	3-4	157497	0,0052
70	*Phragmites australis* (Cav.) Trin. ex Steud.	5-6	247495	0,0082
71	*Plantago lanceolata* L.	7-8	337493	0,0112
72	*Plantago major* L.	5-6	247495	0,0082
73	*Poligonum argurocoleon* Steud. ex G. Kuntze	2-3	112498	0,0037
74	*Polygonum aviculare* L.	16-17	742484	0,0247
75	*Potentilla supine* L.	2-3	112498	0,0037
76	*Ricinus communis* L.	1	44999	0,0015
77	*Rorippa sylvestris* (L.) Bess.	1-2	67499	0,0023
78	*Symphyotrichum graminifolium* (Spreng.) G.L.Nesom	5-6	247495	0,0082
79	*Symphyotrichum novi-belgii* (L.) G.L. Nesom	4-5	202496	0,0067
80	*Schoenoplectiella mucronata* (L.) J. Jung	2-3	112498	0,0037
81	*Stelarria media* (L.) Vill.	11-12	517489	0,0172
82	*Seteria viridis* (L.) P.Beauv	20-21	922480	0,0307
83	*Sisymbrium irio* L.	15	674985	0,0224
84	*Sonchus arvensis* L.	2-3	112498	0,0037
85	*Tagetes patula* L.	19-20	877481	0,0292
86	*Taraxacum bicorne* Dahlst	8-9	382492	0,0127
87	*Tribulus terrestris* L.	3-4	157497	0,0052
88	*Trifolium pratense* L.	10-11	472490	0,0157
89	*Trifolium repens* L.	10-15	562488	0,0186
90	*Veronica polita* Fr.	7-8	337493	0,0112

91	*Xanthium albinum* (Widd.) Scholz-Sukopp	1-2	67499	0,0023
92	*Zínnia elegans* Jacq.	13-14	607487	0,0202
93	*Zygophyllum oxianum* Boriss.	2-3	112498	0,0037
Total (S)			30081117	
Value of the Complexity Coefficient Function (C_d)		0.9892		
Value of the Shannon Index ($\overline{H}$)		4,1348		
Value of the Capacity of Biodiversity (M)		0,0000		
Level of Capacity of Biodiversity according to Table 1:		Low Level of Capacity of Biodiversity		

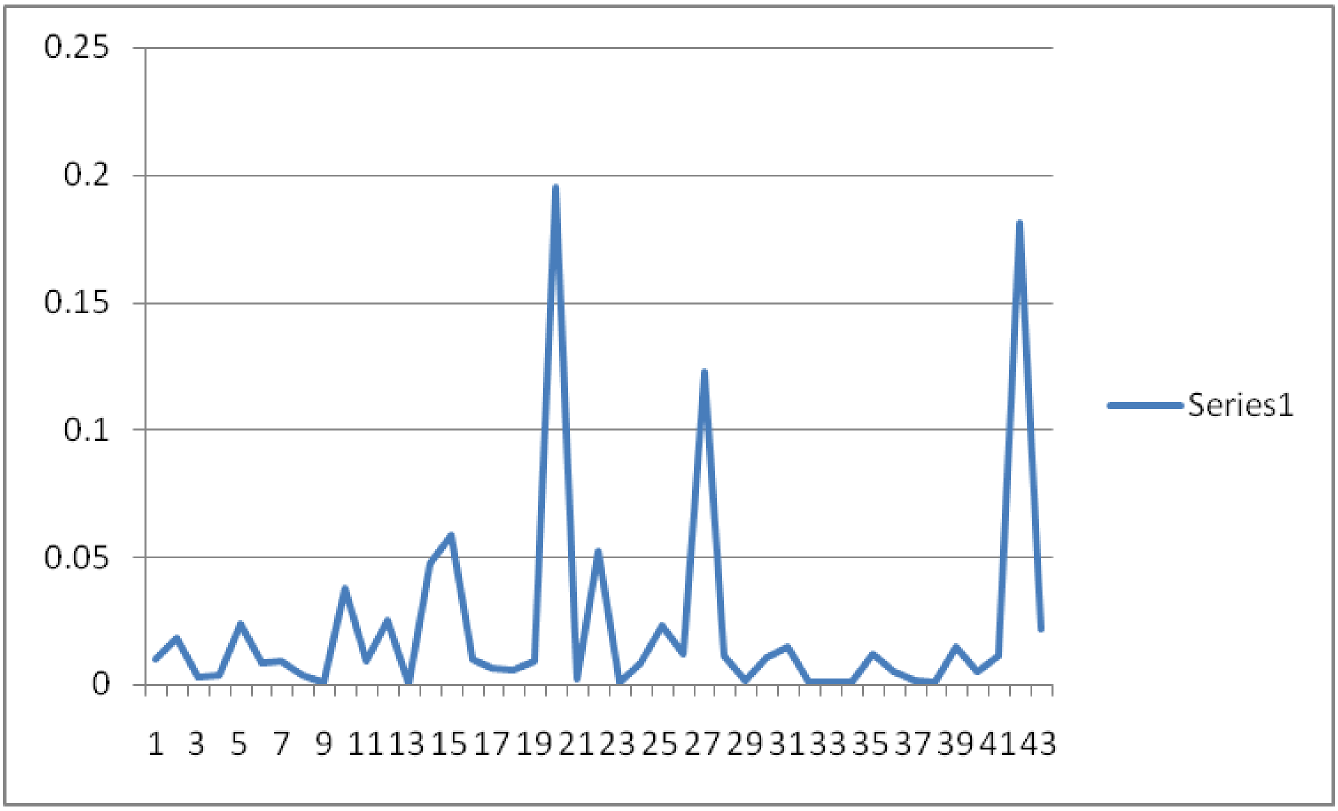

Fig. 2: Graphical representation of the frequency of occurrence of tree species in the urban flora of Bukhara city, RUz. The evenness of species abundance is absent.

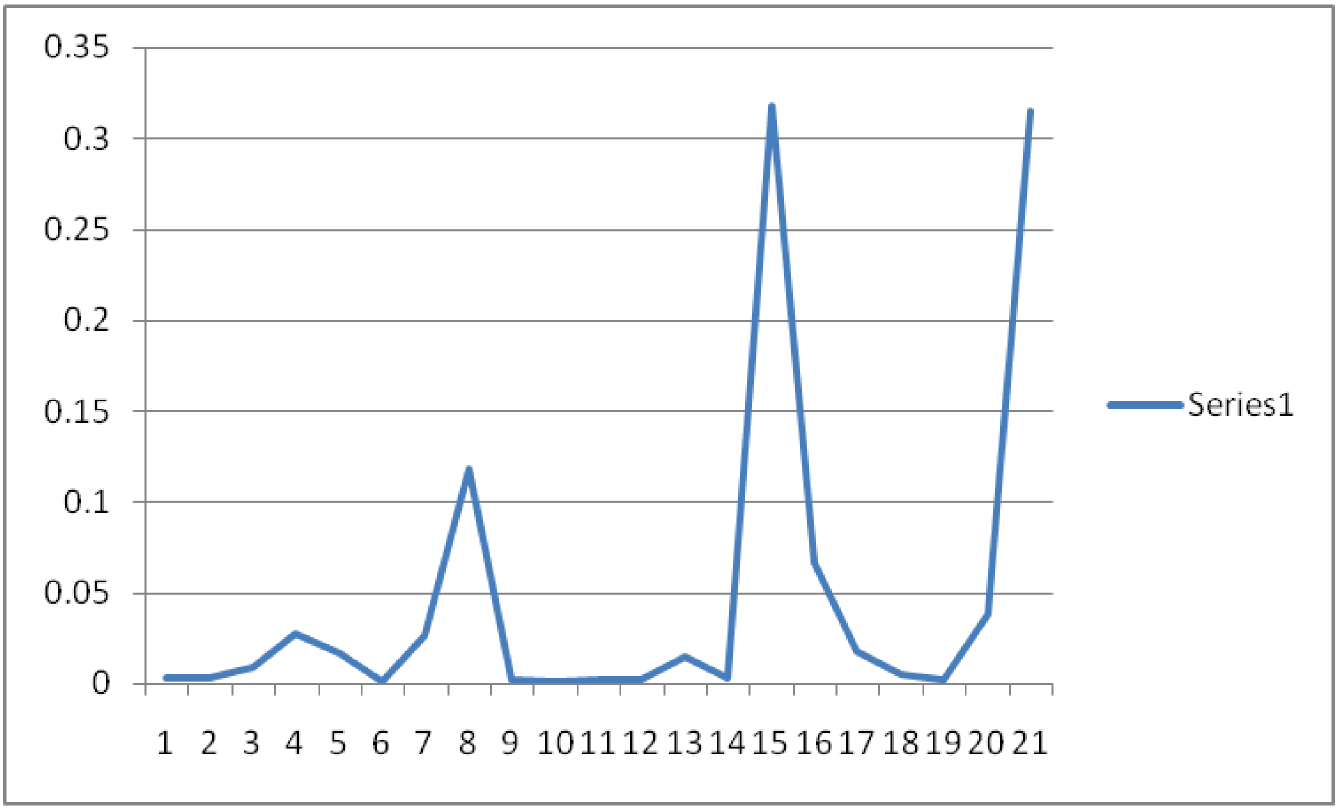

Fig. 3: Graphical representation of the frequency of occurrence of shrub species in the urban flora of Bukhara city, RUz. The evenness of species abundance is absent.

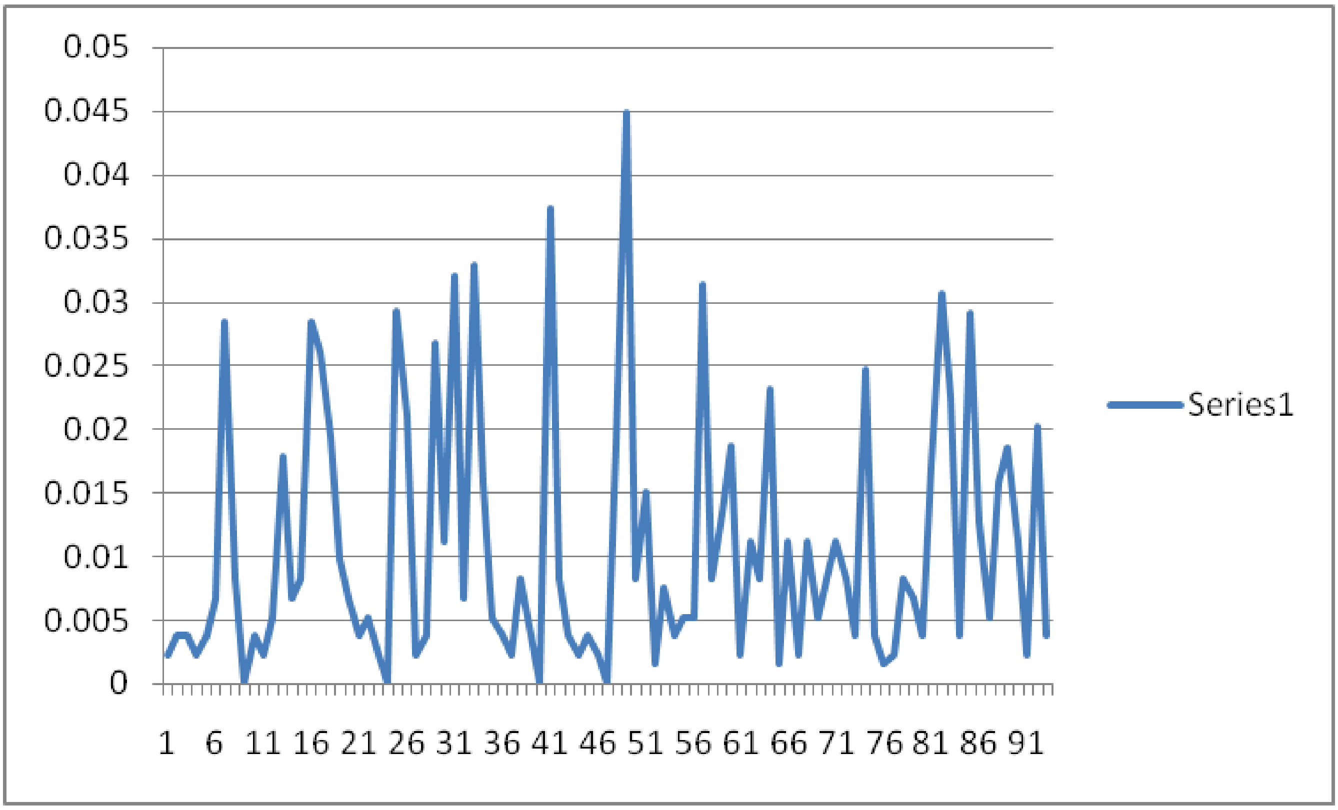

Fig. 4: Graphical representation of the frequency of occurrence of herb species in the urban flora of Bukhara city, RUz. The evenness of species abundance is absent.

III. DISCUSSION OF RESULTS

Our analysis of the biodiversity of Bukhara city's urban flora reveals:

Uneven distribution of species abundance: Dominance of several tree species (*Pinus brutia var. eldarica*, *Ulmus parvifolia*, *Platycladus orientalis*), shrub species (*Rosa chinensis*, *Yucca filamentosa*), and herb species (*Hordeum bulbosum* L.; *Descurainia Sophia* L.; *Seteria viridis* (L.) P.Beauv; *Coreopsis lanceolata* L).

Relatively high complexity index (C_d): Indicating diversity of life forms within the community.

Low Shannon index ($\overline{H}$): Suggesting a low level of biodiversity.

Low capacity (M) of biodiversity: Indicating the ecosystem's limited ability to support species diversity.

These results are presented in Tables 2, 3, 4 and Figures 2, 3, 4.

If we perceive the complexity index (C_d) as a compromise between species, then its relatively high level indicates a balanced coexistence of species in the community (Gulamov, 2017 b). This means that species are in a state of dynamic equilibrium, where each species occupies its ecological niche, minimizing competition and contributing to the stability of the ecosystem.

In addition, a high level of the complexity index indicates a low level of combination of environment-forming ecological factors. Environment-forming factors, such as various types of flora, form non-stationary scalar ecological survival fields that determine the conditions for the existence and development of species (Gulamov, 2021). In urban ecosystems, where environmental conditions are often variable and subject to anthropogenic influences, such survival fields can be unstable, which affects the structure and dynamics of vegetation.

Thus, at a low level of capacity (M) of biodiversity and relatively high values of the complexity index (C_d), an ecological tolerance zone is created. This means that there is an acceptable combination of species in this community that are able to survive and coexist in urbanized environments. However, such a situation may also indicate a decrease in the ecosystem's resistance to external influences and the need to take measures to maintain and restore it.

Table 5: The results obtained from tables 2, 3, and 4 (correspondence in ascending order) are presented in

	N	S	C_d	$\overline{H}$	M
Shrubs	22	1287	0,9524	1,9031	0,0163
Trees	43	4548	0,9767	2,8267	0,0095
Herbs	93	30081117	0,9892	4,1348	0,0000

From the data in Table 5, it is evident that the tendency of the value of the indicator M to a minimum relative to the values of $\overline{H}$ and C_d is explained by the fact that in these life forms of plants, the tendency of the ratio N/S to a minimum, that is, the tendency of the value of N to a minimum and the value of S to a maximum. This condition is especially characteristic of herbs (the value of S is too high). The convergence of the values of N and S can lead to an increase in the value of M and to the equalization of the abundance of species in all life forms of plants.

Since n_i is the number of individuals of the i - th species, and P_i is the probability (frequency of occurrence) of the i - th species, which is a discrete random variable, the Shannon index can be taken as the entropy defined by the Boltzmann formula (Stratonovich, 1975):

$$H = -\sum_{\xi} P(\xi) \ln ln\, P(\xi) .$$

With this approach, the increase in the number of species (N) and the total number of individuals of all species (S), respectively, leads to an increase in the values of the complexity index (C_d) and entropy (a measure of disorder) ($\overline{H}$), while the value of their capacity (M) decreases accordingly. A consequence of complication is an increase in entropy, which, in turn, after a certain time, leads to structural disintegration, that is, the potential (capacity) of the ecosystem to resist external influences is minimized. This scenario of events is natural.

The advantage of complexity and capacity indicators of biodiversity compared to the Shannon index is that, for calculating complexity and capacity indicators of biodiversity, unlike the Shannon index, only the number of species (N) and the sum of individuals of all species (S) of biodiversity are needed. At the same time, for the Shannon index, in addition to the number of species (N) and the sum of individuals of all species (S) of biodiversity, an additional calculation of the probability of occurrence frequency P_i for each species of biodiversity is required, which requires significant time and labor costs. Nevertheless, each of the indicators we consider only complements each other when analyzing the species biodiversity of the flora.

If the tree, shrub, and herb species under consideration (listed in Tables 2, 3, and 4) were in natural conditions, there would be a high probability of their extinction. However, since they are part of the urban flora, their artificial support ensures their existence. All urban floras are artificially maintained, similar to agriculture.
In the city of Bukhara, as in other cities, urban services are engaged in maintaining and renewing vegetation, including trees, shrubs, and herbs. These plants beautify the urban landscape until they require replacement or renewal. This practice is part of the city's policy on landscaping and maintaining public amenities.

Based on the results we obtained, it can be asserted that further development of the city's construction without a significant improvement in the biodiversity of Bukhara's urban flora is practically impossible. Currently, life in Bukhara during the summer becomes unbearable. It is necessary to create green corridors between buildings with diverse plant species.

A characteristic principle for natural ecosystems is the absence of identity, a unified logic, harmony, purpose, and order (Gulamov, 2016). In urban ecosystems, this principle is violated, since a subjective logic, harmony, purpose, and order are introduced into them. This is the main reason for the above-mentioned results for the indicators: C_d, P_i, $\overline{H}$ and M.

The low level of biodiversity capacity observed in all studied objects is characteristic of any urban flora. Given that the number of species in urban ecosystems is often determined by subjective factors, the results we obtained are quite plausible.

To achieve optimal values of indicators C_d, P_i, $\overline{H}$ and M, which increase the resilience and capacity of urban flora biodiversity in resisting external environmental impacts, it is necessary to strive for a convergence of the number of species (N) and the sum of individuals of all species (S). In other words, increasing the number of species and reducing the number of individuals of each species contributes to increasing the stability of the ecosystem. This approach is supported by research, for example, the work of Galina Yu. Morozova (2024), which notes that the use of population research methods makes it possible to select species adapted to the stresses of urbanization and create ecologically stable plantings.

IV. CONCLUSION

1. From a botanical point of view, the biodiversity capacity of trees, shrubs, and herbs is different, so they should be evaluated separately for more accurate analysis. This approach allows taking into account the characteristics of each group of plants and their contribution to the ecosystem.
2. The calculation of complexity and capacity indicators of flora biodiversity is an important tool for assessing and monitoring biodiversity in natural ecosystems. These indicators help to determine the degree of species diversity, their evenness, and the overall condition of the ecosystem, which is important for developing effective measures for the conservation and restoration of natural communities.
3. Equalizing the abundance of species is an important tool for assessing the structure of a community in different ecosystems. This indicator allows determining the degree of uniformity in the distribution of individuals among species, which helps to identify key species that play an important role in ecosystems. In addition, the analysis of the equalization of species abundance contributes to the identification of ecological trends or changes over time, which is important for monitoring the state of ecosystems and developing effective measures for their conservation and restoration.

The analysis of urban flora biodiversity in the arid zone of Bukhara city revealed the following features:

a. Uneven abundance of species (P_i): The dominance of several species of trees, shrubs, and herbs is observed, which indicates a low level of evenness in the distribution of species in the community.
b. High level of complexity (C_d): The presence of a significant number of species and their interactions indicates a complex structure of the community, which indicates a balance in the coexistence of species.
c. Shannon Index ($\overline{H}$): The biodiversity of herbs is twice as high as that of trees and three times higher than that of shrubs, which reflects the higher diversity of the herbaceous layer compared to the tree and shrub layers.
d. Capacity indicator (M): A low level of capacity indicates a limited stability of functioning, adaptation, and recovery of the urban flora of Bukhara city.

5. To increase the resilience and adaptability of urban flora, the following is recommended: Increasing species diversity: The introduction of additional plant species can contribute to increasing the stability of the ecosystem. Creation of green corridors: The development of green spaces between buildings helps to improve the microclimate and increase biodiversity. Monitoring and management of vegetation health: Regular checks on plant health and timely intervention to prevent diseases and pests help maintain a balance between the number and area of species. The application of these measures will help achieve a more balanced distribution of species and increase the biodiversity of the urban flora of Bukhara city.
6. A characteristic principle for natural ecosystems is the absence of identity, a unified logic, harmony, purpose, and order. In urban ecosystems, this principle is violated, since a subjective logic, harmony, purpose, and order are introduced into them.

GLOSSARY

1. The capacity of an ecosystem's flora biodiversity is the ecosystem's ability for sustainable functioning, adaptation, and recovery.
2. Complexity is understood as a compromise between species, that is, an indicator of the level of species coexistence or an indicator of the combination of environment-forming ecological biotic factors.

ACKNOWLEDGMENTS

We are grateful to the head of the Bukhara city landscaping department, A.T. Akhmedov, for providing data on vegetation and cadastral maps of Bukhara.

Funding Source

This research did not receive any specific grants from funding agencies in the public, commercial, or non-profit sectors.

Author’s Contributions

Mukhamad Isakovich Gulamov: Designed the project, analyzed the data and wrote the manuscript.
Saida Muhamadjonovna Gafarova: Conducted fieldwork and sample collection during the 2021-2024 field season, analyzed data and was involved in writing some parts of the manuscript.

Ethics

This material is the authors’ own original work, which has not been previously published elsewhere.

Competing Interests

The authors declare that they have no competing interests.

REFERENCES

1. A Global Standard for the Identification of Key Biodiversity Areas, 2016. Version 1.0. IUCN, Gland, Switzerland.
2. Alves, B., 2024. Biodiversity loss – statistics & facts. Available from: https://www.statista.com/topics/11263/biodiversity-loss/
3. Brodsky, A.K., 2002. Introduction to problems of biodiversity. St. Petersburg: St. Petersburg State University Press [in Russian]
4. Ceplová, N., Kalusová, V., Lososová Z., 2017a. Effects of settlement size, urban heat is land and habitat type on urban plant biodiversity. Landscape and Urban Planning 159: 15–22. https://doi/org/10.1016/j.landurbplan.2016.11.004
5. Conservation and Restoration of Biodiversity. Moscow: NUMC.2002.156 p. [in Russian]
6. Christenhusz MJ, Reveal JL, Farjon A, Gardner MF, Mill RR, Chase MW (2011) A linear sequence of extant families and genera of lycophytes and ferns. Phytotaxa 19: 7–54. https://doi.org/10.11646/phytotaxa.19.1.2
7. Čeplová, N., Kalusová, V., Lososová, Z., 2017b. Does the size of settlement matter? Effects of urban heat island, settlement size and habitat type on urban plant biodiversity. Landscape and Urban Planning 159: 15–22. https://doi.org/10.1016/j.landurbplan.2016.11.004
8. Esanov, H.K., 2016a. New Plant Species in the Flora of Bukhara Oasis. Turczaninowia, 19, 77-81. https://doi.org/10.14258/turczaninowia.19.2.10 [in Russian]
9. Esanov, H.K., 2016b. The alien fraction of the flora of Bukhara oasis. Stapfia 105:92-98 [in Russian]
10. Esanov HK, Sharipova VK (2020) Addition to the flora of Bukhara region (Uzbekistan). Turczaninowia 23(1): 126–128. https://doi.org/ 10.14258/ turczaninowia.23.1.13 [In Russian]

11. Galina Yu. Morozova. Plant Viability in an Urbanized Environment// Lesnoy Zhurnal . Russian Forestry Journal. 2024. No. 6 p.106-120. [in Russian]
12. Gafarova, S.M., Gulamov, M.I., 2021. Modern physical-geographical and environmental characteristics of the city of Bukhara. Universum: Chemistry and Biology 12(90). https://doi.org/10.32743/UniChem.2021.90.12.12566 [In Russian]
13. Gafarova, S.M., Gulamov, M.I., Esanov, H.K., Umedov, A.M., 2024. Urban floristic diversity in the arid zone: a case study of Bukhara city. Acta Biologica Sibirica 10: 197–213. https://doi.org/10.5281/zenodo.10934573
14. Geography and monitoring of biodiversity. 2002. Moscow: NUMC Press. [in Russian]
15. Gulamov, M.I., 2016. Reflections on the nature of diversity. Universum: Chemistry and Biology, 4(22). Retrieved from http://7universum.com/ru/nature/archive/item/3024 [in Russian]
16. Gulamov, M.I., 2017. On the nature of biodiversity renewal. Universum: Chemistry and Biology, 10(40). Retrieved from http://7universum.com/ru/nature/archive/item/5124 [in Russian]
17. Gulamov, M.I., 2017. On the complexity parameter of diversity. Universum: Chemistry and Biology, 2(32). Retrieved from http://7universum.com/ru/nature/archive/item/4247 [in Russian]
18. Gulamov, M.I., 2021. On the concept of "Ecological field of survival". Universum: Chemistry and Biology, 6(84). Retrieved from https://7universum.com/ru/nature/archive/item/11707 [in Russian]
19. Gulamov, M.I., 2022a. ON QUESTION OF THE DYNAMICS OF STRUCTURAL CHANGES IN BIODIVERSITY. Journal of science. Lion, 31, 3-8. https://doi.org/10.5281/zenodo.6627922 [in Russian]
20. Gulamov, M.I., 2022b. On the question of the mechanisms of structural changes in diversity. Danish Scientific Journal 65: 3–6. https://doi.org/10.5281/zenodo.7274464 [in Russian]
21. Gulamov, M.I., 2023. On the Capacity Parameter of Biodiversity. Universum: Chemistry and Biology, 5(107). Retrieved from https://7universum.com/ru/nature/archive/item/15412 [in Russian]
22. Jovanović S, Glišić M (2021) Research analysis on urban flora and vegetation in Southeast Europe. Acta Botanica Croatica 80(1): 74–81. https://doi.org/10.37427/botcro-2021-004
23. Kate W (2022) Six charts that show the state of biodiversity and nature loss – and how we can go nature positive. Available from: https://www.weforum.org/agenda/2022/10/nature-loss-biodiversity-wwf/
24. Lebedeva, N.V., Krivolutsky, D.A., 2002. Biological diversity and methods of its assessment. In Geography and monitoring of biodiversity. Moscow: NUMC Press. p. 253. [in Russian]
25. Megarran, E., 1992. Ecological diversity and its measurement. Moscow: Mir. [in Russian]
26. Nikolaikin, N.I., Nikolaikina, N.E., Melihova, O.P., 2003. Ecology. Moscow: Drofa. [in Russian]
27. Odum, E.P., 1986. Ecology (Vol. 2). Moscow: Nauka. [in Russian]
28. Stratonovich R.L. Information Theory. Moscow: Soviet Radio Publishing House. 1975. P.10. [in Russian]
29. Tretyakova A, Veselkin DV, Senator SA, Golovanov YaM (2018) Factors of Richness of Urban Floras in the Ural-Volga Region. Russian Journal of Ecology 49(3): 201–208. https://doi.org/10.1134/S1067413618030098.

Electrochemical and Microscopic Studies of the Mild Steel (MS) Surface by using Metronidazole Drug as a Green Inhibitor in 1M HCl Medium

Adel H. Ali

Taiz University

ABSTRACT

In this paper, using the metronidazole pharmaceutical drug compound as a green corrosion inhibitor that can be decreasing the rate of corrosion on metallic surface, as a result of the adsorption of metronidazole on the metal surface. In this regard, we simultaneously present an overview of metronidazole compound performance, as a corrosion inhibitor in 1M HCl, and with presence different concentrations of the drug. By using Electrochemical techniques (open-circuit potential, Potentio-dynamic polarization (PP), Electrochemical Impedance Spectroscopy (EIS), Electrochemical Frequency Modulation (EFM)) that illustrate the nature of adsorption. The surface examination by scanning electron microscopy (SEM), energy dispersive X-ray (EDX), atomic force microscopy (AFM), and Fourier transforms infrared (FT-IR) are confirmed the formation thin film that adsorbed on the metal surface according to the mechanism of the adsorption processes on the polarized metal surface.

Keywords: electrochemical techniques OCP, PP, EIS, EFM and surfaces analysis SEM, EDX, AFM, FT-IR.y.

Classification: LCC Code: QD571

Language: English

Great Britain
Journals Press

LJP Copyright ID: 925644
Print ISSN: 2631-8490
Online ISSN: 2631-8504

London Journal of Research in Science: Natural & Formal

Volume 25 | Issue 4 | Compilation 1.0

Electrochemical and Microscopic Studies of the Mild Steel (MS) Surface by using Metronidazole Drug as a Green Inhibitor in 1M HCl Medium

Adel H. Ali

ABSTRACT

In this paper, using the metronidazole pharmaceutical drug compound as a green corrosion inhibitor that can be decreasing the rate of corrosion on metallic surface, as a result of the adsorption of metronidazole on the metal surface. In this regard, we simultaneously present an overview of metronidazole compound performance, as a corrosion inhibitor in 1M HCl, and with presence different concentrations of the drug. By using Electrochemical techniques (open-circuit potential, Potentio-dynamic polarization (PP), Electrochemical Impedance Spectroscopy (EIS), Electrochemical Frequency Modulation (EFM)) that illustrate the nature of adsorption. The surface examination by scanning electron microscopy (SEM), energy dispersive X-ray (EDX), atomic force microscopy (AFM), and Fourier transforms infrared (FT-IR) are confirmed the formation thin film that adsorbed on the metal surface according to the mechanism of the adsorption processes on the polarized metal surface.

Keywords: electrochemical techniques OCP, PP, EIS, EFM and surfaces analysis SEM, EDX, AFM, FT-IR.

Author: Department of Physics, Faculty of Science brunch of Al-Tourba, Taiz University, Yemen.

I. INTRODUCTION

Most organic compounds containing nitrogen (N-heterocyclic), sulfur, long carbon chain, or aromatic, and oxygen atoms are used as a corrosion inhibitor. Among them, organic compounds have many advantages such as large molecular size, soluble in water, availability, cheap, low toxicity, easy for uses, and easy production **[1]**. Natural heterocyclic mixes have been utilized for the corrosion inhibitor on the C-steel **[2]**, copper **[3]**, aluminum **[4]**, and various metals in various aqueous medium **[5]**. Adsorption of the drug molecules on the metal surface facilitates its inhibition **[6]**. Heterocyclic mixes have demonstrated more hindrance effectiveness, for C-steel in both HCl **[7]** and H_2SO_4 arrangements **[8]**, such as the medications are used inhibitors, that can compete favorably with green inhibition of corrosion, and the most medications can be synthesized from natural products. Selection of some medication as corrosion inhibitors due to the followings: (1) drug molecules contain oxygen, sulfur, and nitrogen as active sites, (2) it is environmentally friendly furthermore vital in organic responses, (3) drugs can be easily produced, and purified, (4) nontoxic compering organic inhibitors. Some medications have been investigated to be great corrosion inhibitors for metals such as Biopolymer gave 86% inhibition efficiency (IE) for Cu in NaCl **[9]**, pyromellitic di-imide linked to oxadiazole cycle gave 84.6% IE for mild steel (MS) in HCl **[10]**, 2-mercaptobenzimidazole gave 82% IE for MS in HCl Antidiabetic Drug Janumet gave 88.7% IE for MS in HCl **[11]**. Januvia gave 79.5 % IE for Zn in HCl **[12]**, Cefuroxime Axetil gave 89.9% IE for Al in HCl **[13]**, Phenytoin sodium gave 79% for MS in HCl **[14]**, Aspirin gave71% IE for MS in H_2SO_4 **[15]**, Septazole gave 84.8% IE for Cu in HCl **[16]** and Chloroquine diphosphate gave 80% IE for MS in HCl **[17]**. Study on Structural, Corrosion, and

Sensitization Behavior of Ultrafine and Coarse Grain 316 Stainless Steel Processed by Multiaxial Forging and Heat Treatment **[18]**. Investigating the corrosion of the Heat-Affected Zones (HAZs) of API-X70 pipeline steels in aerated carbonate solution by electrochemical methods **[19]**. Predictions of corrosion current density and potential by using chemical composition, and corrosion cell characteristic MS in micro alloyed pipeline steels **[20]**. Predictions of toughness, and hardness by using chemical composition, and tensile properties in microalloyed line pipe steels **[21]**.

The scope of this article is used metronidazole drug as save corrosion inhibitor for MS in the acid medium by electrochemical method, and to elucidate the mechanism of corrosion inhibition.
Experimental.

2.1 Metal samples

The sample of MS was used in this study that, has the chemical composition of the metal sample was determined by using an emission spectrometer, with the aid of ARL quant meter (model 3100-292 IC) and listed in the Table 1.

Table 1: Chemical compositions of carbon steel sample

Constituent	C	Mn	P	S	Iron
Composition %	0.1	0.4	0.06	0.026	Rest

2.2 Metronidazole drug as an inhibitor

Metronidazole drug information's is described in *Table 2*.
Table 2 The Components and molecular structure of investigated inhibitor

Inhibitor Structure		IUPAC Name	Molecular weight	Active centers	Chemical Formula
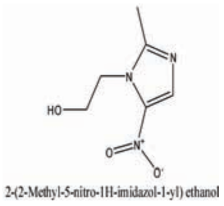	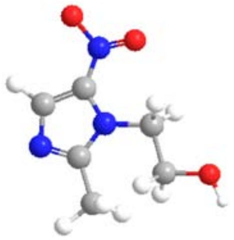	2-(2-Methyl-5-nitro-1H-imidazol-1-yl) ethanol	171.156 g.mol^{-1}	3N, 3O, 3π	$C_6H_9N_3O_3$

2.2 Solution

The aggressive solution, 1M HCl was prepared by diluting of analytical grade 36% of HCl with bi-distill water. The concentration range of the inhibitor was used between 50 ppm to 250 ppm.

2.4 Potentio-dynamic polarization technique

Electrochemical polarization experiments using three electrodes in electrochemical cell such as saturated calomel electrode (SCE) that, couple to a fine Lugging capillary acts a reference electrode, platinum is counter electrode, and working electrode made up from a square cut of metal (MS) sheet fixed in epoxy resin. The surface area that exposed to the electrolyte 1.0 cm^2 only. The working electrode was prepared with polisher paper (SiC) by different sizes (800, 1000 and 1200), and immersed in the corrosive medium at the natural potential for 10 min until it reaches a steady state.

The potential was started from - 600 to + 600 mV vs. open circuit potential (E_{ocp}). Calculation of inhibition efficiency (% IE), and the degree of surface coverage (θ) as follows [22]:

$$IE\ \% = \theta \times 100 = [1- (i_{corr\ (inh)} / i_{corr\ (free)})] \times 100$$

Where, $i_{corr\ (free)}$ and $i_{corr\ (inh)}$ are the corrosion current densities in the absence, and presence of metronidazole, respectively.

2.5 Electrochemical Impedance Spectroscopy (EIS) technique

The measurements of EIS were achieved at 25±1°C over a wide frequency range of ($1x10^5$ Hz to x 0.1 Hz). The potential perturbation was 10 mV in amplitude peak to peak.

The inhibition efficiencies (% IE), and the surface coverage (θ) obtained from the impedance measurements were calculated by the following relation:

$$IE\ \% = \theta \times 100 = [1- (R^{o}_{p}/R_{p})] \times 100$$

Where, R^{o}_{p} and R_p are the charge transfer resistance in the absence and presence of inhibitor, respectively.

The obtained diameters of the capacitive loops increase in the presence of inhibitor and decrease the capacitance double layer (C_{dl}), which is defined as equation [23]:

$$C_{dl} = 1/ (2 \pi f_{max} R_p)$$

Where, f_{max} is the maximum frequency.

2.6 Electrochemical Frequency Modulation (EFM) technique

The measurements of EFM were achieved by using a potential perturbation signal with have abundance of 10 mV with two sine waves of 2 and 5 Hz based on three factors:

1- Large peaks were used to calculate the corrosion current density (i_{corr})
2- Tafel slopes (β_c & β_a)
3- Causality factors (CF_2 & CF_3).

The inhibition efficiencies (% IE_{EFM}) were calculated as follows:

$$\%\ IE_{EFM} = [1- (i_{corr.} / i^{o}_{corr.})] \times 100$$

Where, i^{o}_{corr} and i_{corr} are corrosion current densities in the absence, and presence of an inhibitor, respectively.

All electrochemical techniques were achieved by using Gamry instrument PCI300/4 Potentiation/Galvanostatic/Zra analyzer, DC105 Corrosion software, EIS300 Electrochemical Impedance Spectroscopy software, EFM140 Electrochemical Frequency Modulation software Echem. Analyst the results were plotted in graph form. The data was fitted, and calculated.

2. 7 Surface Examinations

The morphology of the MS surface is used for analysis, examination nature of the surface and study the changing, that was appeared on the metal surface. The specimens were prepared by abraded mechanically by using different emery papers up to 1200 grit size and immersed in 1M HCl acid (blank) and with 300 ppm of metronidazole at room temperature for one day (24 h). Then, after this immersion time, the specimens were washed gently with distilled water, carefully dried, and taken carefully to the system. The surfaces were examined, such as using scanning electron microscope (SEM), energy dispersive x-ray (EDX), FT- IR spectroscopy, and atomic force microscope (AFM).

III. RESULT AND DISCUSSION

3.1 Electrochemical Techniques

3.1.1 Open circuit potential (E_{OCP})

From the Fig. 1 and Table 3 are shown several interesting points:

1. The E_{OCP} in the blank solution was started at -562.1 mV then was shifted anodically, and the steady state is occurred after 300 S. This indicating that the initial dissolution process (the attack on the surface of metal), and then the formed oxide film.

2. In the presence of metronidazole, the E_{OCP} started at relatively positive potential compared with that in the absence of the inhibitor, and then shifted anodically, that starting from 483.3 to 475.1 mV according to the increasing the concentration 50 to 300 ppm respectively. The steady state is attained rapidly, compared with the blank. With increasing the concentration of the metronidazole, make shift in the open circuit potential, that increases in the active direction pointing, this means the inhibitor might act mainly as a mixed type inhibitor [24]. The classification of a compound as an anodic or cathodic type inhibitor is based on the E_{OCP} displacement; if the shift in E_{OCP} is at least ±43 mV compared to the one measured in the blank solution, it can be classified as an anodic or cathodic inhibitor. However, from *Fig. 1,* the shift in E_{OCP} on adding metronidazole is about 15 mV revealing that the present inhibitor acts slightly more as an anodically inhibitor.

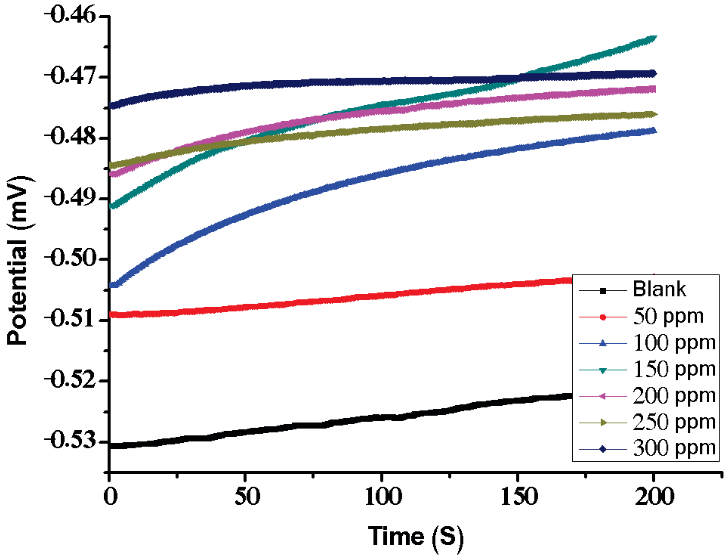

Fig. 1: Open circuit potential, *E*OCP vs. time relations for MS submersed in 1M HCl in the nonexistence and the existence of metronidazole drug at 25°C.

Table 3: E_{OCP} of the MS in the nonexistence and the existence of metronidazole drug at 25° C

Conc.(ppm)	$-E_{Min}$ (mV)	$-E_{Max}$ (mV)
Blank	526.1	507.1
50	483.6	480.2
100	479.3	471.5
150	478.9	475.2
200	476.9	469.3
250	475.1	469.3
300	475.1	458.7

3.3.2 Potentiodynamic polarization (PP)

The results are drawn in nonexistence and with existence deferent doses of metronidazole drug in Fig. 2. The obtained potentio-dynamic polarization parameters are given in Table 4. These results indicating that the cathodic, and an anodic curve according to Tafel-type behavior. The form of the curves is slightly similar either in the cathodic or in the anodic side, which indicates that the mechanisms of MS dissolution, and hydrogen reduction apparently remain in the presence of the inhibitor. Addition of metronidazole decreased both the cathodic, and anodic current densities. The carves are shown mainly parallel displacement to the more negative and positive values respectively, i.e. the presence of metronidazole in solution inhibit both the hydrogen evolution, and the anodic dissolution processes with overall shift of E_{corr} to slightly fewer negative values.

The graphical also are shown that the anodic, and the cathodic Tafel slopes (β_a and β_c) are slightly changed on increment of the doses of the metronidazole. It obvious that no change of the mechanism of inhibition in existence, and nonexistence of metronidazole drug. The fact that the values of β_c are slightly higher than the values of β_a refer to the cathodic action of the metronidazole inhibitor. It is obvious that the action of inhibitor control over the electrochemical reaction slightly cathodic control. This means that the metronidazole is mixed type inhibitor, but the cathodic is more specially polarized than the anodic. The values of Tafel slope is higher referred to the surface kinetic process instead of the diffusion-controlled process [25]. Ether the cathodic slope that obtained from the electrochemical measurements confirm the hydrogen evolution reaction was activation or cathodic controlled [26].

The addition of the inhibitor did not modify the mechanism of this process but appears that the inhibition mode of the metronidazole was used by simple adheres of the surface by adsorption process.

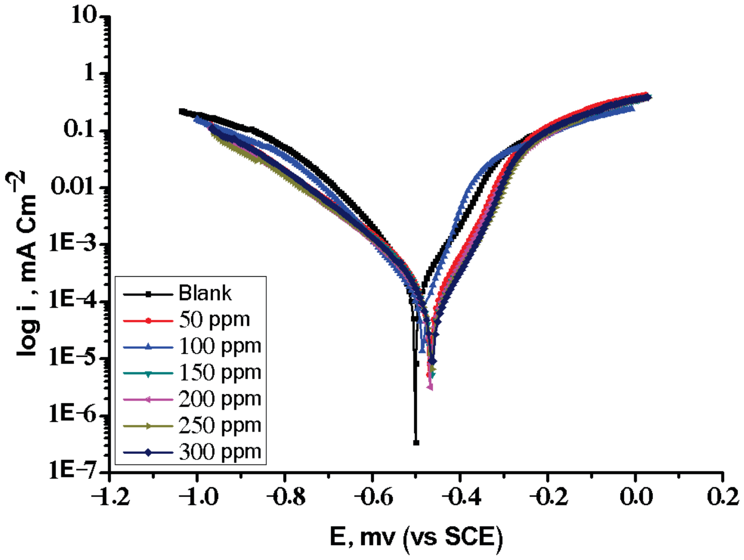

Fig. 2: PP curves for the corrosion of MS in 1 M HCl in the nonexistence and existence of various doses of metronidazole at 25°C

Table 4: PP parameters (E_{corr}, i_{corr}, β_a and β_c), θ and % IE in nonexistence and with existence various doses of metronidazole in 1 M HCl medium at 25 °C

Conc. ppm	$I_{corr.}$ mA/cm^{-2}	-$E_{corr.}$ mV(SCE)	β_a mV dec^{-1}	β_c mV dec^{-1}	C. R. Mpy	Θ	% IE
0.0	147.0	498	153	344	96.5	----	----
50	61.1	465	77.1	94.4	27.9	0.71	71
100	78.6	464	97.9	99.1	35.9	0.628	62.8
150	92.7	465	109.9	110.2	42.4	0.561	56.1
200	125	466	95.9	106.2	57.3	0.406	40.6
250	129	467	152.2	129.9	58.8	0.391	39.1
300	136	469	105.7	136	62.2	0.355	35.5

3.3.3 Electrochemical Impedance Spectroscopy (EIS)

The Nyquist, and Bode impedance diagrams studies between 0.1 Hz and 100KHz frequencies rang abundance signal at E_{OCP} for MS in 1M HCl in the nonexistence, and with existence of various doses of metronidazole are obtained. The equivalent circuit that describe for metal, and electrolyte are seen in Fig. 3, EIS variables and (% IE) are determination, and recorded in Table 5.

The obtained Nyquist, and Bode plotting for metronidazole are shown in Figs. 4 a,b. Nyquist spectrum is characterized by a single full half-circle. The curves are shown, that the corrosion of mild steel is controlled by a charge transfer process [27]. The diameters of the capacitive loop obtained increases in the presence of metronidazole are indicated that the increasing the inhibition process [28]. It was observed from the obtained EIS data, that R_p increases but C_{dl} decreases with the increasing of inhibitor concentrations. The increases of R_p values deal the increasing of the inhibition efficiency, due to the gradual replacement of water molecules by the adsorption of the inhibitor molecules on the metal surface to form an adherence film on the metal surface. This suggests the degree of coverage on the metal surface by formation film decreases the double layer thickness. Also, enhance the decreasing of C_{dl} with increasing the inhibitor concentration, that occur as a result from a decreases in local dielectric constant, and replacement water molecules by inhibitor molecules which, indicating that, the inhibitor was adsorbed on the surface of both anodic, and cover somewhat of cathodic sites [29].

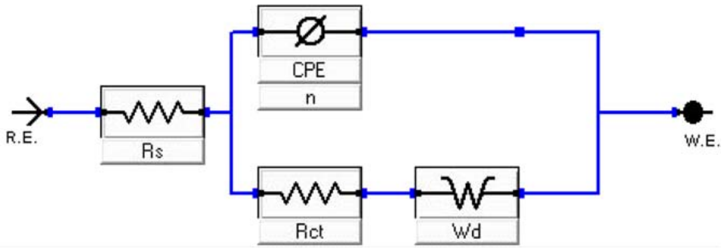

Fig. 3: Electrical equivalent circuit model use to fit the experimental results, R_s is the solution resistance and R_p is the charge transfer resistance

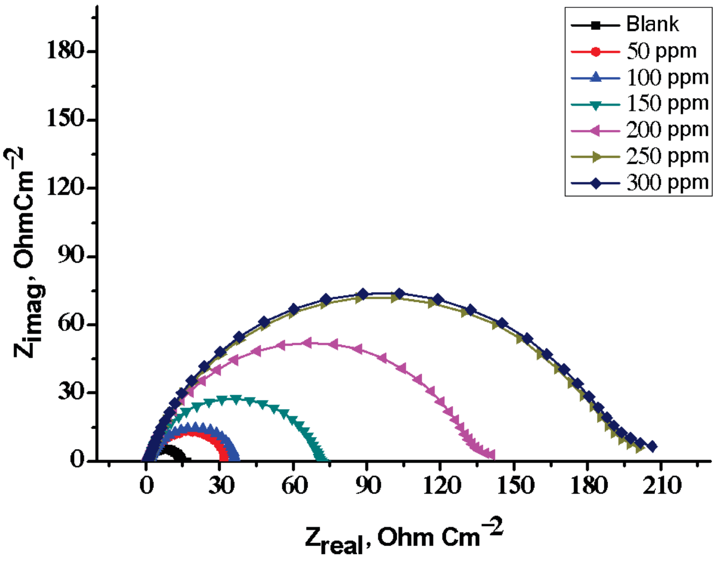

(a) Nyquist

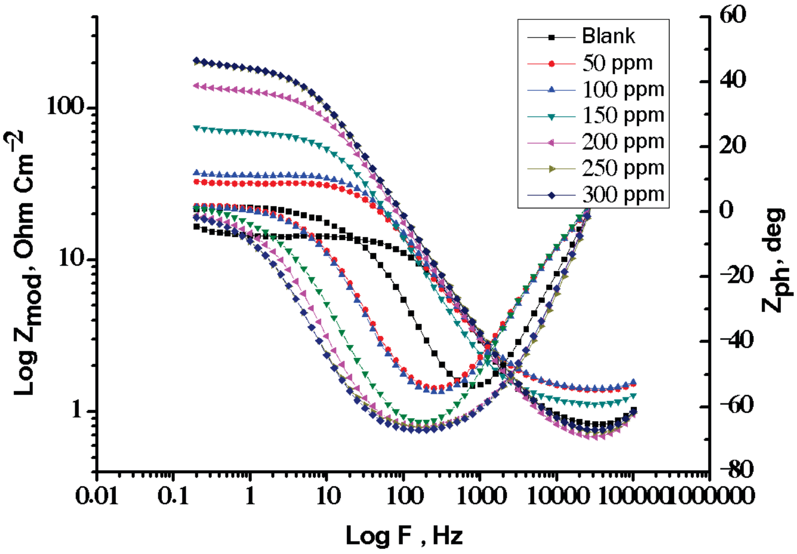

(b) Bode

Figs. 4 a, b: The Nyquist (a), and Bode (b) curves for corrosion of MS in 1 M HCl in the nonexistence and with existence of various doses of metronidazole at 25 °C

Table 5: Electrochemical kinetic variables obtained by EIS technique for MS in 1 M HCl without and with various doses of metronidazole at 25 °C

Conc. ppm	R_p Ω cm²	C_{dl} µF cm²	ϴ	% IE
0.0	8.5	908.5	-----	-----
50	31.2	879.2	0.564	56.4
100	35.4	864.9	0.616	61.6
150	69.5	863.4	0.804	80.4
200	133.7	852.3	0.898	89.8
250	190.6	849.8	0.929	92.9
300	193.2	841.5	0.930	93.0

3.3.4 Electrochemical Frequency Modulation technique (EFM)

EFM is regarded a very good technique to determination corrosion information directly, and quickly because EFM is nondestructive technique to determination corrosion **[30]**. The measurements data of EFM are became a valid data when the practical causality factors (CF2 and CF3) are equals or near the hypothetical values (2 and 3) which determination from the frequency spectrum of the current reaction. **Fig. 5**, illustrated the EFM inter-modulation spectrum of MS in 1 M HCl in nonexistence, and existence deferent concentrations of metronidazole drug. It is clearly that, the treatment EFM data utilizing two various models: (1) the activation model by solved three nonlinear equation, and assuming no change of the corrosion potential due to the polarization of the working electrode (2) cathodic reaction controlled by complete diffusion **[31]**.

The corrosion current density i_{corr}, β_a , β_c , CF2, and CF3 are calculated from the two large peaks of inter-modulation spectrum, and then are listed in Table 6. It is obviously, that the addition of the metronidazole drug at different doses to the corrosive medium reducing the i_{corr}, indicating that, the metronidazole drug inhibits the corrosion of MS by the adsorption process. The CF2 and CF3 are equal or near the hypothetical values 2 and 3 indicating that, the estimation information data are valid, and good value **[32]**. The % IE $_{EFM}$ values are incremented by expanding the doses of metronidazole drug, which determination and are recorded in Table 6.

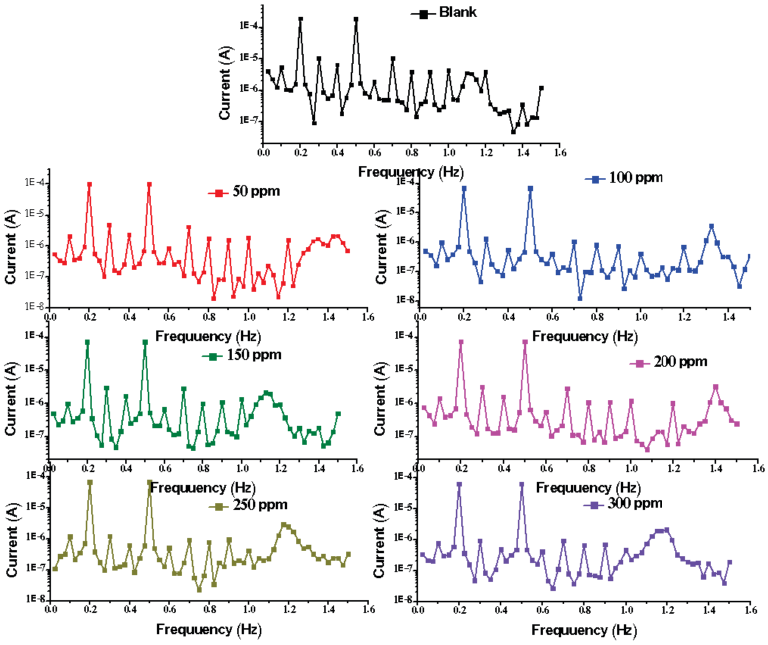

Fig. 5: EFM for MS in 1M HCl unlucky deficiency and vicinity of distinctive convergences of metronidazole

Table 6: Electrochemical kinetic parameters obtained by EFM technique for MS in 1 M HCl without and with various doses of metronidazole at 25 °C

Comp.	Conc. ppm	$I_{corr.}$ μAcm^{-2}	β_a x 10^{-3} $mVdec^{-1}$	β_c x 10^{-3} $mVdec^{-1}$	CF (2)	CF (3)	CR Mpy	ϴ	% IE
Blank	0.0	425.8	69.5	91	1.9	2.8	203.2	----	----
Metronidazole	50	138	801	102.3	2.1	2.2	63.1	0.676	67.6
	100	114.9	101.6	113.6	2.5	2.2	52.5	0.73	73
	150	107.9	88.7	113.8	1.9	1.7	49.3	0.746	74.6
	200	103.6	83.8	106.1	2.2	2.9	47.4	0.757	75.7
	250	86.2	79.5	85.9	2.0	3.2	39.4	0.798	79.8
	300	84.6	85.5	92.6	1.9	3.5	38.7	0.80	80

3.3.5 Scanning Electron Microscopy (SEM)

The micrographs are obtained for MS specimens in the nonexistence, and in the existence of 300 ppm of metronidazole drug after exposure for immersion one day in corrosive medium 1M HCl. It is clear, that the MS has suitable surfaces for corrosion attack in the blank or corrosive medium only **`b and c**. When add the metronidazole to the corrosive medium, the morphology of MS surfaces was shown quite different from the previous one, and the specimen surface was seen smoother. It is clear that the formation of a thin film layer adsorbed on the metal surface, which distributed in a disorder way overall the surface of the metal **[33]**. This may be due to the adsorption of the metronidazole on the MS surface, and made up the passive film that block and attract to the active site on the metal surface. The metronidazole molecule is interacted with active sites of MS surface, resulting the be decreasing contact between MS, and the corrosive medium. From the above sequentially metronidazole is exhibited excellent inhibition effect.

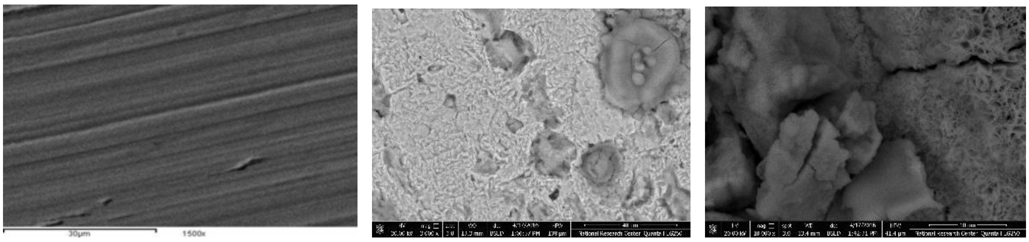
a-Free sample b- Blank in 1M HCl c-In 1M HCl with existence

300 ppm of Metronidazole

Figs. 6 a, b and c: SEM micrographs for MS in the nonexistence, and the existence of 300 ppm of the metronidazole after submersion for 1 day

3.3.6 Energy Dispersion Spectroscopy (EDX) [34]

To determination the elements, and molecules, that existence are adsorbed on the surface of MS after one day that immersion in acid with optimum doses of metronidazole by using the EDX spectra. The EDX analysis of MS in 1M HCl with in the presence of 300 ppm of the metronidazole is given in **Fig. 7**. The spectra show additional lines, demonstrating the existence of C (owing to the carbon atoms of some metronidazole). These data show that the carbon, nitrogen, and oxygen atoms are covered the specimen surface. The EDX analysis is indicated that only carbon, nitrogen, and oxygen are detected, and are shown that the passivation film is contained the chemical formula of the metronidazole drag, that adsorbed on the MS surface. It is clear that, the percent weight of adsorbed elements C, N, and O were presented in the spectra, and recorded in Table 7.

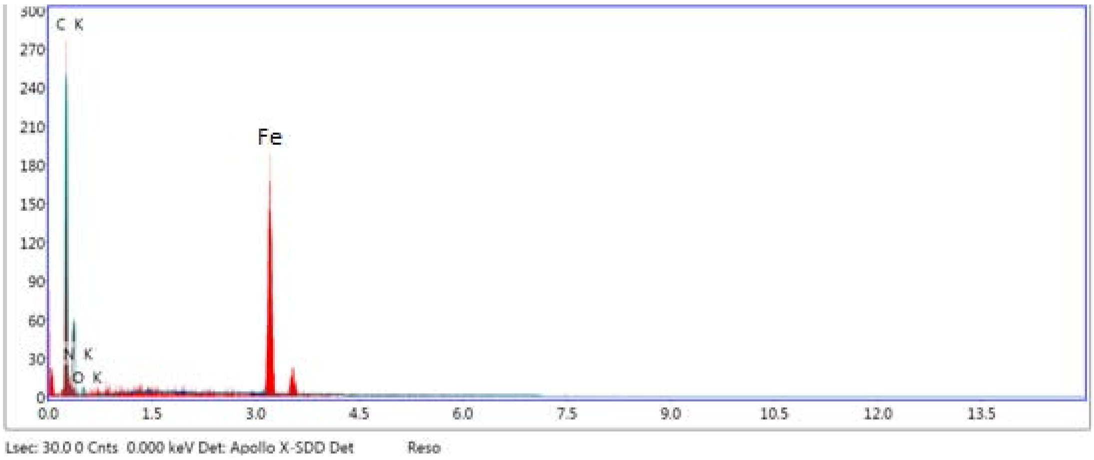

Fig. 7: EDS analysis on the MS in the existence 300 ppm of the metronidazole drug for 1 day that immersion in 1M HCl.

Table 7: Surface composition (wt %) of MS after one day that immersion in 1M HCl with 300 ppm of the metronidazole

Wt %	Fe	C	N	O
Metronidazole	75.97	43	50	5.21

3.3.7 Atomic Force Microscopy (AFM)

AFM is a powerful tool to investigate the surface morphology of various samples at nano- micro scale, that is currently used to study the influence of corrosion inhibitor on the metal solution interface. From the analysis, it can be gained regarding the roughness on the surface. The roughness profile values are played an important role to identifying, and reported the efficiency of the inhibitor under study. Among the roughness is tacked a role for the explanation of adsorption, and illustrated the nature of the adsorbed film on the metal surface *[35-36]. Fig. 8 a and b,* show the 3D images as well as elevation profiles of polished of the MS in the absence, and the presence the metronidazole an inhibitor. From analysis the values, indicating that the higher value of Z parameter reached, which found (2.60 µm) for the blank solution which placed in 1M HCl one day and analyzed. The observation of the metal surface which immersed in 1M HCl in the presence of 300 ppm of the metronidazole as an inhibitor possess small roughness (488.6 nm) compared with the blank solution. It can be noted that the value is lower than that of the blank value. The decrease in the roughness value reflected to the adsorption of inhibitor molecule on metal surface thereby reducing the rate of corrosion.

Conclusion: The image (a) is exposed to corroded solution affected the structure with large vales, and deep crack but the image (b) the surface reveal that is covering by thin film, that adsorbed on the metal surface. The adsorption film is protected the surface of the metal from corrosion process.

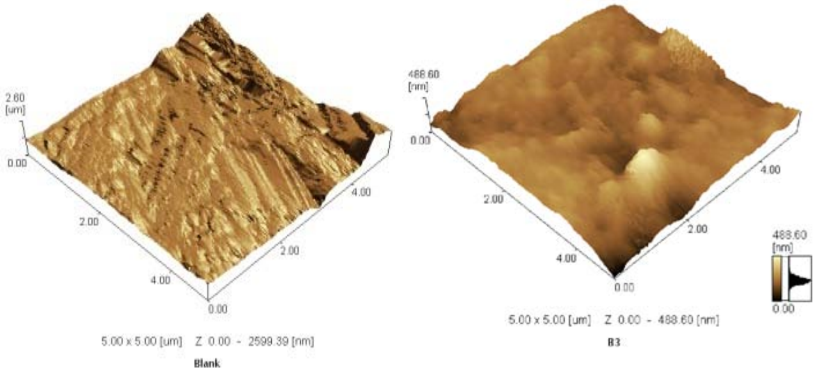

a-Blank b-In 300 ppm of Egy- dronate drug

Figs. 8 a and b: The 3D of optical images of AFM in the nonexistence, and the existence of the metronidazole drug.

3.3.8 Fourier transforms infrared spectra (FT – IR)

The (FT – IR) spectrophotometer is a powerful instrument, that can be used to identify the function group, that presence in metronidazole, and the type of interaction that occur between function group with metal surface. Since, pharmaceutical drug compound contain variety of organic compound, and these organic compounds (inhibitor) are adsorbed on the metal surface by formation thin film that protection them against corrosion, they can be analyzed by using (FT – IR). To confirm the nature of the chemical constituent that adsorbed on the metal surface, by the Fourier transform infrared (FT – IR) spectra [37].

The pharmaceutical drug compounds are contained certain function group according to the chemical formula like OH, N═C, C=C and N=O. In order to find the nature of constituents involved in the adsorption using (FT – IR) spectrum of material that are coated the metal surface gives in Fig. 9. The spectrum of metronidazole before, and after adsorption that seen the wave number of the function groups OH abroad peak at 3400 cm^{-1} starching, C=C is sharp peak at 1630 cm^{-1} starching, and N=O a sharp peak between 1140 – 1000 cm^{-1} starching. It is clear that the function groups of metronidazole inhibitor appear on the metal surface that confirm to the adsorption process [38].

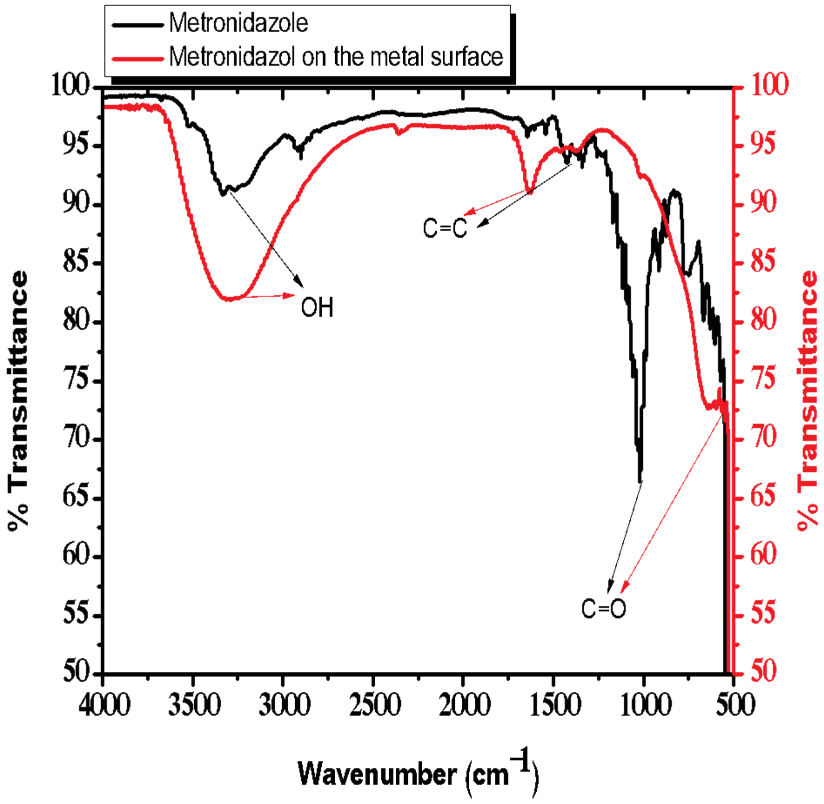

Fig. 9: FT – IR spectrum of metronidazole before and after adsorption on the MS surface.

3.4 Mechanism of inhibition

To illustrate the mechanism of inhibition of corrosion on the MS surface in acid medium by using pharmaceutical drug compound as an inhibitor, it is must be knowing the nature of metal surface, and the nature of the component of inhibitor structure. The MS is regarded the metal α-phase [39], It is obvious that α-phase state consists of grains, and grain boundaries in the surface of the metal, Fig. 10. A cross-section of a piece or specimen of the metal that is a corroding to clarify that there are both anodic, and cathodic sites in the metal surface structure.

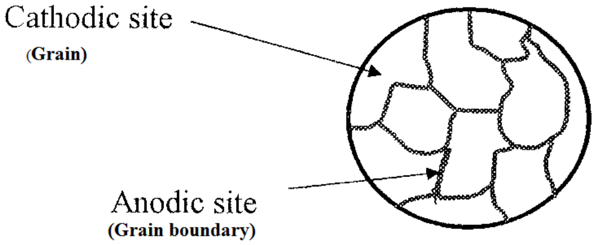

Fig. 10: Schema models of metalα- phase

The surface of iron is usually, coated with a thin film of iron oxide. However, if this iron oxide film develops some cracks, anodic area are created on the surface, while other metal parts acts as cathodic sets. It follows that the anodic areas are small surface, while nearly the rest of the surface of the metal large cathodes. Electrochemical corrosion involves flow of electric current between the anodic, and cathodic areas called inter-granular corrosion. *Fig. 11*, SEM image is shown the corrosion of the MS in 1M HCl in one day immersion that illustrated inter-granular corrosion.

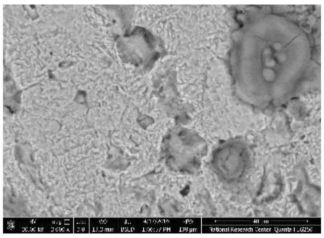

Fig. 11: SEM image illustrated inter-granular corrosion after immersion the specimen in 1M HCl one day

All previous results prove that the pharmaceutical drug compound under study were actually inhibit the corrosion of the MS in 1M HCl solution as a corrosive medium. The corrosion inhibition is due to their physical, and chemical adsorption for formation of protection thin film adsorbed on the metal surface. The effect of metronidazole as inhibitor may be corresponding to the accumulation of the inhibitor molecules on the metal surface, which prevent the direction contact of the metal surface with corrosive environment. The surface of the MS sample has positively charge in aqueous acid solution, and the adsorption occur according to [40-41]:

1- The unshared electrons of nitrogen, oxygen atoms, and electron density of π bonding donate to the vacant orbital on the metal surface make chemisorption.
2- The partial negative charge that present in function group containing Oxygen, nitrogen, and electron density of π-bond in metronidazole may be adsorbed on the positively charge of the metal surface like electrostatic attraction between the opposite charge, in the form of neutral molecules, that involving displacement of water molecules from the metal surface.

The inhibition action of the metronidazole can be accounted by the interaction between the lone pair of electrons in the nitrogen, oxygen, and electron density of π-bond with positively charged (anodic sites) on the metal surface, and the skeleton of inhibitor compound cover the cathodic sites this action form thin layer adsorbed on the metal surface and prevent corrosion processes *Fig. 12*.

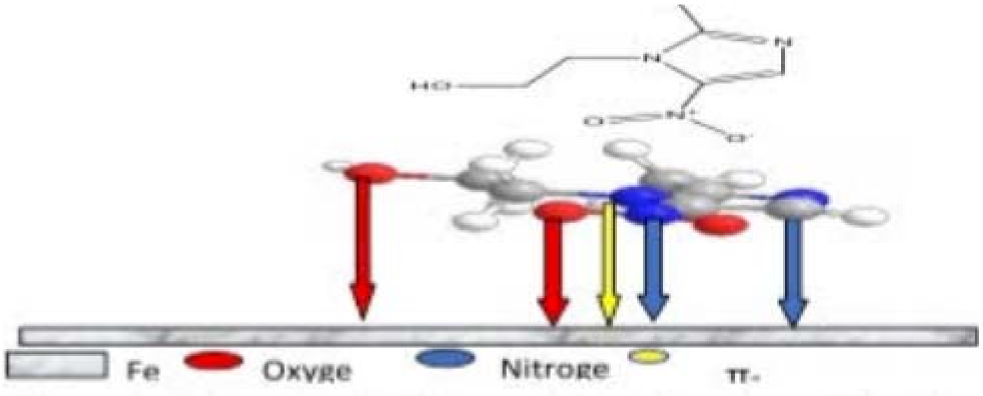

Fig. 12: Schema model illustrated the adsorption of the metronidazole structure on the MS surface.

This meaning, the metronidazole molecule attached with anodic site, and covered somewhat of cathodic area, so that the corrosion rate in presence of metronidazole is anodic-cathodic control.

IV. CONCLUSION

Inhibition of the corrosion of the MS in 1M HCl solution by metronidazole is determine by potentio-dynamic polarization, Evans techniques, and surface examination by Scanning Electron Microscopy (SEM), Energy Dispersive X-ray (EDX), Atomic Force Microscopy (AFM), and Fourier Transforms Infrared (FT-IR). It was found that the inhibition efficiency depends on concentration, nature of metal surface, and the type of adsorption of the inhibitor. The observed corrosion data in the presence the metronidazole as an inhibitor:

1) The tested metronidazole inhibitor establishes a very good an inhibition efficiency for the MS corrosion in 1M HCl solution.
2) Metronidazole inhibits the MS for the corrosion by the adsorption on its surface, and make thin film layer protective them from corrosion process.
3) The inhibition efficiencies of the metronidazole increase with the increasing of their concentrations.
4) The values of inhibition efficiencies obtained from all techniques that using are seen the validity of the obtained results.
5) The metronidazole molecule attached with anodic site, and covered somewhat of cathodic area, so that the corrosion rate in the presence of the metronidazole is anodic-cathodic control.

REFERENCES

1. I. A. Raspini, (1993) Influence of Sodium Salts of Organic Acids as Additives on Localized Corrosion of Aluminum and Its Alloys, Corrosion, 49, 821-828.
2. M. A. Migahed, E. M. S. Azzam, A. M. Al-Sabagh, (2004) Corrosion inhibition of mild steel in 1 M sulfuric acid solution using anionic surfactant Mater. Chem. Phys., 85, 273-279.
3. R. F.V. Villamil, P. Corio, J. C. Rubim, M. L. Siliva, (1999) Effect of sodium dodecylsulfate on copper corrosion in sulfuric acid media in the absence and presence of benzotriazole, J. Electroanal. Chem., 472, 112-119.
4. S. S. Abd El Rehim, H. Hassan, M. A. Amin, (2003) The corrosion inhibition study of sodium dodecyl benzene sulphonate to aluminum and its alloys in 1.0 M HCl solution Mater. Chem. Phys., 78, 337-348.
5. R. Guo, T. Liu, X. Wei, (2002) Effects of SDS and some alcohols on the inhibition efficiency of corrosion for nickel, Colloids Surf., A, 209, 37-45.
6. V. Branzoi, F. Golgovici, F. Branzoi, (2002)Aluminum corrosion in hydrochloric acid solutions and the effect of some organic inhibitors, Mater. Chem. Phys., 78, 122-131.
7. M. Elachouri, M. S. Hajji, M. Salem, S. Kertit, J. Aride, R. Coudert, E. Essassi, (1996) Some Nonionic Surfactants as Inhibitors of the Corrosion of Iron in Acid Chloride Solutions, Corrosion, 52,103-108.
8. A. S. Algaber, E. M El-Nemma, M. M. Saleh, (2004) Effect of octylphenol polyethylene oxide on the corrosion inhibition of steel in 0.5 M H_2SO_4, Mater. Chem. Phys., 86, 26-32.
9. R. Oukhrib, B. El Ibrahimi, H. Bourzi, K. El Mouaden, A. Jmiai, S. El Issami, L. Bammou, L. Bazzi, (2017) Quantum chemical calculations and corrosion inhibition efficiency of biopolymer “chitosan” on copper surface in 3% NaCl, JMES, 8 (1), 195-208.
10. A. M. Al-Azzawi, and K. K. Hammud, (2016) Newly antibacterial / anti-rusting oxadiazole poro-mellitic di-imides of carbon steel / hydrochloric acid interface: Temkin isotherm model, IJRPC, 6 (3), 391-402.

11. M. Sani1 Umar, Umar Usman, (2016) Electrochemical Corrosion Inhibition of Mild Steel in Hydrochloric Acid Medium Using the Antidiabetic Drug Janumet as Inhibitor, International Journal of Novel Research in Physics Chemistry & Mathematics, 3 (3), 30-37.
12. A. M. Kolo, U.M. Sani, U. Kutama, and U. Usman, (2016) The Pharmaceutical and Chemical Journal, 3 (1), 109-119.
13. P. O. Ameh and U. M. Sani, (2015) Cefuroxime Axetil: A Commercially Available Pro-Drug as Corrosion Drug for Aluminum in Hydrochloric Acid Solution, Journal of Heterocyclic, 1(1), 2 – 6.
14. H. I. Al-Shafey, R. S. Abdel Hameed, F. A. Ali, A. S. Aboul-Magd, M. Salah, (2014) Effect of Expired Drugs as Corrosion Drugs for carbon steel in 1M HCL Solution, Int. J. Pharm. Sci. Rev. Res. 27(1), 146-152.
15. Kushwah Rupesh, R. K. Pathak, (2014) Inhibition of Mild Steel Corrosion in 0.5 M Sulphuric Acid Solution by Aspirin Drug, International Journal of Emerging Technology and Advanced Engineering, 4 (7), 880-884.
16. A. S. Fouda, M.N. EL-Haddad, and Y. M. Abdallah, (2013) Septazole: Antibacterial Drug as a Green Corrosion Drug for Copper in Hydrochloric Acid Solutions, IJIRSET, 2 (12), 7073-7085.
17. S. U. Ofoegbu and P. U. Ofoegbu, (2012) Corrosion inhibition of MS in 0.1 M hydrochloric acid media by chloroquine diphosphate, ARPN Journal of Engineering and Applied Sciences, 7 (3), 272-276.
18. S. R. Kiahosseini, S. J. M. Baygi, G. Khalaj, A. Khoshakhlagh, and R. Samadipour, (2018) Study on Structural, Corrosion, and Sensitization Behavior of Ultrafine and Coarse Grain 316 Stainless Steel Processed by Multiaxial Forging and Heat Treatment, Journal of Materials Engineering and Performance, 27, 271–281.
19. K Gholamreza, K. Mohammad-Javad, (2016) Investigating the corrosion of the Heat-Affected Zones (HAZs) of API-X70 pipeline steels in aerated carbonate solution by electrochemical methods, International Journal of Pressure Vessels and Piping, 145, 1-12.
20. N. Narimani, B. Zarei, H. Pouraliakbar, G. Khala, (2015) Predictions of corrosion current density and potential by using chemical composition and corrosion cell characteristics in microalloyed pipeline steels, Measurment, 62, 97-107.
21. M. J. Faizabadi, G. Khalaj, H. Pouraliakbar and M. R. Jandaghi, (2014) Predictions of toughness and hardness by using chemical composition and tensile properties in microalloyed line pipe steels, Neural Computing and Applications, 25, 1993–1999.
22. A. S. Fouda, R.M. Abou-shahba, W. A Husien, E. S. EL-Habab, Chemical and Electrochemical Study on the Effectively of *Melilotus Officinalis* Extract as A Green Inhibitor for Corrosion of Aluminum Alloy in 1 M HCL, International Journal of Recent Research in Physics and Chemical Sciences (IJRRPCS), 2, (2) (2016), (1-18)
23. A. S. Fouda, G. Y. El-Ewady and Adel H. Ali, Corrosion Inhibition of Carbon Steel in hydrochloric acid medium using Gliclazide drug, Journal for Electrochemistry and Plating Technology, (2018) 1-20.
24. Adel H. Ali, Abd El-Aziz S. Fouda, Amal H. Tilp, Electrochemical behavior for corrosion protection of mild steel (MS) in 1M HCl medium by using lidocaine drug as an inhibitor, Zastita Materijala, 61 (4) (2020), 286 - 305
25. A. S. Fouda, A. M. El- Defrawy, and M. W. El-Sherbeni, Pharmaceutical compounds as save corrosion inhibitors for carbon steel in 1M H_2SO_4 solution, Reprint form the Mansoura, J, Chemistry, 39 (2) (2012) 1-27.
26. O. A. Hazazi, A. Fawzy, M. Awad, Synergistic Effect of Halides on the Corrosion Inhibition of Mild Steel in H_2SO_4 by a Triazole Derivative: Kinetics and Thermodynamic Studies, Int. J. Electrochem. Sci., 9, (2014) 4086 – 4103.
27. A. S. Fouda, A. A. Al-Sarawy, E. E. El-Katori, Pyrazolone derivatives as corrosion inhibitors for MS HCl solution, Desalination, 201 (2006),1-13.

28. O. Benalli, L. Larabi, M. Traisnel, L. Gengembra, Y. Harek, Electrochemical, theoretical and XPS studies of 2-mercapto-1-methylimidazole adsorption on carbon steel in 1 M $HClO_4$, Appl. Surf. Sci., 253 (2007), 6130-6139.
29. S. Kshama Shetty and A. Nityananda Shetty, Ionic Liquid as an Effective Corrosion in hibitor on 6061Al-15 Vol. PCT. SIC (p) Composite in 0.1M H_2SO_4 Medium, An Ecofriendly Approach, 3 (2015) 41-64.
30. E. Kus and F. Mansfeld, an Evaluation of the Electrochemical Frequency Modulation (EFM) Technique, Corros. Sci. 48 (2006) 965-979.
31. G. A. Caigman, S. K. Metcalf, E. M. Holt, Thiophene substituted di hydropyridines, J. Chem. Cryst. 30 (2000) 415-422.
32. Abd El-Aziz S. Fouda, Adel H. Ali, (2018(, Egy- dronate drug as promising corrosion inhibitor of C - steel in aqueous medium, protection material journal, 59 (1) 126 – 140.
33. A.S. Fouda, G. El-Ewady, A.H. Ali, (2017) Modazar as promising corrosion inhibitor of carbon steel in hydrochloric acid solution, Green Chem. Lett. Rev., 10 (2), 88–100.
34. A.S. Fouda, G. El-Ewady, Adel H. Ali, (2017) Corrosion protection of carbon steel by using simvastatin drug in HCl medium, J. Applicable Chem., 6 (5),701-718.
35. Adel H. Ali, (2023) Electrochemical Study for using Eg-dronate drug as a Green Corrosion Inhibitor in 0.5 M H2SO4 Solution by Applied: Potentio-dynamic and Evans Techniques, London Journals Press, Volume 23, Issue 3, 27-44.
36. Adel H. Ali, (2018) Electrochemical study of candesartan drug as corrosion inhibitor for carbon steel in acid medium, J. Adv. Electrochem., 4 (1),152–157.
37. Jan Mohammad Mir, R.C. Maurya, P.K. Vishwakarma, (2017) Corrosion resistance and thermal behavior of acetylacetonato-oxoperoxomolybdenum (VI) complex of maltol: Experimental and DFT studies, Karbala International Journal of Modern Science, 3, 212-223.
38. Abd El-Aziz S. Fouda, Ahmed A. El-Hossiany, Ramadan Heba M., (2017) Calotropis procera plant extract as green corrosion inhibitor for 304 stainless steel in hydrochloric acid solution, Zastita Materijala 58 (4), 541 - 555
39. Adel H. Ali, Abd El-Aziz S. Fouda, Amal H. Tilp, (2020) Electrochemical behavior for corrosion protection of mild steel (MS) in 1M HCl medium by using lidocaine drug as an inhibitor, Zastita Materijala 61 (4), 286 – 305
40. Adel H. Ali, (2020) Electrochemical Behavior of Quenching Low Carbon Steel (LCH) by using Simvastatin Drug as a Corrosion Protection in 0.5 H_2SO_4 Medium by Applied: Potentio-dynamic and Evans Techniques, Global Journal of Science Frontier Research: B Chemistry, 20 (2), 23-39
41. Adel H Ali (2023). The Relation Between Adsorption of Metronidazole as Green Inhibitor and the Microstructure of Carbon Steel (CS) in 1M HCl Medium, J Eng Tech & App Sci 1(1), 01-08.

Scan to know paper details and
author's profile

Effect Acrylamide Grafted Starch on the Properties of a Water based Mud

Akintola Sarah, Oluwaseyi Olora & Ehwarieme Favour Omoyoma

University of Ibadan

ABSTRACT

Modified starches have gained popularity in recent years due to the availability of starch. Graft polymerization is one of the ways to improve the properties of starch. Starch was obtained by process of wet milling from four genotypes Cassava tubers (TMS 96/1632, TMS 98/0581, TMS 07/ 0593 and TMS 01/1371), assigned as A, B, C, and D, respectively, were grafted with PAM and synthesized by polymerization method. Potassium Persulfate (PPS) was used as an initiator with ethanol-water solution used to remove the homo-polymer acrylamide (PAM). The starch-grafted copolymer was characterized by Fourier transform infrared spectroscopy. From the result, it was observed that the FTIR spectra for the four starches grafted onto Polyacrylamide Monomer showed the presence of PS-g copolymer with new absorption bands at the range of 1644cm^{-1} – 1654cm^{-1} this indicates a primary amide group in the polyacrylamides. The drilling fluids treated with the PS-g copolymer showed mud weights between 8.6 – 9.0 with genotype D S-g-PA copolymer presenting a better rheology properties and fluid loss control. All drilling fluids prepared with copolymerized starch exhibit shear thinning and pseudoplastic properties.

Keywords: graft copolymerization, cassava starch, acrylamide, Water based mud rheological properties.

Classification: LCC Code: TP248.65.P62

Language: English

Great Britain
Journals Press

LJP Copyright ID: 925645
Print ISSN: 2631-8490
Online ISSN: 2631-8504

London Journal of Research in Science: Natural & Formal

Volume 25 | Issue 4 | Compilation 1.0

Effect Acrylamide Grafted Starch on the Properties of a Water based Mud

Akintola Sarah[α], Oluwaseyi Olora[σ] & Ehwarieme Favour Omoyoma[ρ]

ABSTRACT

Modified starches have gained popularity in recent years due to the availability of starch. Graft polymerization is one of the ways to improve the properties of starch. Starch was obtained by process of wet milling from four genotypes Cassava tubers (TMS 96/1632, TMS 98/0581, TMS 07/ 0593 and TMS 01/1371), assigned as A, B, C, and D, respectively, were grafted with PAM and synthesized by polymerization method. Potassium Persulfate (PPS) was used as an initiator with ethanol-water solution used to remove the homo-polymer acrylamide (PAM). The starch-grafted copolymer was characterized by Fourier transform infrared spectroscopy. From the result, it was observed that the FTIR spectra for the four starches grafted onto Polyacrylamide Monomer showed the presence of PS-g copolymer with new absorption bands at the range of 1644cm^{-1} – 1654cm^{-1} this indicates a primary amide group in the polyacrylamides. The drilling fluids treated with the PS-g copolymer showed mud weights between 8.6 – 9.0 with genotype D S-g-PA copolymer presenting a better rheology properties and fluid loss control. All drilling fluids prepared with copolymerized starch exhibit shear thinning and pseudoplastic properties.

Keywords: graft copolymerization, cassava starch, acrylamide, Water based mud rheological properties.

Author α σ: Petroleum Engineering, University of Ibadan, Ibadan, Nigeri).
ρ: (Triumphant College, Windhoek, Namibia).

I. INTRODUCTION

Drilling fluids are an important part of drilling operations. Drilling fluids are complex mixtures of solids and liquids. During drilling operations, additives are added in order to enhance the properties of the drilling fluid. These additives perform different functions in drilling fluids such as increase mud weight, reduce viscosity, reduce fluid loss. However, most of these additives are currently not suitable for continuous use due to their adverse environmental effects resulting from high toxicity and poor biodegradability (S. Wysocki et al. 2005), Polymers have been used as additives and one of this is the use of polymeric additives and starch being the was the first and the most widely. Recent studies have used products obtained from biomaterials such as starch, xanthan gum, ginger and guar gum (Akinwumi et al. 2018) as suitable alternatives to the conventional additives to obtain desired rheological and filtration properties.

Starch is an effective colloid and it decreases the filtration of water by dispersing drilling fluids and increasing viscosity. Cassava (Manihot esculenta Crantz) , a polysaccharide polymer, is a root crop which has been investigated to exhibit different properties that have potential for a wide end use. In recent years, starch has been gaining significance in the oil industry as an additive in drilling fluid. Its use is widespread due to its availability and low cost (Peter Adewale et al. 2022). Native starch from corn, cassava, potato, and banana has been used as an additive in drilling fluids as a viscosifier and as an alternative to Carboxymethyl Cellulose and Polyanionic Cellulose.

Studies have shown that native starch degrades and destroys the integrity of the drilling fluid due to their poor temperature resistance (Shadfar et al. 2024). In response to the degradability and unstable nature of native starch, researchers have come up ways to improve the properties of starch via modification. Starch has been modified by different methods such as chemical modification (etherification, esterification, acid hydrolysis, oxidation), physical modification (Pregelatinization) and enzymatic modification (degradation) (Haq Hawaz et al. 2020).

Modified starch in drilling increases its resistance to bacterial attack and also improves the rheological properties of the drilling mud this starch is prepared with (Diana Soto et al. 2020). This study describes the development and evaluation of modified starch using graft polymerization method. The graft copolymerization of starch is highly necessary in order to reduce its limitations and applications and is employed to enhance its properties without altering its intrinsic properties (Haq Hawaz et al. 2020, Vidyagauri V. L et al. 2018) and it is one of the effective ways to improve the properties of natural polymers.

Graft copolymerization combines the properties of the starch and the homopolymer which then produces unique and advanced properties as opposed to the original materials (Monica R.N et al. 2022).

II. MATERIALS AND METHODS

Four (4) genotypes of native cassava, TMS 96/1632, TMS 98/0581, TMS 07/ 0593 and TMS 01/1371 were obtained from IITA (International Institute of Tropical Agriculture), Ibadan, Nigeria. Acrylic acid, Potassium Persulfate and Ethanol were all analytical grade and obtained from Oarsman chemicals in Ibadan, Nigeria.

2.1 Cassava starch

The cassava tubers were processed using the wet milling method

2.2 Copolymerization of Cassava Starch

Preparation of S-gPAM copolymer was performed using the following 20g of starch obtained from cassava stems was dissolved in 100ml distilled water and heated in a water bath at 50 °C for 15 min. 10 g of acrylic acid was added and 2% of initiator (Potassium Per sulfate) was added. Temperature was kept at 50 °C for 120 min under reflux with vigorous stirring on magnetic stirrer. Reaction product was precipitated in 200 mL of ethanol. After filtration, precipitate was washed with 20 mL of ethanol at ambient temperature and then 4 times with ethanol-water solution (80:20) to ensure complete removal of homo-polymer acrylamide (PAM). The resulting starch grafted polyacrylamide (S-gPAM) was oven-dried for 24hours to remove water. This procedure was carried out for the 4 genotypes of cassava starch (Vidyagauri & Savita, 2021)

2.3 Characterization of the Grafted Starches

The determination of carbonyl, carboxyl and other group contents present in the copolymerized starch was carried out using the Fourier Transform Infrared Spectroscopy. The analysis was carried on both the native starch and the copolymerized starch for evidence of grafting. The spectra were obtained using a FTIR spectrophometer (spectrum one, Perkin Elmer/PIKE MIRacle™ Technologies, Wellesley, MA, USA) using KBr pellets and measured in ATR mode with a special resolution of 0.5cm^{-1} used.

2.4 Mud Preparation and Tests

The drilling mud was prepared in accordance with the API 13A recommended practice. 15 mud samples were prepared using 21.5g of bentonite gradually added to 350 ml of distilled water and mixed to obtain a homogenous mixture using a Hamilton Beach mixer. The samples were labelled A, B, C, D and CMC was allowed to stay from 16hours allowing for proper hydration before an electronic weighing balance was used to measure 10g of barite into each mud suspension before varying concentration of the modified starches (2g. 4g and 6g) into the labelled mud samples the suspension was thoroughly mixed for about 20minutes, with a spatula used to scrap the polymer clinging to the beaker walls The suspension was poured into the Fann35A viscometer cup and sheared, and dial readings at 600, 300, 200, 100, 60, 30, 6, and 3 rpm were taken

2.5 Physico-Chemical, Rheological and Filtering Properties

The Physico-chemical, rheological and filtering properties of the different Water -Based Muds were determined. The density of the drilling fluids was determined using a mud balance. The pH was determined using a pH meter.

2.5.1 Determination of Mud Sample Density and pH

The density of the drilling fluids was determined using a Bariod Mud Balance while the pH was determined using the pH meter.

2.5.2 Rheological Properties

The readings obtained from the Fann 35A viscometer were used to determine the plastic viscosity, apparent viscosity and yield point. at 20 °C, 40°C and 70°C. using the equations 1.0,2.0 and 3.0, respectively.

$$PV(cp) = \theta_{600} - \theta_{300} \tag{1.0}$$

$$AV = \frac{\theta_{600}}{2} \tag{2.0}$$

$$YP(lbs/100ft) = \theta_{300} - PV \tag{3.0}$$

Power law model

This is a two parameter model that relates shear stress to shear rate in a non-linear manner (Alderman et al. 1988; Okafor & Evers, 1992). The model does not consider an excess yield stress and states the relation in equation 4 as;

$$\tau = K\gamma^{n} \tag{4. 0}$$

Where K and n are consistency index and flow index respectively, τ is the shear stress and γ is the shear rate.

2.5.3 Filtration Properties

The American Petroleum Institute (API) filter press was used to determine the filtrate loss of the drilling fluids. The filtrate loss test is used to determine the quantity of fluid lost during drilling and the type of mud cake formed. Drilling fluids with poor filtrate loss control produce thick filter cakes that can pose issues in the wellbore. Such issues include but are not limited to; reduced rate of penetration, stuck pipe, excessive torque. Minimizing fluid loss and forming a thin permeable mud cake is crucial in drilling activities (Hanyi Zhong et al., 2022)

III. RESULTS AND DISCUSSION

3.1 Starch Characterization: Fourier Transform Infrared Spectroscopy

The Fourier Transform Infrared (FTIR) spectra in Figures 1.0 to 5.0 were obtained for a native starch (TMS 95/0289) and the copolymerized cassava starches from TMS 96/1632(A), TMS 98/0581 (B), TMS 07/ 0593 (C) and TMS 01/1371(D). The Figure 1.0 presents the spectrum of native cassava starch showing peaks at 3200cm^{-1} to 3500cm^{-1} and 2923cm^{-1} corresponding to OH and CH stretching while peaks at 1639cm^{-1} and 1416cm^{-1} correspond to OH and CH bonding. The native cassava starch also showed the short range order structures of the starch double helix at 1020 cm^{-1} and 930cm^{-1}. while those of the others S-gPAM showed a strong absorption band at 3300cm^{-1} - 3500cm^{-1} which is attributed to NH stretching vibration of the NH_2 group.

The band for OH stretching vibration was seen around 2908cm^{-1} – 2938cm^{-1}. New absorption bands at 1644cm^{-1} – 1654cm^{-1} indicates a primary amide group in polyacrylamides. NO asymmetric stretch bands were also observed around 1530cm^{-1}. Absorption bands at 1411cm^{-1} to 1416cm^{-1} shows scissoring vibrations of $-CH_2$ group. Absorption bands around 1080cm^{-1} corresponds to valence vibrations $-OCH\text{-}O\text{-}CH_2$ groups. The absence of the strong 1639cm^{-1} (C=N) absorption band in the copolymers indicate that copolymerization has taken place (Vidyagauri and Savita, 2021).

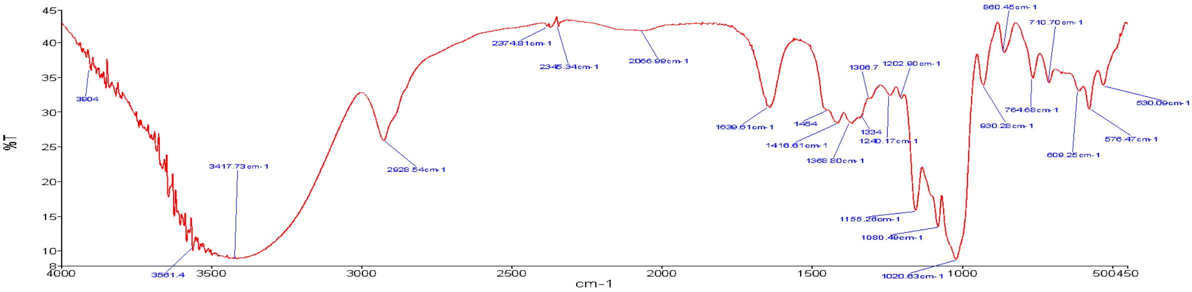

Figure 1.0: FTIR spectra of native starch

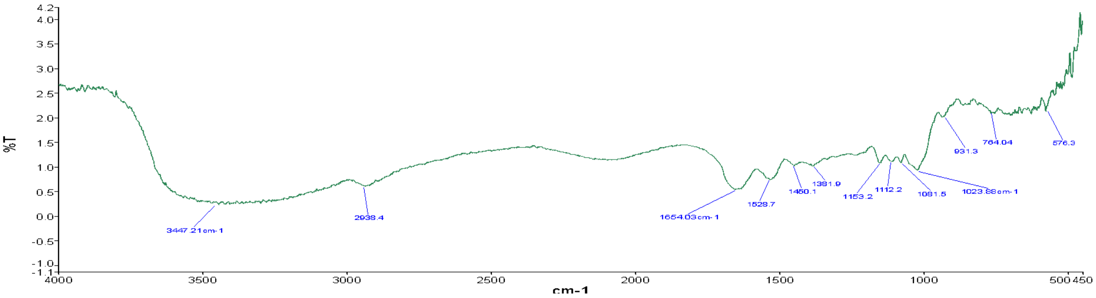

Figure 2.0: FTIR spectra of sample A

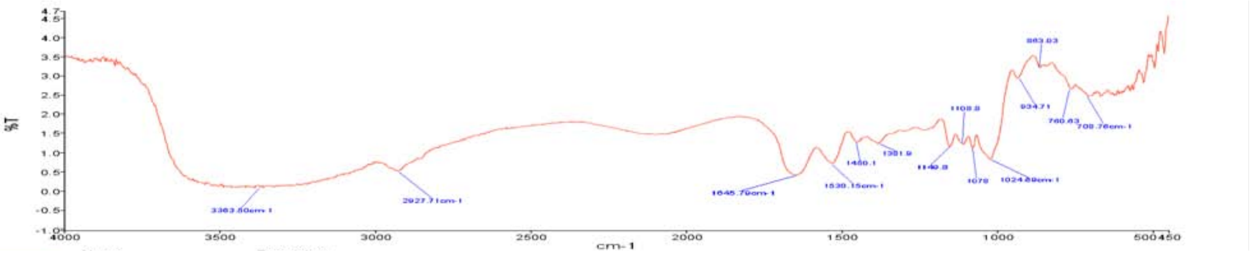

Figure 3.0: FTIR spectra of B

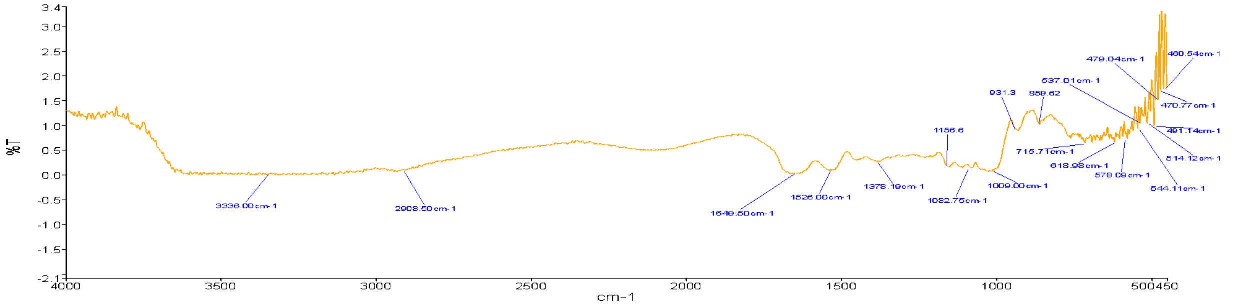

Figure 4.0: FTIR spectra of C

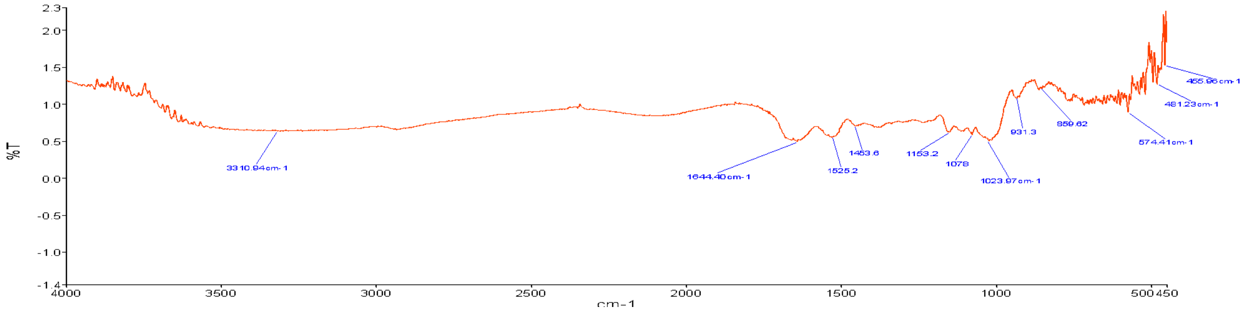

Figure 5.0: FTIR spectra of D

3.2 Mud weight

The Figure 6.0 presents the result of the mud weight of all the mud samples. from the result it can be observed that mud samples treated with polymerized starch had weights higher than the control mud. Also there is a minimal increase in the mud weight as the weight of the additive, copolymerized starch, increases.

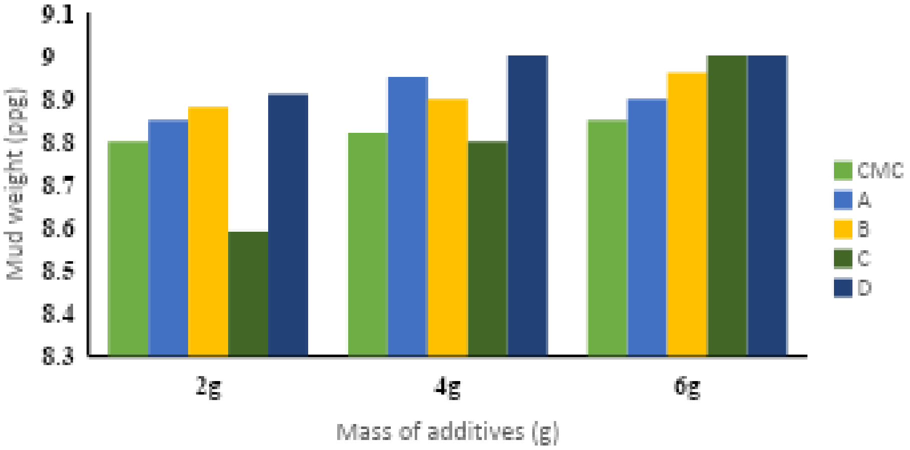

Figure 6.0: Mud weight of mud samples

3.3 pH of Drilling Fluids

The pH of the drilling fluids increased with increasing weight of the copolymerized starch as presented in the Figure 7.0. The mud samples pH is within the range of 8.6 to 8.9. These mean that the modified starch reduced the hardness of water by precipitating the calcium ions in the water thereby increasing the pH of water. Therefore, modified starch can be used to reduce the mud acidity which could lead to corrosion of bottom equipment during drilling (Aliyu, et al. 2020).

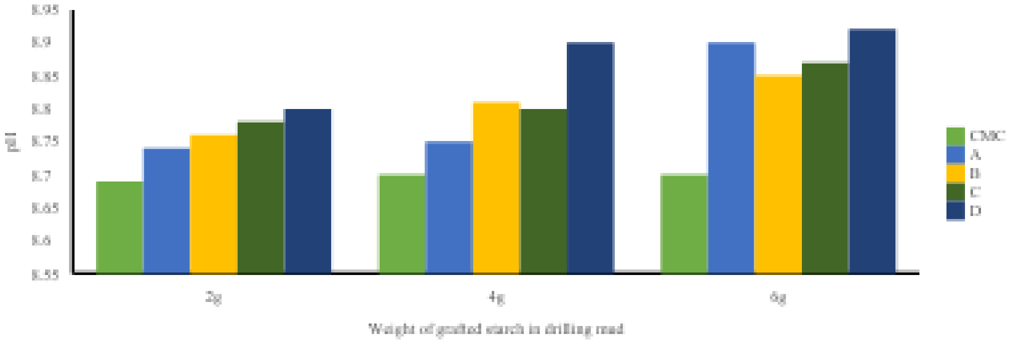

Figure 7.0: pH of mud samples

3.4 The Mud Samples Rheological Properties

The dial readings of the drilling fluid samples after the addition of copolymerized starch were taken.

3.4.1 Plastic Viscosity

The results for the plastic viscosities of the mud samples are shown in Figures 8.0 to 10.0.. The API specification for high performance is below 35cp which the mud samples exhibited. . Mud sample prepared with 6g of CMC at 40℃ had the highest PV at 18cp followed by 2.0g of D at 70℃ at 15cp.

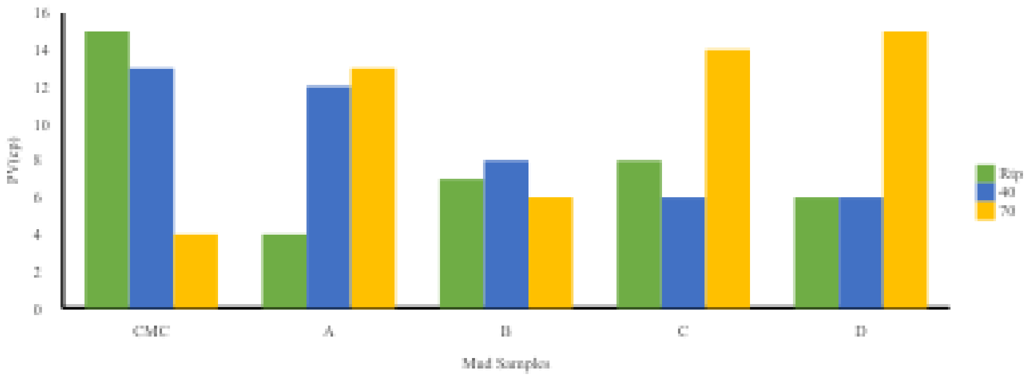

Figure 8: Plastic Viscosity of 2g of mud samples at Rtp, 40℃ and 70℃

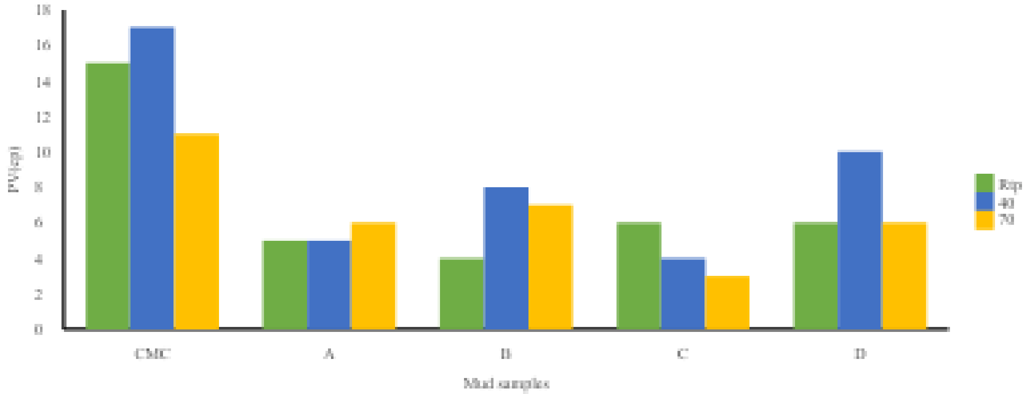

Figure 9: Plastic Viscosity of 4g of mud samples at Rtp, 40℃ and 70℃

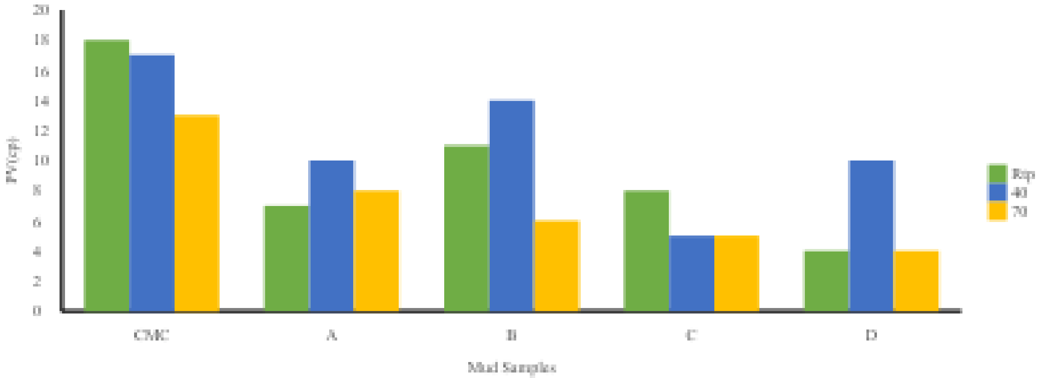

Figure 10: Plastic Viscosity of 6g of mud samples at Rtp, 40℃ and 70℃

3.4.2 Apparent Viscosity

The apparent viscosity of mud samples treated with copolymerized starch are presented in figures 11.0 to 13.0. The apparent viscosity for all mud samples prepared with CMC had the highest values going as high as 47cp. At 70℃, C and D had a value of 25cp while 6g of B at 40℃ had a value of 30cp.

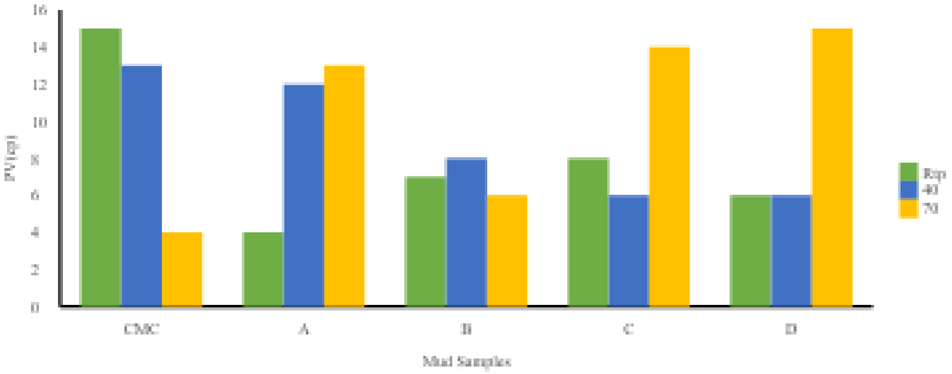

Figure 11.0: Apparent Viscosity of 2g of mud samples at Rtp, 40℃ and 70℃

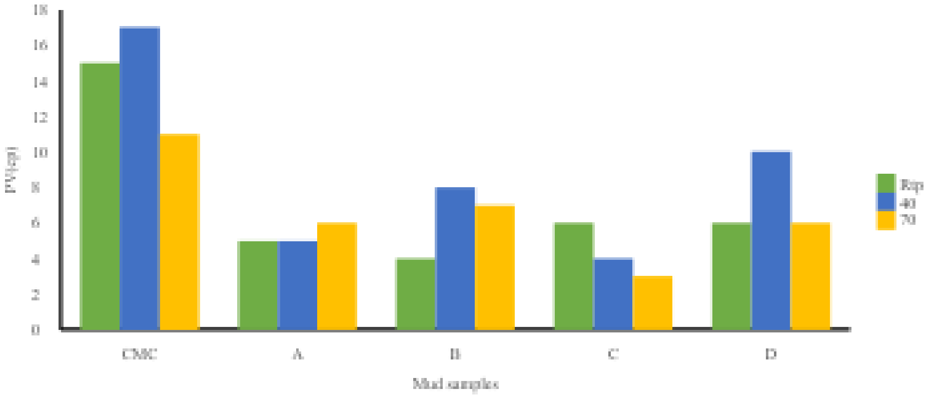

Figure 12: Apparent Viscosity of 4g of mud samples at Rtp, 40℃ and 70℃

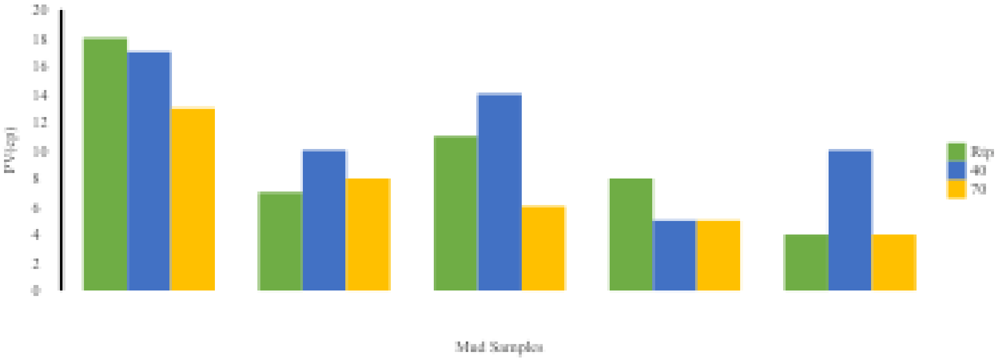

Figure 13: Apparent Viscosity of 6g of mud samples at Rtp, 40℃ and 70℃

3.4.3 Yield Point

The yield point of the mud samples in varying concentrations are shown in figures 14 to 16. High YP means an increase in mud rate. Yield point indicates the ability of drilling mud to lift drill cuttings from the wellbore. The API specification for high performance is between 15-25cp. The higher the YP, the better the mud lifts drill cuttings but excessive YP could lead to pressure loss during drilling mud circulation which could damage the formation. Mud samples prepared with 6g of CMC at all temperatures had the highest yield point with the highest at 58cp. 2g of B at r.tp had the lowest YP at 11cp. All other mud samples had YP within the API specification except 2g of D at 40℃ with 32cp.

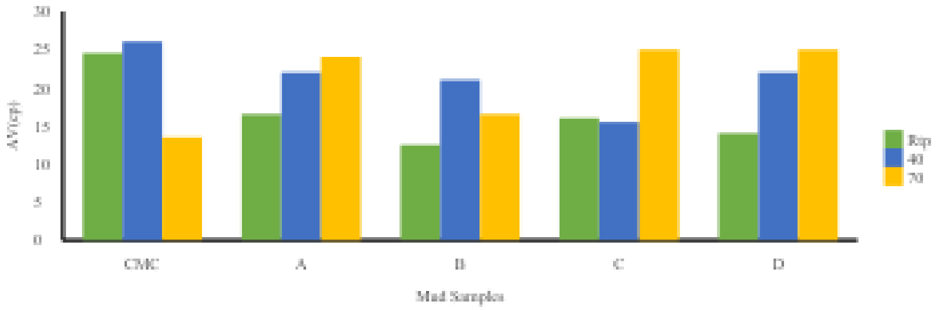

Figure 14: Yield Point of 2g of mud samples at Rtp, 40℃ and 70℃

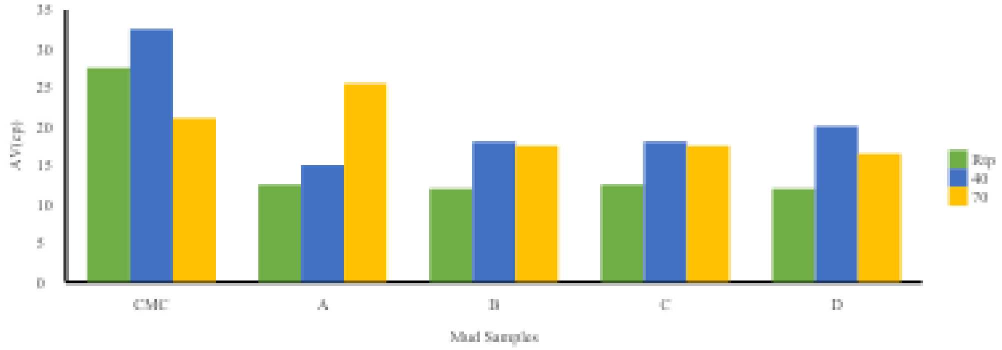

Figure 15: Yield Point of 4g of mud samples at Rtp, 40℃ and 70℃

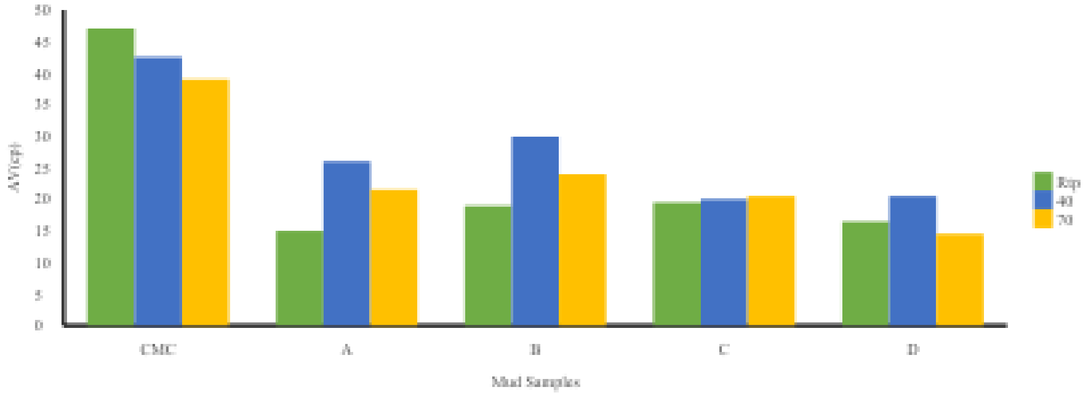

Figure 16: Yield Point of 6g of mud samples at Rtp, 40℃ and 70℃

2.4.4 Gel Strength

The API specification for the difference between the 10secs and 10mins gel strength is 20, if it exceeds 20, more pump power is needed to start the circulation after the static condition. Figures 17 to 19 show the gel strength values of mud samples taken at 10seconds and 10minutes at r.tp, 40℃ and 70℃. All copolymerized mud samples showed difference between 10secs and 10mins gel strength to be less than 20, therefore less pump power is needed to start the circulation after the static condition (Aliyu et al.

2020). The drilling mud sample prepared with 2g of copolymerized starch of genotype B at 40℃ had the same value at 10secs and 10min gel strength. The same was also observed for drilling mud sample prepared with 6g of copolymerized starch of genotype B at 70℃.

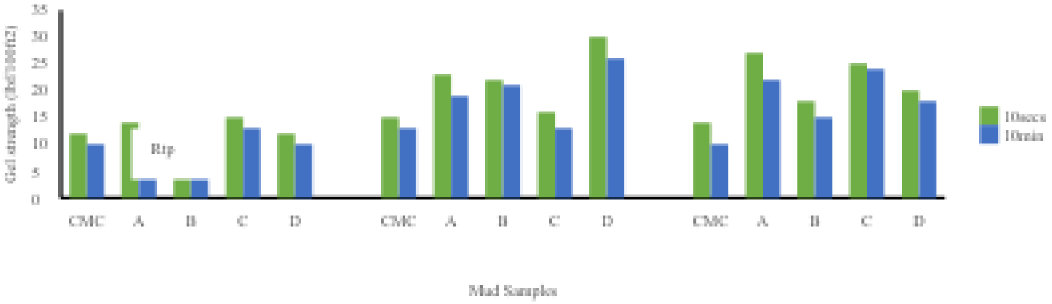

Figure 17: Gel strength of mud samples containing 2g of copolymerized starch at 10secs and 10mins

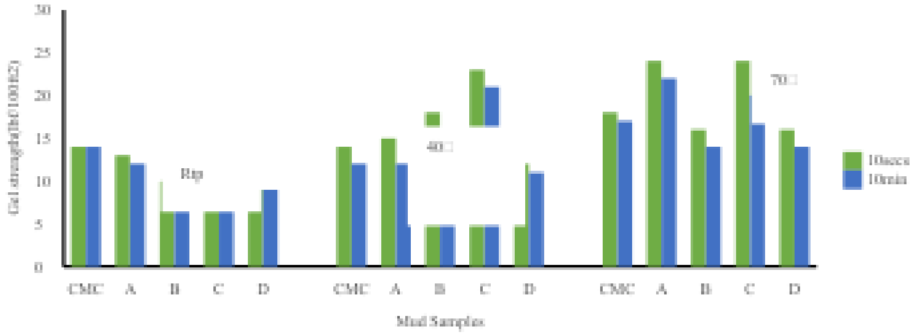

Figure 18: Gel strength of mud samples containing 4g of copolymerized starch at 10secs and 10mins

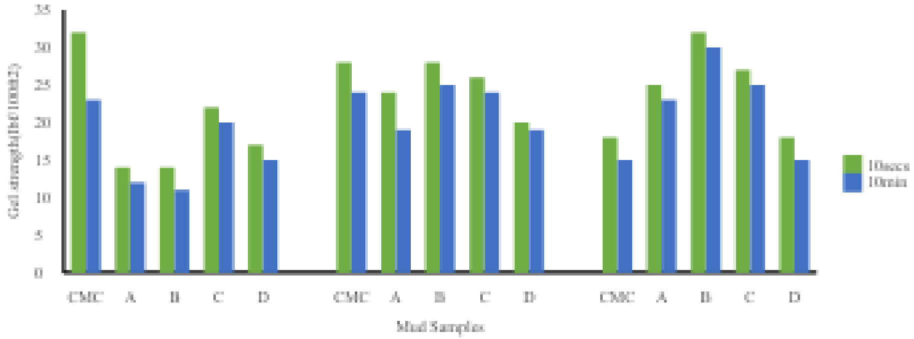

Figure 19: Gel strength of mud samples containing 6g of copolymerized starch at 10secs and 10mins

3.5 Filtration Properties and Mud Cake Thickness

The filtrate volume and cake thickness of all mud samples are shown in figures 20 to 22. The filtrate loss and mud cake properties of the samples were evaluated using the API filtration tests for 30mins. The test measured the quantity of water lost from the drilling mud at 30mins. All drilling mud samples produced thin permeable filter cake which indicates that formation damage will be minimized because of reduced fluid invasion (Imtiaz Ali et al. 2022). Drilling mud samples prepared with 2g of A, B and D all had filtrate volume ranging from 18.3 to 18.5ml while C sample had a filtrate loss value of 13.7ml.

For the 4g mud samples, D had the least filtrate loss volume at 15.5ml and the thinnest filter cake at 0.15ml.

Drilling mud samples prepared with 6g of the copolymerized starches all showed reduced filtrate loss volume with D showing the highest filtrate loss at 17.5ml while B showed the thickest filter cake at 0.5mm. Mud samples prepared with CMC at different weights all outperformed the drilling muds prepared with the copolymerized starches.

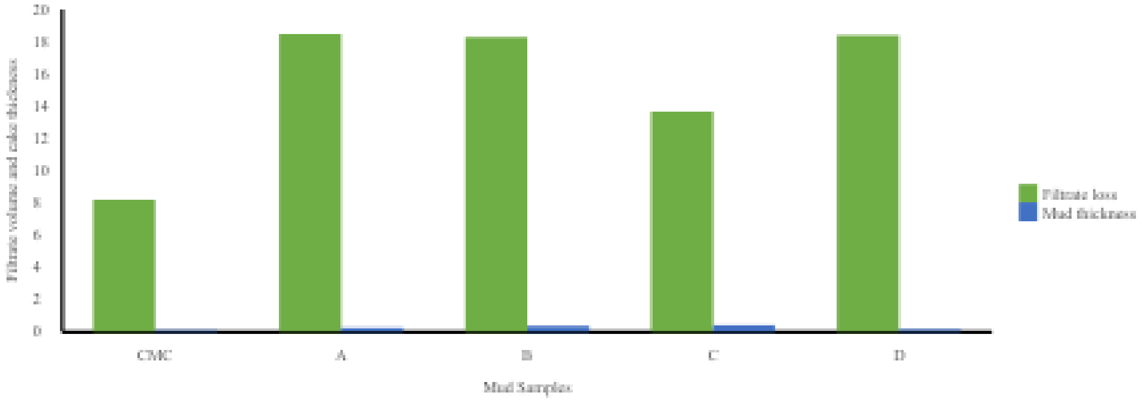

Figure 20: Filtrate volume and mud cake thickness for mud samples containing 2g of copolymerized starch

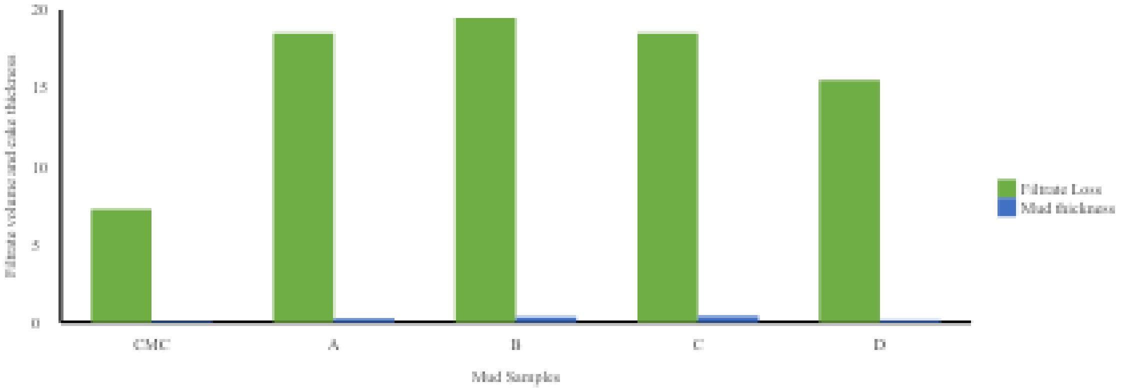

Figure 21: Filtrate volume and mud cake thickness for mud samples containing 4g of copolymerized starch

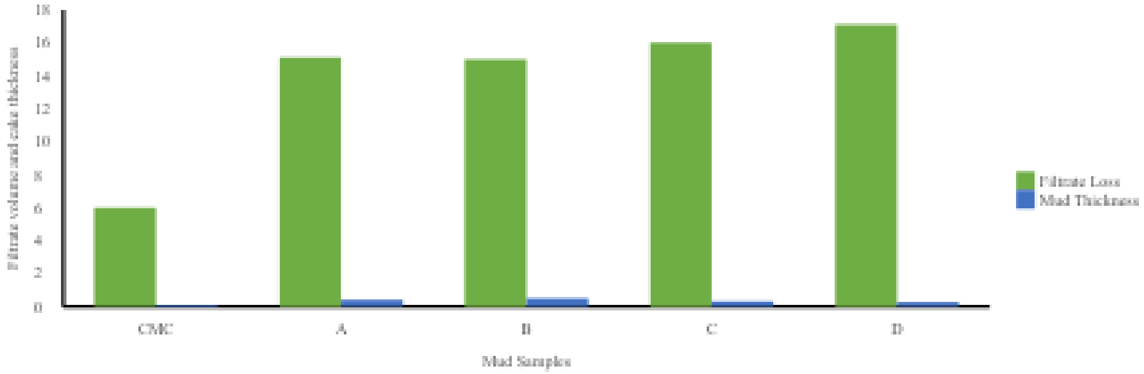

Figure 22: Filtrate volume and mud cake thickness for mud samples containing 6g of copolymerized starch

IV. CONCLUSION

Native starch was modified by graft copolymerization and the effect of these on the properties of water based mud was compared to mud formulated with CMC. All mud samples were alkaline in nature, the mud samples prepared with 2g of copolymerized starch had the lowest pH. The mud sample containing 2g of D at 70℃ had PV of 15cp and is capable of lifting drill cuttings.

Mud samples prepared with copolymerized D had the least filtrate loss volume at 15.5ml and the thinnest filter cake at 0.15ml, hence a good filtrate loss reducer compared to the other starch samples. Therefore, mud sample treated with D had better rheological properties and filtration loss control. From the results, increasing concentrations of the modified starch does not have a significant effect on the mud properties; however, there are differences in the mud properties based on genotype of the cassava. It was also observed that mud samples containing modified starch are shear thinning, pseudoplastic and therefore have acceptable flow characteristics.

Declaration of conflict of Interest

On behalf of all the co-authors, the corresponding author states that there is no conflict of interest

REFERENCES

1. Akinwumi E. Akinade, Okologume C. Wilfred A.M Akin-Taylor, 2018. Improving the Rheological Properties of Drilling Mud Using Local-Based Materials. American Journal of Engineering Research (AJER), Vol 7, Issue 9, pp 58-63
2. Alderman N.J., Gavignet A., Guillot D., Maitland G.C., 1998. High Temperature, High Pressure Rheology of Water-Based Mud. PN: SPE-18035-MS, https://doi.org/10.2118/18035-MS
3. Aliyu Adebayo Sulaimon, Sarah Abidemi Akintola, Mohd Adam Bin Mohd Johari, Sunday Oloruntoba Isehunwa, 2020. Evaluation of Drilling Muds Enhanced with Modified Starch for HPHT Well Applications. Journal of Petroleum Exploration and Production Technology (2021) 11:203–218, https://doi.org/10.1007/s13202-020-01026-9
4. Diana Soto, Orietta Leon, Jose Urdaneta, Alexandra Munoz – Bonilla, Marta Fernandez – Garcia, 2020. Modified Starch as a Filter Controler in Water Based Drilling Fluids.
5. Hanyi Zhong, Xin Gao, Xianbin Zhang, Anliang Chen, Zhengsong Qiu, Xiang zheng Kong, Weian Huang, 2022. Minimizing the Filtration Loss of Water-Based Drilling Fluid with Sustainable Basil Seed Powder. Petroleum, https://doi.org/10.1016/j.petlm.2021.02.001

6. Haq Hawaz, Mubashir Nawaz, Rashem Waheed, Dure Shahwar, 2020. Physical and Chemical modifications in Starch Structure and Reactivity.
7. Imtiaz Ali, Maqsood Ahmad, Tarek Ganat, 2022. Biopolymeric Formulations for Filtrate Control Applications in Water-Based Drilling Muds: A review, Journal of Petroleum Science and Engineering, Volume 210.
8. Monica R. Nemtanu, Mirela Brașoveanu, Elena Pincu and Viorica Meltzer, 2022. Water-Soluble Starch-Based Copolymers Synthesized by Electron Beam Irradiation: Physicochemical and Functional Characterization. Materials (Basel, Switzerland), 15(3), 1061. https://doi.org/10.3390/ma15031061
9. Okafor M.N. and Evers J.F., 1992. Experimental Comparison of Rheology Models for Drilling Fluids. PN: SPE-24086-MS, https://doi.org/10.2118/24086-MS
10. Peter Adewale, Marziehossadat Shokrollahi Yancheshmeh, Edmond Lam, 2022. Starch Modification for non-food, Industrial applications: Market Intelligence and Critical Review. Carbohydrate Polymers: Volume 291
11. Shadfar Davoodi, Mohamed Al-Shargabi, David A. Wood, Konstantin M. Minaev, Valeriy S. Rukavishnikov, 2024. Modified-Starch Applications as Fluid-Loss Reducers in Water-Based Drilling Fluids: A Review of Recent Advances. Journal of Cleaner Production, Vol 434.
12. Vidyagauri Lele and Ms, Savita Kumari, 2021. Synthesis and Characterization of Graft Copolymer of Sago Starch-g-Poly (Acrylamide) using Potassium Persulphate Initiator. Journal of Scientific Research, vol. 65, Issue 2
13. Vidyagauri V. Lele, Savita Kumari, Harshada Niju, 2018. Syntheses, Characterization and Graft Copolymers of Sago Starch - A Review.
14. Wysocki, S. Bielewicz, D.. Knez, D 2005. Environmental Biodegration and Drilling Performance of Water Based Polyampholyte Drilling Fluid. SPE-95640-STU